PONTIFICIA UNIVERSIDAD CATÓLICA DEL PERÚ

Escuela de Posgrado

Implementation of a triboelectrical workstation for the investigation of the influence of electrical parameters on the tribological properties of thin films in real - time

Tesis para obtener el grado académico de Maestro en Ingeniería Mecatrónica que presenta:

Diego Ricardo Cardenas Cullash

Asesor:

Francisco Aurelio Rumiche Zapata

Lima, 2025

Informe de Similitud

Yo, Francisco Aurelio Rumiche Zapata, docente de la Escuela de Posgrado de la Pontificia Universidad Católica del Perú, asesor(a) de la tesis titulada(o) Implementation of a triboelectrical workstation for the investigation of the Influence of electrical parameters on the tribological properties of Thin Films in real-time, de el autor Diego Ricardo Cardenas Cullash, dejo constancia de lo siguiente:

- El mencionado documento tiene un índice de puntuación de similitud de 16%. Así lo consigna el reporte de similitud emitido por el software *Turnitin* el 9/05/2025.
- He revisado con detalle dicho reporte y la Tesis o Trabajo de investigación, y no se advierte indicios de plagio.
- Las citas a otros autores y sus respectivas referencias cumplen con las pautas académicas.

Lugar y fecha:

Lima, 9 de Mayo de 2025.

Apellidos y nombres del asesor / de la asesora: Rumiche Zapata, Francisco Aurelio	
DNI: 10491814	Firma 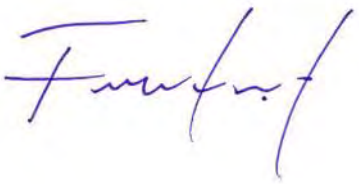
ORCID: 0000-0001-9318-8425	

Dedicatoria

En este espacio deseo agradecer a la Pontificia Universidad Católica del Perú y a la TU Ilmenau por haberme instruido en este proceso de formación. En especial, al profesor Ph.D. Francisco Rumiche y al profesor Ph.D. Rolf Grieseler por su guía y paciencia durante el desarrollo de este trabajo de tesis de maestría.
A mis colegas y amigos que me acompañaron durante todo el proceso de estudios de maestría tanto en Perú como en Alemania.
Finalmente, quisiera mencionar el apoyo de mi familia. En especial a mis padres y mi hermano. Mi familia siempre me ha impulsado a mejorar y seguir adelante.
Gracias por apoyarme siempre.

Resumen

La aplicación de peliculas delgadas se ha incrementado en varios campos de la mecánica (reducción de fricción), la química (sensores de gases químicos) y la electricidad (elementos piezoelectricos). Además, los nuevos procedimientos para crear peliculas delgadas permiten a los investigadores la oportunidad de experimentar con nuevos materiales. El objetivo de esta tesis de maestría es desarrollar una estación de trabajo tribo-electrica para la investigación sobre la influencia de los parámetros eléctricos sobre las propiedades tribológicas (coeficiente de fricción) de peliculas delgadas en tiempo real. El sistema esta compuesto por un tribómetro Basalt® MUST (Modular Universal Surface Tester) desarrollado por Tetra GmbH, dos multímetros KEITHLEY Model 2000 Multimeter, una fuente de energía KEITHLEY Model 2400 Series Source Meter ® y una estación de trabajo pórtatil desasrrollado por National Instruments (NI) con un módulo NI PXI-1042 como hardware y un NI PXI-8105 como su computador. Estos equipos fueron interconectados y configurados manualmente para ser controlados mediante un programa desarrollado en LabVIEW 2008. El programa emplea una interfaz gráfica con el usuario para ingresar los parámetros requeridos para un ensayo de tribología sobre una pelicula delgada, tambien se ingresan los parámetros eléctricos que van a afectar la muestra durante el ensayo tribológico y finalmente guia al usuario para ejecutar dicho ensayo. El programa va ha grabar todos los datos tribológicos y eléctricos recolectados durante le ensayo en un archivo de texto (el coeficiente de fricción de la muestra asi como el voltaje y la corriente obtenida durante todo el ensayo). Esta información es filtrada mediante un algoritmo desarrollado en MATLAB para eliminar ruido y los datos innecesarios para el análisis de la muestra. Finalmente, los datos obtenidos se guardaran para un análisis posterior en un programa especializado compatible con el formato de MATLAB (por ejemplo Origin Pro 2016). En conclusión, el sistema proporcionará información detallada sobre el comportamiento del coeficiente de fricción de las peliculas delgadas sometidas a variaciones eléctricas en un tiempo establecido para analizar resultados con peliculas delgadas creadas con diferentes materiales y con diferentes métodos de fabricación.

Abstract

The applications of thin films have been increasing in many fields as Mechanics (friction reduction), Chemistry (sensors for gaseous chemicals) and Electricity (piezoelectric devices). Also the new procedures to create thin films offers to the researchers the opportunity to experiment with new materials. The aim of this master thesis is to develop a triboelectrical workstation to investigate the influence of electrical parameters on the tribological properties of thin films in real-time. The components used for this investigation are one Basalt®MUST tribometer (Modular Universal Surface Tester) developed by Tetra GmbH, two KEITHLEY Model 2000 Multimeters, one KEITHLEY Model 2400 Series Source Meter ® and one portable workstation developed by National Instrument (NI) with a NI PXI-1042 as a cage and a NI PXI-8105 embedded as computer. These devices were interconnected and configured manually to be controlled by a program developed in LabVIEW 2008. The program features a graphical user interface (GUI) to input the tribological parameters, the electrical parameter (current flow) that affects the thin film during the sample and to guide the user to perform the test. Also, the program records all the data of the test (coefficient of friction, voltage and current during the test) in a text file. The obtained data is then filtered using a MATLAB program to remove noise and unnecessary data for further analysis. Finally, the obtained information can be displayed and analysed with any program compatible with MATLAB (for example Origin Pro 2016).
In conclusion, the system brings information about the behavior of the coefficient of friction of the thin films affected by a flow of current in real time. This result help to analyse the properties of different thin films created from different material and different methods of fabrication.

Contents

List of Tables

List of Figures

Introduction

1 Motivation

According to Braunovic, "An electrical contact is defined as the interface between the current-carrying members of electrical or electronic devices that assure the continuity of electric circuit, and the unit containing the interface" (ref [1]). Nowadays, electrical contacts are used in many aspects of everyday life, from domestic tasks until industrial applications. The increase in applications has led researchers to develop electrical contacts on a microscopic scale. Consequently, numerous challenges that were never been considered by previous generations of researchers and engineers have arisen (ref [1]).

The sliding wear and fretting are key factors in the performance of many electrical contacts (ref [2]). Therefore, knowledge of the tribological properties of micro-materials is important in the development of new materials for electrical contacts (ref [1]). However, the available commercial system that can measure the effect of the electrical current and the contact resistance of the material under a tribological test in real time are limited to low current values. The goal of this thesis is to implement a triboelectrical workstation for the investigation of the influence of electrical parameters on the tribological properties of thin films in real time using the four point method in order to measure the electrical parameter during the tribological test. Also the current values applied are higher than 1 milliampere (mA) to focus on the interaction of an electrical arc with the material. Commercial tribometer systems do not achieve this two points because they use less intense currents.

The group of Materials for Electronics at TU Ilmenau provides a tribometer to study the tribological properties of thin films and modules to provide electrical current and multimeters to measure electrical properties. The tribometer used in the laboratory is a Basalt® MUST (Modular Universal Surface Tester) developed by Tetra GmbH. Others modules are one KEITHLEY Model 2400 Series Source Meter ® and two KEITHLEY Model 2000 Multimeters. Both devices have a measurement accuracy of microvolts and can provide a low level of voltage and current respectively (ref [3],ref [4]).

Previous studies have implemented a triboelectrical workstation based on this tribometer and the Keithley modules (ref [5]). This previous work used two different programs developed in LabVIEW to control the parameters of the tribometer and to use the Keithley modules for measuring the electrical parameters during one tribological test. These two programs can collect the electrical and tribological data from the experiment, however this information was not acquired from the same experiment because they were in different programs. On this basis, there was imposible to establish a direct relation between the electrical and the tribological parameters at each moment in time (ref [5]). Additionally, both programs (the tribological and the electrical) had issues that needed to be improved in order to obtain reliable data. The previous work presents the following problems that need to be solved:

- There must be just one program that controls the tribometer functions and the electrical parameters during the experiment in order to store the electrical and tribological data in real time to investigate the relationship between both parameters during the test.
- The previous graphical user interface (GUI) of both programs were difficult to understand for new users. Therefore, a new program with a user-friendly GUI has been developed.
- The previous program does not have any safety algorithms to prevent collision between the fiber optic sensors and the tribometer mirrors (both are sensible components of the tribometer,as explained in Chapter 2.2.1).
- The previous GUI lacked emergency stops. Every electro mechanical machine should have emergency stops to avoid accidents that could damage the user or the device. In this case, the tribometer has delicate components, such as the mirrors or the cantilever that can be broken due to improper use of the tribometer motors and the calibration that the user must perform before conducting an experiment.
- The coefficient of friction obtained by the previous tribological program shows irregular data. This suggest that the normal force value set by the user may not match the value recorded by the program. This phenomenon was caused by the low accuracy of the cantilever's initial approach to the sample. Additionally, there was no control in the program to adjust the normal force during the experiment.
- The final data include segments where the coefficient of friction is zero. Due to the nature of the experiment (explained in section c of the Chapter 2.1.1.6), there are moments when the tribometer motors slow their velocity to change the direction of movement. At those moments, the tribological data is irrelevant in order to study the relation between the tribological and the electrical parameters in real time.
- The current data recorded in some tests exhibit an irregular behavior. After a period of time from the beginning of the test, the current value drops to zero. This could be due to an open circuit during the test, indicating a separation between the cantilever and the sample.

2 Objectives

2.1 General Objectives

The primary objective of this master's thesis is to design and develop a triboelectrical workstation capable of studying the influence of high current values (greater than 1mA) on the tribological properties of thin films in real time. This workstation will be controlled by a LabVIEW program running on a portable National Instruments (NI) workstation, enabling the simultaneous measurement of electrical and tribological properties during the experiment.

2.2 Specific Objectives

1. **Enhance the accuracy of the normal force control:**
   To develop and implement a LabVIEW program that improves the accuracy in setting the desired normal force in comparison to the measured normal force, both during the initial approach and throughout the entire experiment.
2. **Address current fluctuations during the experiment:**
   To design a system that prevents current value drops during the test, ensuring stable electrical conditions for accurate tribological analysis.
3. **Establish reliable communication between system components:**
   To ensure seamless and reliable communication between the Keithley modules, the tribometer, and the computer, allowing real-time control of the entire system through a single LabVIEW program.
4. **Improve the graphical user interface (GUI):**
   To enhance the LabVIEW graphical user interface (GUI) for user-friendly operation, providing intuitive control over the entire experimental process.
5. **Simultaneously record electrical and tribological data:**
   To develop a system capable of simultaneously recording both electrical and tribological properties during the experiment for integrated analysis.
6. **Develop a MATLAB-based post-processing tool to filter irrelevant data:**
   To create a post-processing program in MATLAB that removes segments with a zero coefficient of friction from the tribological data after the experiment is completed and filters unnecessary data before conducting further analysis.
7. **Compare the experimental results with previous studies:**
   To compare the data obtained from the developed system with results from previous studies, demonstrating the improvements and effectiveness of the newly designed triboelectrical workstation.

CHAPTER 1

Fundamental Theory and State of the art

1.1 Theoretical knowledge

1.1.1 Tribology

To determine the application field of a material, it is necessary to characterize its properties, whether mechanical, electrical or chemical. Tribology is the science and technology that studies surfaces in relative motion and involves the areas of friction, lubrication and wear (ref [6]). These concepts will be discussed below.

1.1.1.1 Contact mechanics

According to Popov: "Contact mechanics and the physics of friction are fundamental disciplines of the engineering sciences " (ref [7]). These contacts are applied in clutches, brakes, tires, bushing and ball bearings, combustion engines, hinges, gaskets, castings, machining, cold forming, ultrasonic welding, electrical contacts and many others. However, scientist are now applying this knowledge in a smaller scale. Consequently, industry and the laboratories are demanding the use of tribological knowledge in micro and nanotechnology applications.
Many models have been created to understand the forces, deformation, wear and stress in the contact between solid bodies. Hertz was a pioneer in the field finding a solution for the normal contact (without adhesion) between elastic bodies with slightly curved surfaces (ref [8]). The most well known scenario of his research is the contact between a rigid sphere and a flat surface (see Figure 1.1)(ref [7]).

Hertz developed a general formula for the stress in any elastic contact created by a force between two objects and then summarized this formula for each special case of

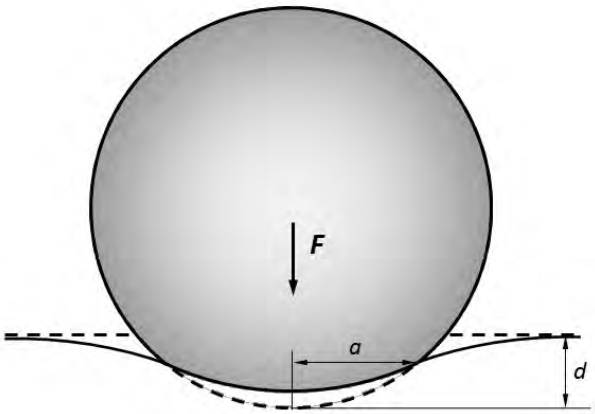

Figure 1.1: Contact between a rigid sphere and a flat surface. Note that F is the load gain; R is the indenter radius (the sphere) and a is the radius of the surface of contact. Based on ref [7].

elastic collision between objects with different surface shapes. In a general case, the first equation has u_z as the displacement in z-axis, E^* as the combined elastic modulus of both objects, p_o as the stress in z-axis, a related to the gain load and r related to the displacements in the x-axis and y-axis. The second equation has F as the force that generate the collision (ref [7]).

$$u_z = \frac{1}{E^*}\frac{p_o}{4a}\pi(2a^2 - r^2) \tag{1.1}$$

$$F = \frac{2}{3}p_o\pi a^2 \tag{1.2}$$

In the specific case of a collision between a spherical indeter an a plane surface, E^* is the combined modulus of the indenter and the specimen defined by ref [8]:

$$\frac{1}{E^*} = \frac{(1-\nu^2)}{E} + \frac{(1-\nu'^2)}{E'} \tag{1.3}$$

In this equation, E and ν describe the elastic modulus and Poisson ratio of the indenter whereas E' and ν' represent the elastic modulus and Poisson ratio of the contact surface (ref [8]).

Also, Hertz developed the following equations for this special case when the maximal pressure:

$$u_z = d - \frac{r^2}{2R} \tag{1.4}$$

$$p_0 = \frac{2}{\pi}E^*\left(\frac{d}{R}\right)^{1/2} \tag{1.5}$$

Then substituting the equation 1.1 into the equation 1.4 the value of a is reduced (ref [7]).

$$a = \sqrt{R\,d} \tag{1.6}$$

Finally after substituting equation 1.5 and equation 1.6 into equation 1.2 the final result is one equation of the force F in function of E^*, R and d.

$$F = \frac{4}{3} E^* R^{1/2} d^{3/2} \tag{1.7}$$

1.1.1.2 JKR-Theory

The theory developed by Johnson, Kendall and Roberts in 1971 along with studies on the adhesive contact between two surfaces caused by attractive forces (e.g. van-der-Waals forces) complements the Hertz's theory which only includes elastic collisions. For example, when an elastic sphere of radius R contacts a rigid surface, the adhesive forces generates a "neck" in the sphere if it separates from the rigid plane (see Figure 1.2a) with a maximum indentation of d (see Figure 1.2b). It is important to note that the points on the surface of the sphere in contact with the rigid plane must be displaced in order to lie on the second one after deformation (ref [7]).

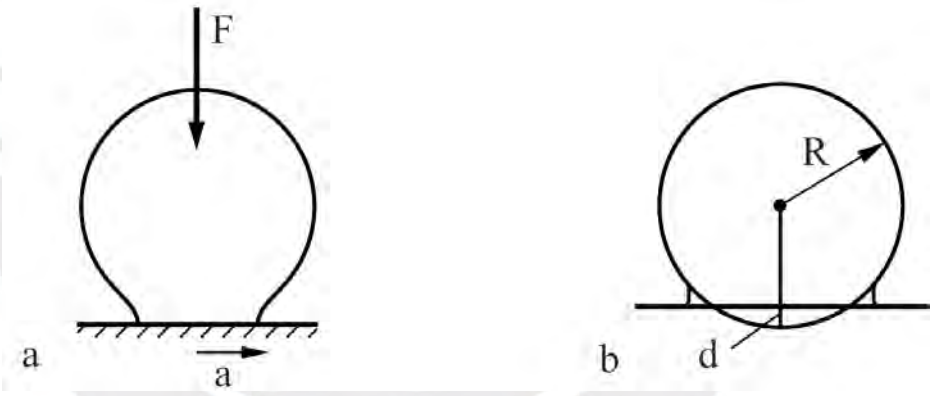

Figure 1.2: Deformation of a sphere: a)"Neck" formed during an adhesive contact, b) Maximun penetration d. Adapted from ref [7].

The radius of the contact area is defined as a, d is much smaller than R. The displacement in the z-axis is obtained from Figure 1.3:

$$u_z = d - \frac{r^2}{2R} \tag{1.8}$$

where

$$r = \sqrt{x^2 + y^2} \tag{1.9}$$

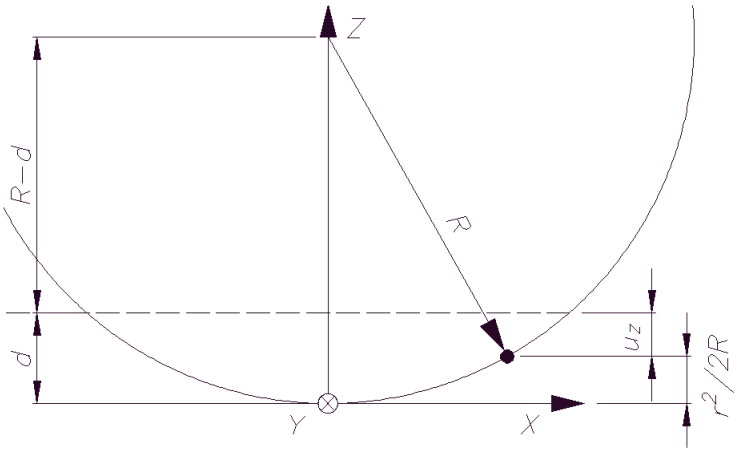

Figure 1.3: Geometric dimensions of the penetration. Adapted from ref [7].

Due to the quadratic distribution of the displacement shown in Equation (1.8), the pressure distribution (p) explained in (1.10) will be used (ref [7]). Parameters r and a were explained in 1.1.1.1, whereas p_0 and p_1 are variables that depend on the depth of the pressure (d).

$$p = p_0 \left(1 - \frac{r^2}{a^2}\right)^{-1/2} + p_1 \left(1 - \frac{r^2}{a^2}\right)^{1/2} \tag{1.10}$$

and the displacement in z axis (u_z) is

$$u_z = \frac{a\pi}{E^*} \left[p_0 + \frac{1}{2} p_1 \left(1 - \frac{r^2}{2a^2}\right)\right] \tag{1.11}$$

from (1.8) and (1.11)

$$d = \frac{a\pi}{E^*} \left(p_0 + \frac{p_1}{2}\right), \qquad \frac{1}{2R} = \frac{p_1 \pi}{4E^* a} \tag{1.12}$$

$$p_1 = \frac{E^* 2a}{\pi R}, \qquad p_0 = \frac{E^*}{\pi} \left(\frac{d}{a} - \frac{a}{R}\right) \tag{1.13}$$

The previous equations have three unknown variables p_1, p_0 and a. To determine the state of deformation and stress for a penetration d, it is assumed that the total energy (U_{tot}), elastic and adhesive, of the system is minimum at a constant d (ref [7]). This assumption yields

$$U_{tot} = E^* \left[d^2 a - \frac{2da^3}{3R} + \frac{a^5}{5R^2}\right] - \gamma_{12} \pi a^2 \tag{1.14}$$

where γ_{12} represents the relative surface energy between the two contacting bodies (one made of material 1 and the other of material 2), and E^* is the combined modulus

calculated by Equation (1.3). The radius a is obtained by requiring that U_{tot} assumes its minimum value:

$$\frac{\partial U_{tot}}{\partial a} = 0 \tag{1.15}$$

This yields:

$$d = \frac{a^2}{R} \pm \sqrt{\frac{2\gamma_{12}\pi a}{E^*}} \tag{1.16}$$

By substituting into equation (1.14) an expression is obtained that relates the total energy as a function of the contact radius (ref [7]):

$$U_{tot} = E^* \left[\frac{8}{15}\frac{a^5}{R^2} + \frac{\gamma_{12}\pi a^2}{E^*} \pm \frac{4}{3}\frac{a^3}{R}\sqrt{\frac{2\gamma_{12}\pi a}{E^*}} \right] \tag{1.17}$$

Equation (1.17) with the minus sign applies to the case of lowest energy (ref [7]). The total force acting on the sphere can be obtained from the derivative of the energy with respect to the displacement d, which yields (ref [7]):

$$F = E^* \left[\frac{4}{3}\frac{a^3}{R} - \left(\frac{8\gamma_{12}\pi a^3}{E^*} \right)^{1/2} \right] \tag{1.18}$$

When the value of a is equal to

$$a = a_{crit} = \left(\frac{9}{8}\frac{\gamma_{12}\pi R^2}{E^*} \right)^{1/3} \tag{1.19}$$

the force F reaches a minimum value equal to

$$F_A = -\frac{3}{2}\gamma_{12}\pi R \tag{1.20}$$

The **adhesive force** is the absolute value of this force. The dimension d reaches its critical value (d_{crit}) in that state and is equal to

$$d_{crit} = -\left(\frac{3\pi^2\gamma_{12}^2 R}{64 E^{*2}} \right)^{1/3} \tag{1.21}$$

In Figure 1.4 it is shown the graphic of equation 1.22, which represents the variation of the normalized force ($\tilde{F} = F/|F_A|$) regarding the normalized contact radius ($\tilde{a} = a/|a_{crit}|$).

$$\tilde{F} = \tilde{a}^3 - 2\tilde{a}^{3/2} \tag{1.22}$$

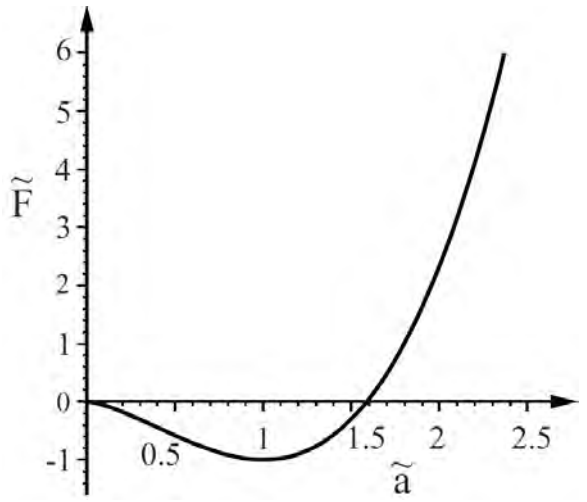

Figure 1.4: Normalized force vs normalized contact radius. Extracted from ref [7].

On the other hand, Figure 1.5 represents the dependence of the normalized force respect to the normalized penetration, which is calculated by $\tilde{d} = d/|d_{crit}|$.

$$\tilde{d} = 3\tilde{a}^2 - 4\tilde{a}^{1/2} \tag{1.23}$$

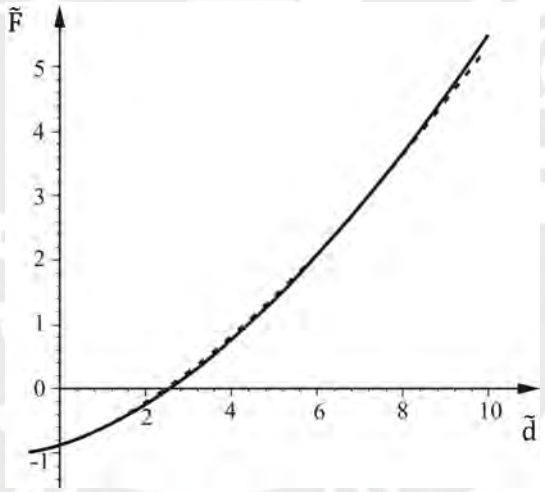

Figure 1.5: Normalized force vs normalized penetration d. Extracted from ref [7].

The distribution of contact forces is shown in the Figure 1.6, where compressive forces appears in the center, while tensional forces occurs at the edge of the contact area (ref [9]).

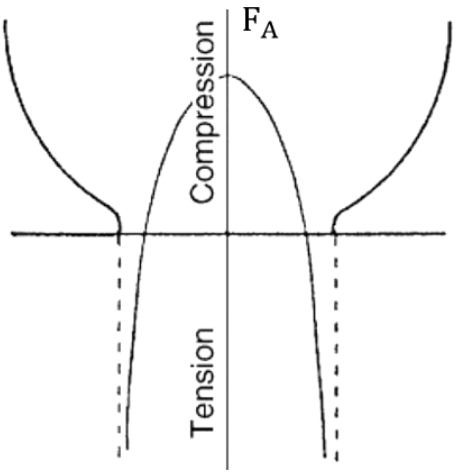

Figure 1.6: Distribution of the adhesion force. Extracted from ref [9].

1.1.1.3 Roughness

Although the surfaces in motion seems to be completely smooth, there are always rough areas as well as undulations (ref [10]). The high points are referred to as peaks while the low points are called valleys. To quantify the roughness of a surface, the following parameters are calculated: the center-line average (R_a), the root mean square value (R_q) and the mean distance between the highest peaks and lowest valleys (R_z) (ref [10]). This can be seen in the Figure 1.7.

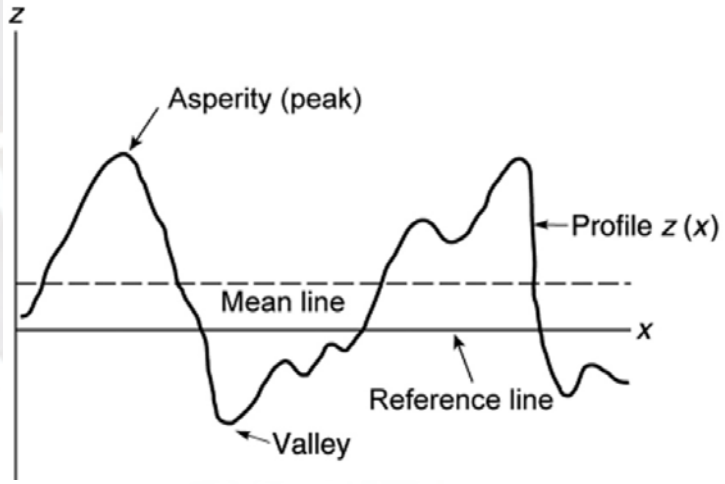

Figure 1.7: Schematic view of the profile $z(x)$ of a surface. Extracted from ref [9].

The center-line average is calculated with the following equation (ref [9]):

$$R_a = \frac{1}{L}\int_0^L |z - m| dx \tag{1.24}$$

Where L is the length of the profile and the parameter m is determined by ref [9]:

$$m = \frac{1}{L}\int_0^L z dx \tag{1.25}$$

The variance (σ_v) is calculated as ref [9]

$$\sigma_v^2 = \frac{1}{L}\int_0^L (z-m)^2\, dx = R_q^2 - m^2 \tag{1.26}$$

and R_q is given as

$$R_q^2 = \frac{1}{L}\int_0^L (z)^2\, dx \tag{1.27}$$

The center-line average is a standard parameter used to describe the roughness of a surface. In microscale, the microroughness is atribuited to manufacturing process of the material. Therefore, the presence of errors in experiments with materials in the micro scale order are common (ref [9]).

1.1.1.4 Real contact area

The irregularities described above interact when two surfaces come into contact. Initially, only the highest peaks make contact, but as the load increases, smaller asperities are also engaged. This interaction generates individual spots and the complete area of these spots constitutes the real contact area (ref [1]).

With this definition, metallic contact can be better understood. Even though the real contact area (A_r) is a fraction of the apparent contact area (A_a), another type of area, called a-spots, provides the sole conductive paths for electrical current transfer (ref [1]). A diagram illustrating these areas is shown in Figure 1.8.

Since the current is confined to flow only through a'-spots, the electrical resistance of the contact is known as constriction resistance, which is influenced by properties such as the electrical resistivity and hardness of the metals (ref [1]). The constriction resistance for a single a'-spot is expressed as ref [1] where ρ_1 and ρ_2 are the resistivities of the materials in contact.

$$R_s = (\rho_1 + \rho_2)/4a' \tag{1.28}$$

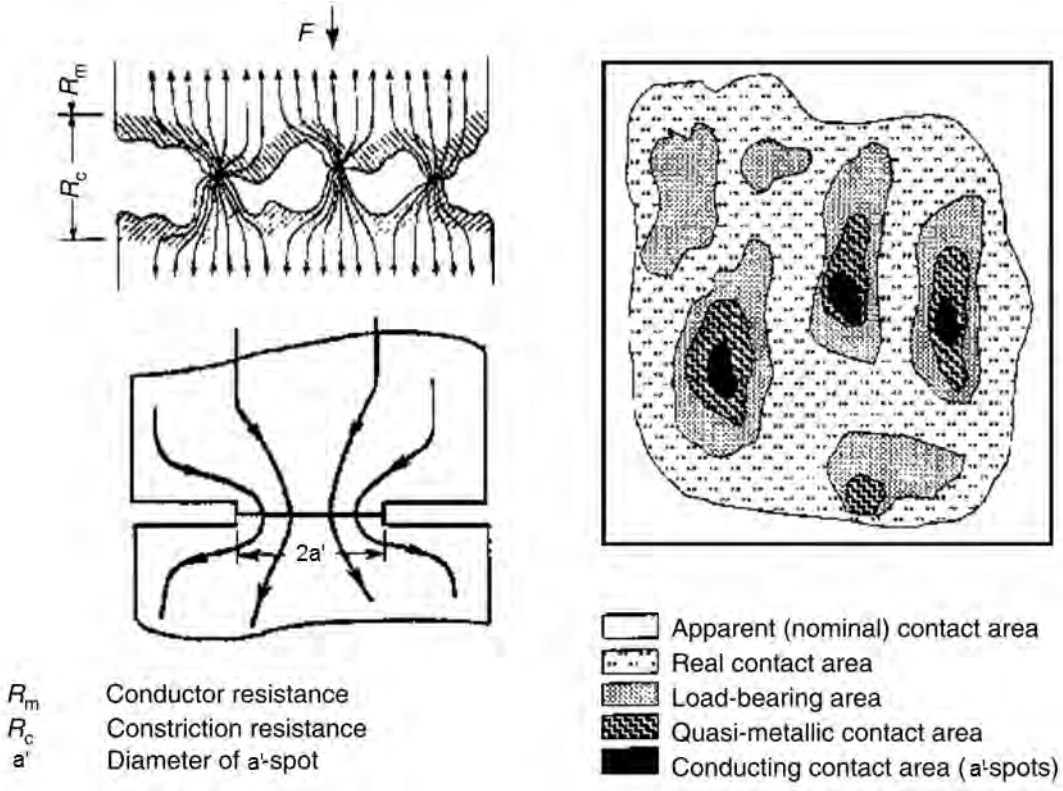

Figure 1.8: Representation of the real contact area. Extracted from ref [1].

The presence of thin oxide, sulphide or inorganic films on surfaces, can affect the flow of electrical current. As a result, the total contact resistance is the sum of R_s and the resistance of the film (R_f) where σ represents the resistance per unit area of the film (ref [1]).

$$R_c = R_s + R_f \tag{1.29}$$

$$R_f = \sigma/\pi a^2 \tag{1.30}$$

1.1.1.5 Friction

The friction is a force defined as the resistance against the movement between two bodies (ref [11]). To produce the relative displacement between them, a tangential force is required to produce it (F_t).

Applying detailed experimental studies Coulomb determined that this force is present between two bodies that are pressed with a normal force (F_N)(see Figure 1.9) (ref [7]).

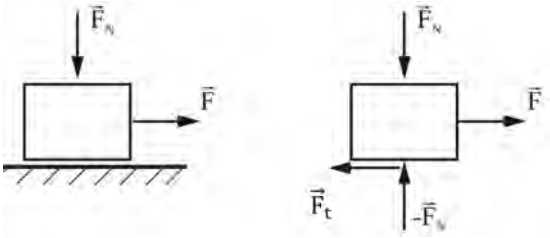

Figure 1.9: Tangential force and normal force actuated on a body. Extracted from ref [7].

As this force increases from zero to a certain value, both bodies stay as one, despite the microdisplacements between them (ref [10]). Hence the tangential force must exceed a limit value in order to generate the relative displacement. This value is known as maximum static friction value (F_s) (ref [10]) and can be seen in the Figure 1.10.

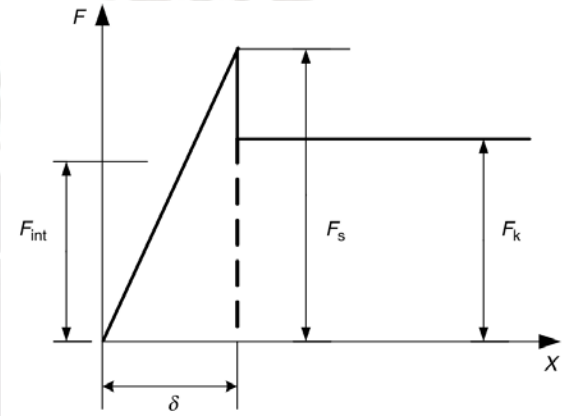

Figure 1.10: From static friction to kinetic friction (ref [1]).

F_s is proportional to the normal force applied to the bodies (ref [7]).

$$F_s = \mu_s F_N \tag{1.31}$$

The coefficient of static friction (μ_s) depends on the material of the bodies in contact, but the roughness of the surfaces and the area of contact has a small influence in its value as was explained in section 1.1.1.3 if the analysis is in micro or nano scale.

On the other hand, the kinetic friction force appears when the relative displacement between the surfaces occurres. Its properties were experimentally determined by Coulomb (ref [7]):

- The kinetic friction force is proportional to the normal force.

$$F_k = \mu_k F_N \tag{1.32}$$

- The kinetic friction force does not depend on the apparent area of contact between the bodies.

- The coefficient of kinetic friction is independent of the relative velocity.

Nevertheless, the coefficient of friction may be affected by some factors such as the time of contact, the normal force, the sliding velocity and temperature.

Dependence on standstill time

Coulomb found deviations from the laws of friction listed above. He discovered that the static friction force increases with the duration of contact, or standstill time (see Figure 1.11)(ref [7]).

The physical reasons for this time dependence can vary. In metallic materials, the real contact area between micro-contacts grows over time due to the creeping process (ref [7]). As the contact area increases, the rate of growth slows, resulting in a logarithmic dependence between the contact area and and the static frictional force (ref [7]). The initial contact at the atomic scale initiates this growth, which continues even after a prolonged period (ref [7]).

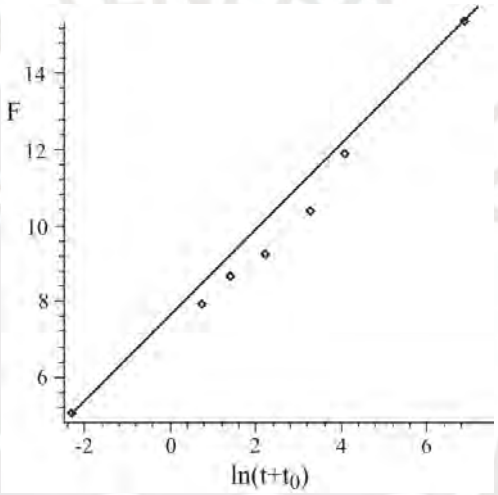

Figure 1.11: Static friction force as function of standstill time (ref [7]).

Dependence on normal force

Although the coefficient of friction under some conditions and for some materials remains constant even if the load is modified (see Figure 1.12a), it may not remain constant for materials with surface films produced by reaction with the environment (ref [9])). In Figure 1.12b), which represents the sliding between copper on copper in air, the variation of the coefficient of friction is shown from low values at low loads to a higher values as the normal load is raised (ref [9]). There are two explanations regarding the low values of the coefficient of friction: as copper easily oxidizes in air, there is an oxide film, which separates the two surfaces and for that reason, their contact to each other is minimal; besides this oxide film has a low shear strength (ref [9]). On the other hand, when load increases, this film disintegrates leading to an intimate metallic contact that causes high friction as well as surface damage (ref [9]). Moreover, in many metallic contacts, the coefficient of friction decreases (see Figure 1.12c) as the load increases due to increase of surface roughness caused by a large quantity of

wear debris (ref [9]).

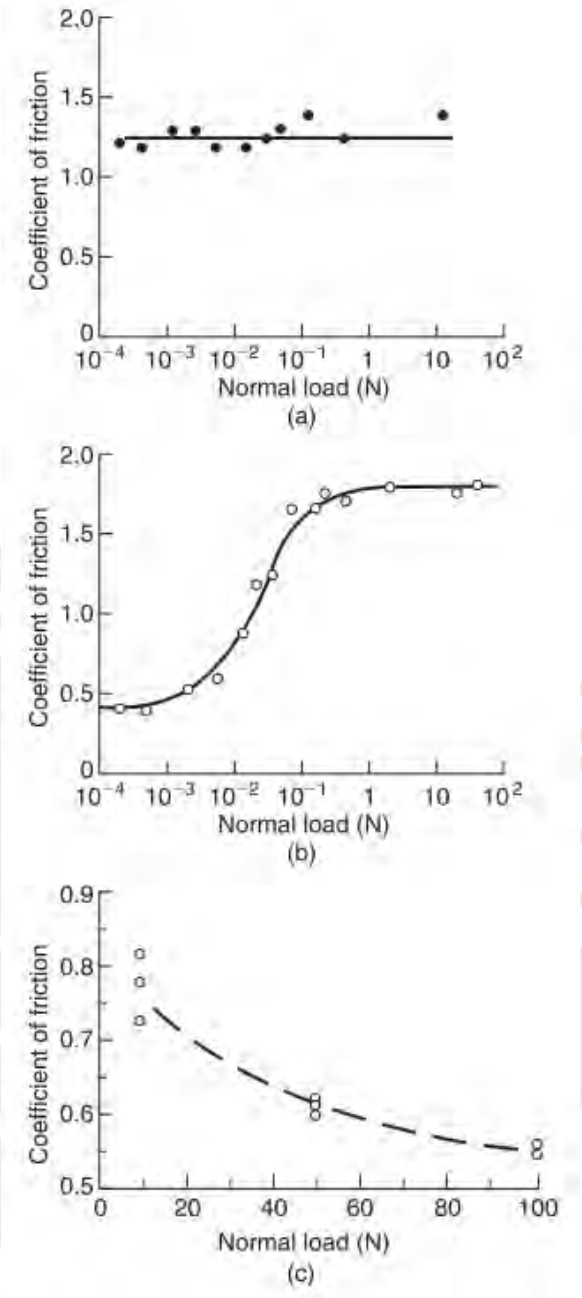

Figure 1.12: Repercussion of normal force on coefficient of friction: (a) steel sliding on aluminum in air, (b) a copper on copper in air and (c) AISI 440C stainless steel on Ni_3Al alloy in air (ref [9]).

Dependence on sliding velocity

Notwithstanding the third rule exposed above, there is a descendant trend between the coefficient of kinetic friction and the sliding velocity. In Figure 1.13a it can be seen that this slope is slight, i.e. the coefficient of friction varies a scanty percent due to a change in velocity of an order of magnitude (ref [9]). However, Figure 1.13b, shows

that the trend decreases readily for a change in velocity in large magnitudes. Bhushan explains this trend as follows: *"High normal pressures and high sliding speeds can result in high interface (flash) temperatures which may form low shear strength surface films and in some cases, high temperatures may result in local melting and reduce the strength of materials. In addition, changes in the sliding velocity result in changes in the shear rate, which can influence the mechanical properties of the mating materials. The strength of many metals and nonmetals (especially polymers) is greater at higher shear strain rates, which results in a lower real area of contact and a lower coefficient of friction in a dry contact."*

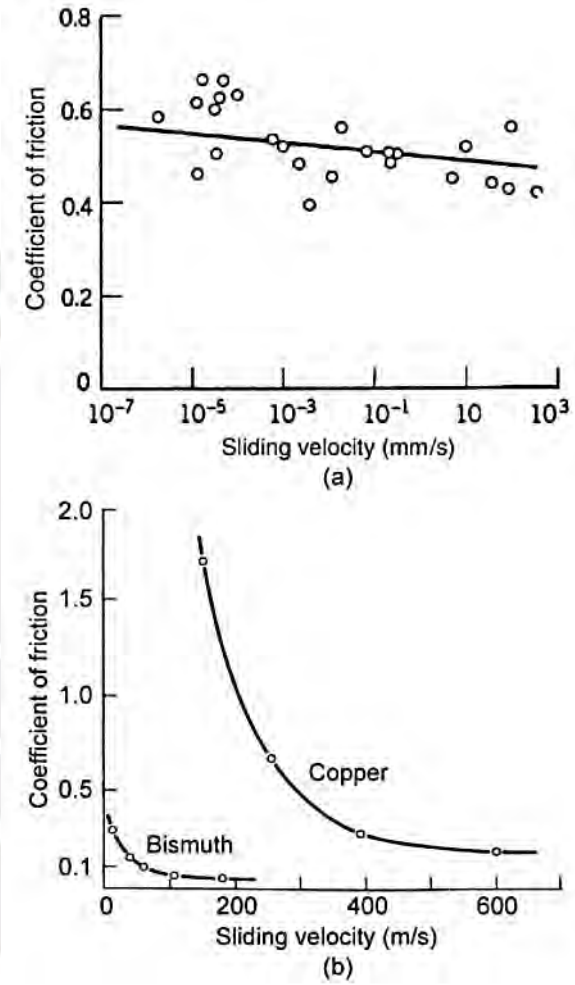

Figure 1.13: Coefficient of frictions vs sliding velocity: (a) titanium sliding on titatium at $F_N = 3\,\mathrm{N}$, (b) pure bismuth and copper sliding on themselves (ref [9]).

Dependence on temperature

In presence of thin and soft layers on the contact surface, the coefficient of friction increases briskly when the melting temperature of the layer is achieved (ref [7]). For metallic layers that occurs abruptly at the melting temperature of the softer metal and in the case of greases or metal soaps, the softening temperature belongs to the grease or the metal soap. In Figure 1.14, the variation of the coefficient of static

friction can be seen: for temperatures below 150°C, the coefficient of friction weakly ascends; however, between 200°C and 300°C occurs an escarpment; and at higher temperatures, it remains almost constant or increases with a smaller slope (ref [7]). At this temperature, it involves softening or decomposition of external layers of the surfaces (ref [7]).

For the low temperature range, the coefficient of friction is constant or relatively small and only weakly dependent of the material combination and varies typically in the range of 0.16 to 0.22 (ref [7]). This area is characterized by the presence of oxide or other layers of foreign materials on the contact surface (ref [7]).

Nevertheless other materials presents another behavior, because an increase in temperature may transform the solid-state phase, which might either improve or deteriorate mechanical properties (ref [9]). At high temperature, the friction rises because the adhesion on the contacts and ductility increase. Furthermore, this growth results from the emergence of thermal diffusion and creep phenomena when a metal approaches its melting point, which cause that its strength sinks rapidly (ref [9]).

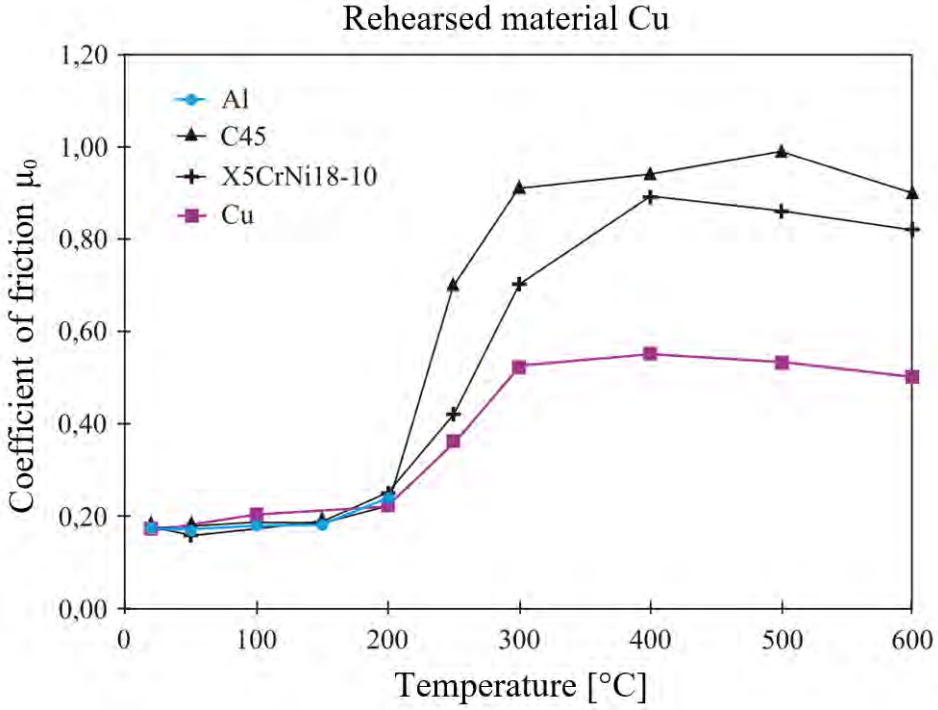

Figure 1.14: Coefficient of static frictions vs temperature (ref [7]).

Furthermore, hight temperatures increase the oxidation ratio leading to low adhesion and friction in many cases (ref [9]). This can be seen in Figure 1.15 for cobalt on stainless steel. At 417 °C cobalt has a phase transformation from a hexagonal close-packed structure to a cubic face centered (fcc) structure and hence its ductility varies: from limited slip to fully ductile. Therefore, a peak in friction can be seen at approximately 500 °C (ref [9]). Above 500 °C there is a drop in friction caused possibly by an increase in oxide thickness and by a change in oxide class from CoO, a poor lubricant, to Co_3O_4 (ref [9]).

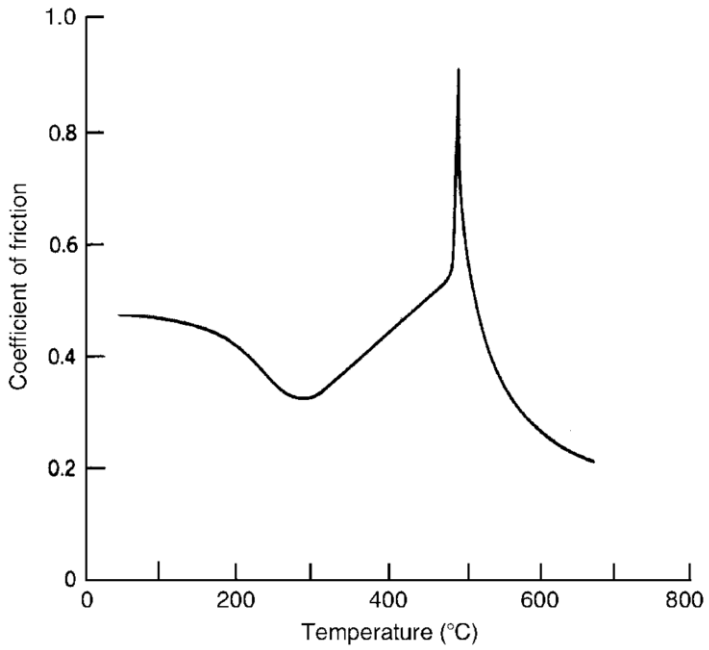

Figure 1.15: Coefficient of kinetic friction vs temperature: cobalt sliding on stainless steel at $F_N = 5\,\mathrm{N}$ and velocity of $25\,\mathrm{mm/s}$(ref [9]).

Besides, according to the definition of friction, there are two cases of relative motion: sliding and rolling. Each one has their own properties and basic mechanisms, which will be explained in the following paragraphs.

a) Sliding friction

Friction can be seen as a dissipative process consisting of the sum of an adhesion energy, or force, and deformation energy (ref [9]). Hence the total intrinsic frictional force needed to shear the adhered connections and the deformation can be calculated as follows (ref [9]):

$$F_i = F_a + F_d \tag{1.33}$$

or the coefficient of friction

$$\mu_i = \mu_a + \mu_d \tag{1.34}$$

Adhesion

Adhesion is the force that appears when two bodies are brought into contact, which bonds the surface of one solid to the other, by a pure normal force or under combined normal and shear forces (ref [9]). The coefficient of adhesion (μ_a) is the proportion of the normal tensile force (W'), used to separate the bodies, and the normal compression force (W) applied at first (ref [9]).

$$\mu_a = \frac{W'}{W} \tag{1.35}$$

The adhesive joint results from the atomic interaction between the surfaces in contact (ref [9]), that is caused by the bonds shown in Figure 1.16.

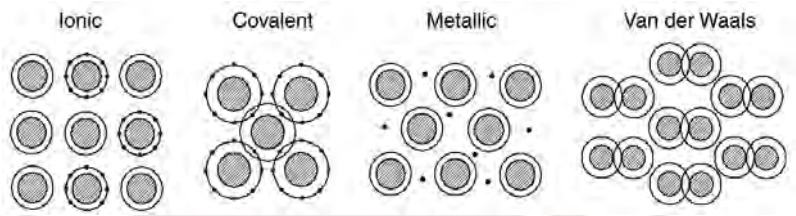

Figure 1.16: Principal bonding interactions (ref [1])

Covalent bond: Bond between neutral atoms, whose electrons overlap (ref [1]).

Ionic or electrostatic bond: Originated when one or more electrons are moved from one atom to another, which forms negative and positive ions (ref [9]). Some material combinations, commonly nonconductive materials, have a "triboelectrical effect" originated when they are electrically charged under frictional load (ref [9]). After loading, discharges of this static electricity may occur leading to a collapse of this static charges and thus to not a permanent adhesion (ref [9]).

Metallic bond: It is the result of the attraction between the periodic structure of positive ions and the sea of valence electrons (ref [9]). In metals, the delocalized electrons, i.e. valence electrons that are free to flow through the entire metal, not bound to any particular atom in the solid, form a sea of electrons or an electron cloud (ref [9]).

Van der Waals bond: It is weaker than the three bonds shown before and appears as dipole-dipole interactions, for polar molecules in contact, or as the interaction of fluctuating dipoles in the individual atoms, in case of nonpolar molecules (ref [9]).

The repeated process of formation and fracture of adhesive bonds is considered as friction (ref [1]). In Figure 1.17, the site where fracture appeared is shown: whether the interfacial bonding is stronger than the cohesive strength (atomic bonding forces associated within a material) (ref [9]) of the weaker material, so this material is fractured and the material transfer happens; on the contrary, fracture occurs at the interface (ref [1]).

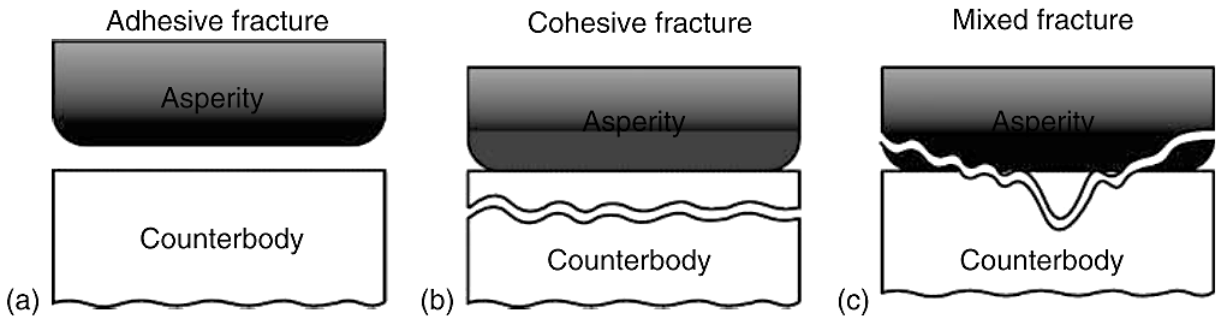

Figure 1.17: Forms of fracture by cause of adhesion: (a) adhesive fracture, (b) cohesive fracture and (c) mixed fracture (ref [1]).

Deformation

During the relative sliding of two surfaces in contact two types of interactions, shown in Figure 1.18, arise. They are described by Bhushan (ref [9]) as follows: *"The microscopic interaction where primarily plastic deformation and displacement of the interlocking surface asperities are required, and the more macroscopic interaction where the asperities of the harder material either plow grooves in the surface of the softer one via plastic deformation or result in fracture, tearing or fragmentation."*. The coefficient of friction μ_d governs the commencement of sliding (ref [9]).

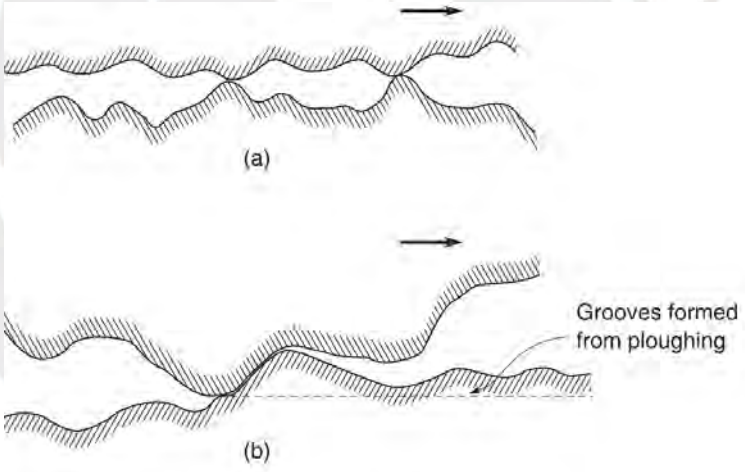

Figure 1.18: Interactions between the surfaces in contact: (a) asperity interaction, (b) macroscopic interplay during sliding (ref [9]).

1.1.1.6 Wear

Wear is defined as the surface wound of material belonging to one of both surfaces during sliding, rolling or impact relative motion between them (ref [9]). It is measured by the wear rate, which can be expressed such as (ref [1]):

- Volume of material removed per any of the followings units: time, sliding distance, revolution of a component or oscillation of a body.
- Loss of volume per unit normal force at unit sliding distance (mm^3/Nm).
- Mass loss per unit time.
- Variation in a certain dimension per unit time.
- Relative change in dimension or volume respect to the same changes in another substance.

a) Stages of wear

As wear increases over time, it is displayed on the graph as a function of time (ref [1]). In Figure 1.19, the three main phases or stages that occur in the wear process are shown. Stage I is the beginning of wear, is the shortest in duration and it is characterized by the erratic state of the tribosystem with a high wear rate that progressively drops (ref [1]). Stage II is longer than the previous one and is outlined by stable conditions of friction and a low wear rate, almost constant. In stage III the rate increases rapidly causing a disastrous wear (ref [1]).

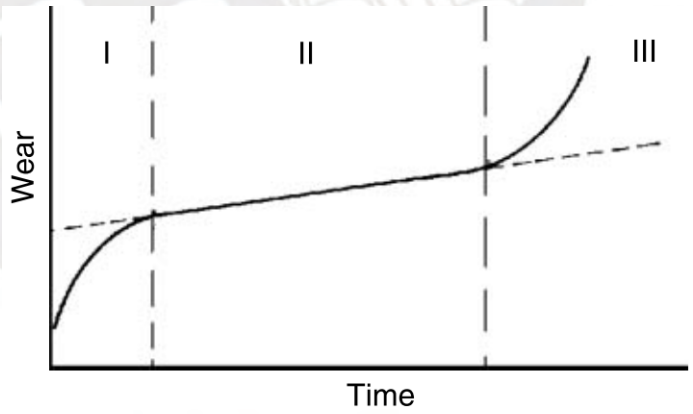

Figure 1.19: Usual phases of wear process (ref [1]).

b) Classes of wear mechanisms

The principal types of mechanisms are the following: adhesive, abrasive, fatigue, impact by erosion and percussion and chemical or corrosive (ref [9]).

Adhesive wear: Its main mechanism is adhesion, which is an important component of friction, as explained above. Hence, it emerges in the same way as adhesion friction (formation, progress and fracture) (ref [1]). The adhesion appears at the asperity contacts sheared by the sliding movement between surfaces leading to a disengagement of a fragment from one surface and attachment to the other surface (ref [9]).

Abrasive wear: It happens when asperities of a rough, hard surface or hard particles slide on the surface of a softer material damaging the interface by plastic deformation or fracture. The two general situations are shown in Figure 1.20.

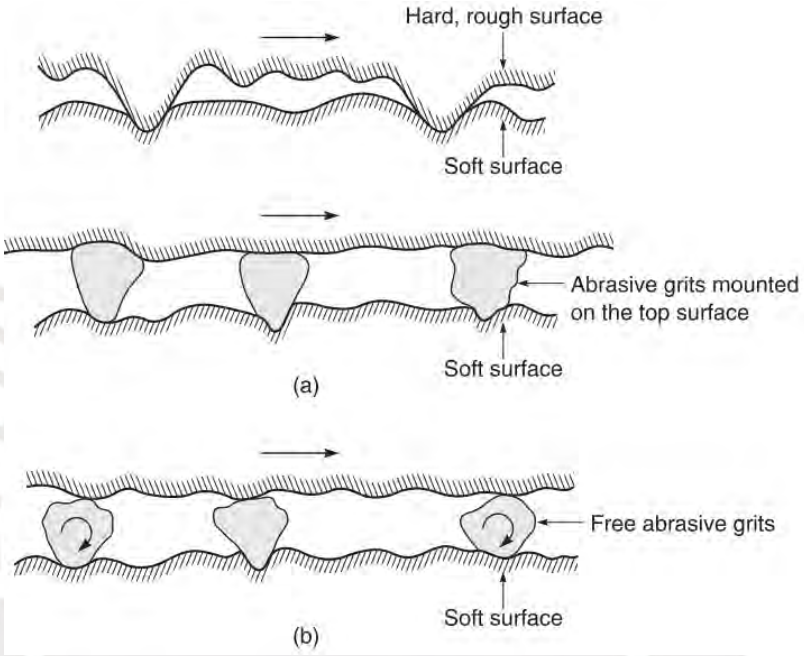

Figure 1.20: Representation of the two general situations: (a) a rough hard surface with abrasive grits sliding on a softer surface, (b) free abrasive grits between surfaces (one softer than the other) (ref [9]).

Impact wear: It is divided in erosive, caused by streams of solid particles, liquid droplets or bubbles implosions; and percussion wear, originated by repetitive solid body impacts (ref [9]).

The solid particle erosion arises when solid particles collide with a surface at high velocity (see Figure 1.21) (ref [9]). Although it is a kind of abrasion, it is treated in another way due to the contact stress that arises from the kinetic energy of the particles, which is dependent on the particle velocity, impact angle and size of particle (ref [9]).

Furthermore, the liquid impingement erosion happens when small drops of liquid hit hard at high velocities (at least 300 $\frac{\mathrm{m}}{\mathrm{s}}$) the surface of a solid leading to high pressures higher than the yield strength of a material (ref [9]). Other kind of erosion occurs

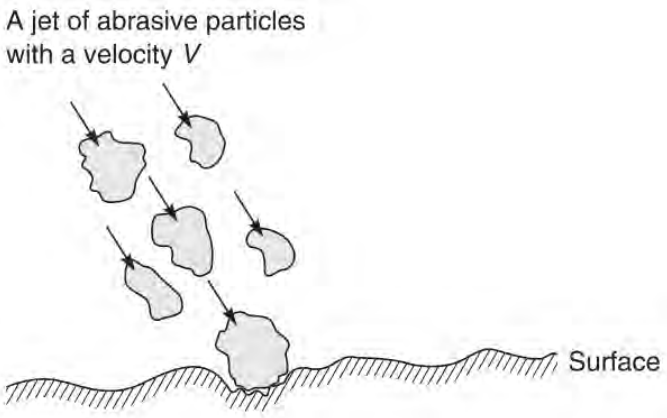

Figure 1.21: Representation of a jet of abrasive particles colliding a surface (ref [9]).

when a cavitation process appears, which is generated by the implosion of bubbles of a liquid, in relative motion with a solid, against the surface of the solid (ref [9]). The energy generated by the impact is absorbed by the solid as elastic deformation, plastic deformation or fracture (ref [9]). This type of erosion is known as cavitation erosion.

On the other hand, percussion erosion emerges under the application of repetitive solid impact on a surface. It involves several of the following mechanisms: adhesive, abrasive, surface fatigue, fracture and tribochemical wear.

Chemical wear: It arises during the sliding in a corrosive environment (ref [9]). Although oxides particles, in the absence of sliding, tend to reduce the oxidation process, the sliding action rub the layer, formed by those particles, thus the chemical attack can advance (ref [9]). Furthermore, according to Braunovic (ref [1]), the chemical wear hinges on the following factors :*"chemical composition and microstructures of the contact surfaces; rigidity and porosity of the contact surfaces, pressure or absence of surface cracks and grain boundaries; degree to which the contact surface has been work-hardened; state of stress in the surface; electrical potentials and current paths between contacting surfaces; temperature and pressure in the contact zone; and the reactivity of the medium interposed between contact surfaces."*

Fatigue wear: It is characterized by the generation and development of cracks and appears when stress is applied cyclically causing a change in the material state (ref [1]). This change is caused by the emerge of two varying stress fields of different strengths in the surface and subsurface regions (ref [1]).

c) Methods to test wear and friction

Typical friction and sliding wear test geometries are shown in Figure 1.22 and are explainedn below (ref [9]):

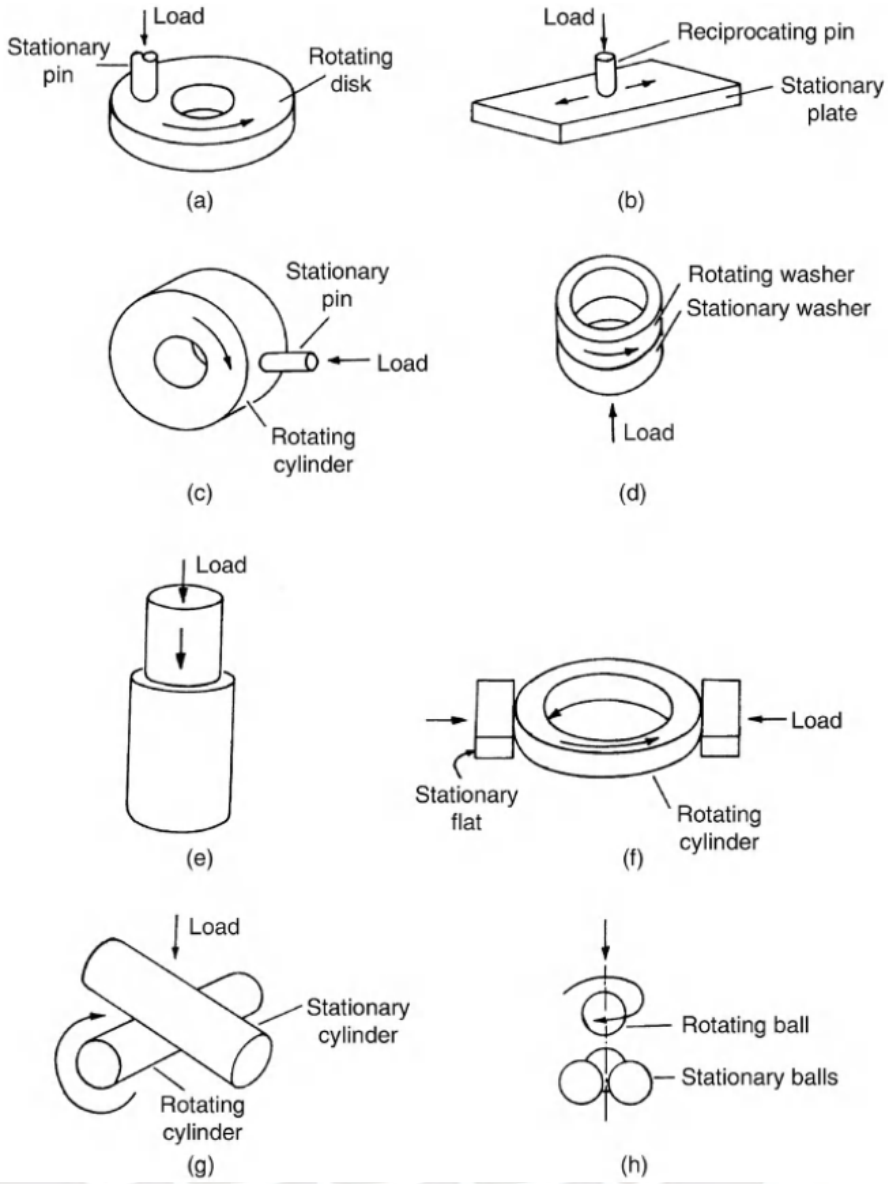

Figure 1.22: Schematic representations of methods to test wear.“a” is Pin-on-disk method, “b” is Pin-on-flat method, “c” is Pin-on-cylinder method, “d” is Thrust washers method, “e” is Pin-into-bushing method, “f” is Rectangular flats on a rotating cylinder method, “g” is Crossed cylinders method and “h” is four ball method (ref [9]).

- Pin-on-disk (face loaded): The pin (a nonrotating ball, a hemispherical tipper ride, a flat-ended cylinder or a rectangular parallelepiped) remains stationary while the disk rotates.
- Pin-on-flat (reciprocating): The pin remains stationary while a flat moves in a reciprocating motion and in some cases the opposite occurs.
- Pin-on-cylinder (edge loaded): It is similar to the pin-on-disk, but in this case the pin is perpendicular to the axis of rotation or oscillation.

- Thrust washers (face loaded): It involves the use of two washers: one stationary and the other rotates or oscillates on the face of the previous one.
- Pin-into-bushing (edge loaded): In this method, a pin applies a normal or axial force on the surface of a bushing generating a radial force, which tends to expand the bushing. The coefficient of friction is calculated by dividing the axial force with the radial force.
- Rectangular flats on a rotating cylinder (edge loaded): Two rectangular flats are loaded perpendicular to the axis of rotation of the disk: one is stationary and the other applies the load.
- Crossed cylinders: It consists of two cylinders, one stationary and the other rotating, at an angle of 90°.
- Four ball: It consists of four balls distributed in an equilateral tetrahedron form. The upper ball rotates and wears the other three fixed balls.

The details of the previous test are explained in Table 1.1 and the comparison of the most common wear test methods, in Table 1.2.

Table 1.1: Details of test for friction and wear. Extracted from ref [9].

Geometry	**Type of contact**	**Type of motion**
1. Pin-on-disk (face loaded)	Point/conformal	Unidirectional sliding, oscillating
2. Pin-on-disk (reciprocating)	Point/conformal	Reciprocating sliding, oscillating
3. Pin-on-cylinder (edge loaded)	Point/conformal	Unidirectional sliding, oscillating
4. Thrust washers (face loaded)	Conformal	Unidirectional sliding, oscillating
5. Pin-into-bushing	Conformal	Unidirectional sliding, oscillating
6. Flat-on-cylinder (edge loaded)	Line	Unidirectional sliding, oscillating
7. Crossed cylinders	Elliptical	Unidirectional sliding, oscillating
8. Four balls	Point	Unidirectional sliding

Table 1.2: Comparison of wear test methods. Extracted from ref [12].

Test	Advantages	Disadvantages
Pin-on-Disk	After run-in, surface pressure remains constant. Easy to determine wear volume and wear rate. The model closely simulates a linear friction bearing.	If the pin does not stand perfectly vertical on the plate, edge contact results. A very long run-in time is therefore necessary. The front edge of the pin can skim off lubricant. This makes a defined lubrication state impossible.
Ball-on-Disk	High surface pressures are possible. The ball skims off lubricant less than a pin does. The model is similar to a linear friction bearing and a radial friction bearing.	Very small contact ratio: The contact surface of the ball is small compared to the sliding track on the disk. The contact area is enlarged by wear. Difficult to determine the wear volume of the ball.
Block-on-disc	The model is capable of simulating a variety of harsh field conditions, e.g., high temperature, high speed, and high loading pressure.	

1.1.1.7 Lubrication

Lubrication is the process employed to reduce friction, wear and heating of machine parts that are in relative motion (ref [13]). The lubricant is a substance inserted between the surfaces that encompasses two types: solid lubrication and fluid film lubrication (ref [9]).

The regimes of lubrication are the following:

- **Hydrostatic lubrication**: It occurs when the surfaces are separated with a thick film of lubricant, which is applied at high pressure into the load-bearing area (ref [13]). Hydrostatic bearings are used in cases with little or no relative motion (ref [9]).
- **Hydrodynamic lubrication**: The surfaces are separated by a nearly thick film of lubricant, which pressure is generated by the movement of the surface itself. this pressure impulses the lubricant between in a shape of a wedge at high velocity required to create the pressure needed to separate the surfaces (ref [13]).
- **Elastohydrodynamic lubrication**: It occurs when the hydrodynamic pressure of the lubricant is so high that deforms elastically the surface asperities (ref [14]).
- **Mixed lubrication**: It appears in the transition between the hydrodynamic/elastohydrodynamic and boundary lubrication regimes (ref [9]).
- **Boundary lubrication**: It happens when the highest asperities of the surfaces may be separated by a very thin lubricant film only several molecular dimensions

(ref [13]). The principal causes are higher bearing loads, lower speeds, insufficient surface area, a decrease in the velocity of the moving surface, a dropping in the amount of lubricant or a decrease in viscosity of the lubricant due to a rise of temperature (ref [13]).

The regimes exposed above can be seen in the Stribeck curve (Figure 1.23), which show the variation of the friction coefficient versus the lubricant film thickness ratio (λ).

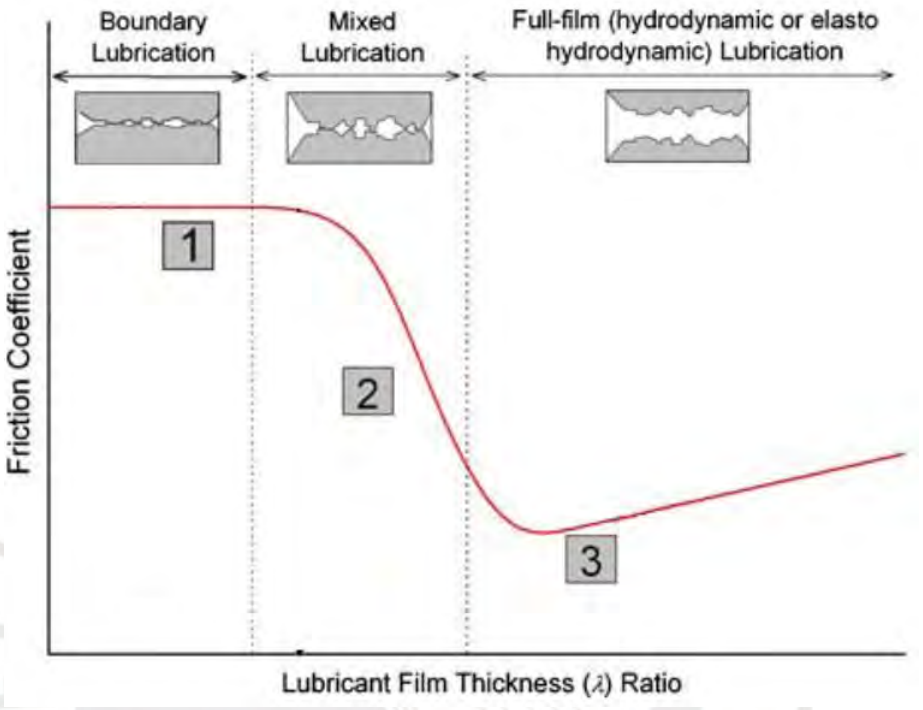

Figure 1.23: Lubrication regimes in the Stribeck diagram (ref [15])

.

It is calculated as film thickness (h) divided by the mean roughness of the surfaces (σ_1 and σ_2) (ref [15]).

$$\lambda = \frac{h}{\sqrt{\sigma_1^2 + \sigma_2^2}} \tag{1.36}$$

1.1.2 Electrical resistivity

The electrical resistivity is a material property that describes the opposition against a current flow. In solids, the knowledge and the understanding of this electrical property can be calculated by considering several factors, specially the type of material (ref [16]).

In the analysis of micro and nano structures is necessary to include the calculation of conduction electron scattering based on some model of the structure. In the presence of a current flow the electrons carry the energy generating chaotic movements inside the material. Atomic and magnetic disorder, strain, and the band structure effects can be altered (ref [17]).

The electrical resistivity in pure metals has a large amount of reliable experimental data over a wide temperature range, which allow to calculate it mathematically. In dilute alloys, composed of a base metal and a second metal in a lower percentage, resistivity can often be assessed using mathematical equations. However, when the base metal is ferromagnetic, the result cannot be calculated using the same method. In concentrated alloys, there are many factors that influence the resistivity including the atomic and magnetic long range order, changes in crystal structure as the composition and the temperature vary, and the concurrence of two or more phases (ref [16]).

1.1.3 Methods of electrical resistivity measure in thin films

The elementary and most widely used method is the four probe method. This method is specially used in metals and alloys, furthermore a variant of this method is used for semiconductor wafers (Van der Pauw method). However, this technique requires contact points on the sample, making it ineffective for brittle or chemically reactive materials. In this cases, non-invasive methods, such as those based on induced eddy currents, are employed (ref [16]).

1.1.3.1 Four probe methods

This method involves two current contacts and two voltage contacts attached to the sample. First, a current flow i s generated in the sample, and the voltage v is measured using the two voltage contact. Also the cross-area a of the sample and the distance l between this two current contacts must be known. The electrical resistivity is calculated with the next equation (ref [16]), (ref [17]):

$$\rho = \frac{va}{il} \tag{1.37}$$

Some conditions must be checked to improve the results in Van der Pauw method. These are the followings conditions(ref [18]):

a) The sample must have a flat shape of uniform thickness.

b) The sample must not have any isolated holes.

c) The sample must be homogeneous and isotropic.

d) All four contacts must be located at the edges of the sample.

e) The area of contact of any individual contact should be at least an order of magnitude smaller than the area of the entire sample.

Examples about recommend positions for the contacts are shown in Figure 1.24.

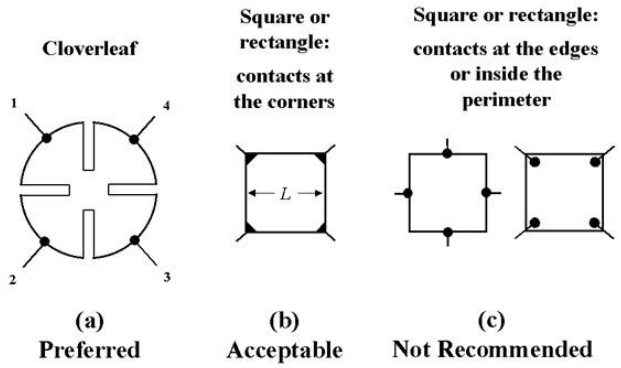

Figure 1.24: Suggested positions for Van der Pauw method. Based on ref [18].

1.1.3.2 Eddy current methods

There are many methods based on induced eddy current. One of the fundamental methods involves using a periodic magnetic field (for example, a sinusoidal) where the field exhibits a step function that abruptly changes from zero to a constant value in the sample. Same result will be achieved if the function changes from a constant to zero (ref [16]). Nevertheless, these methods have low accuracy and can sometimes yield erroneous results. The following considerations are employed to reduce the error:

a) The eddy currents are not uniformly distributed throughout the sample when the period magnetic field is applied. Therefore, selecting an appropriate frequency will solve the issue.

b) If the sample generates magneto-resistance due to the motion of the electrons within itself, the data could be misleading. In this case, the solution is to use a coil around the entire sample to induce the eddy currents and employ circuit capable of de-energizing the coil. The flux change will be detected by a secondary coil (ref [16]).

1.1.3.3 Four wire resistance method

The Kelvin resistance measurement method is similar to the four probe method. Nevertheless, the special configuration of the connection between the multimeters and the sample ensures an accurate resistance measurements for low values of electrical resistance (equal or less than 100 Ohms ref [19]). Although this method could also be used

with two wires, noise in the wires during recording can affect the measurement if the values are in millivolts or milliamperes. The configuration used is shown in the Figure 1.25 and this configuration is used in the present thesis.

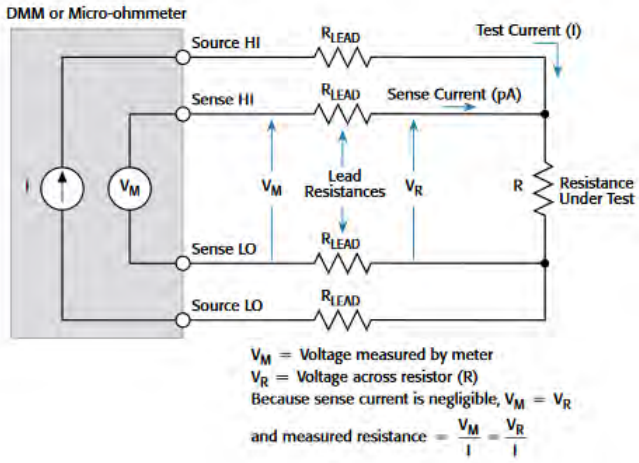

Figure 1.25: Four-wire resistance measurement configuration. Extracted from ref [19].

1.2 Devices and previous research

1.2.1 Tribometer

The tribometer is based on the pin-on-disc method, mounted in an oscillating module, to perform the tribological test also known as pin-on-flat, using a spherical pin. This method is described in the section 1.1.1.6 subsection c. Besides, it has two main parts: the header (Basalt® MUST 2D-FM 1N) and the base unit (Basalt® MUST LMS20) (ref [20]), which can be seen in Figure 1.26 and Figure 1.27. The technical specifications of basalt are presented in Table 1.3 (ref [20]).

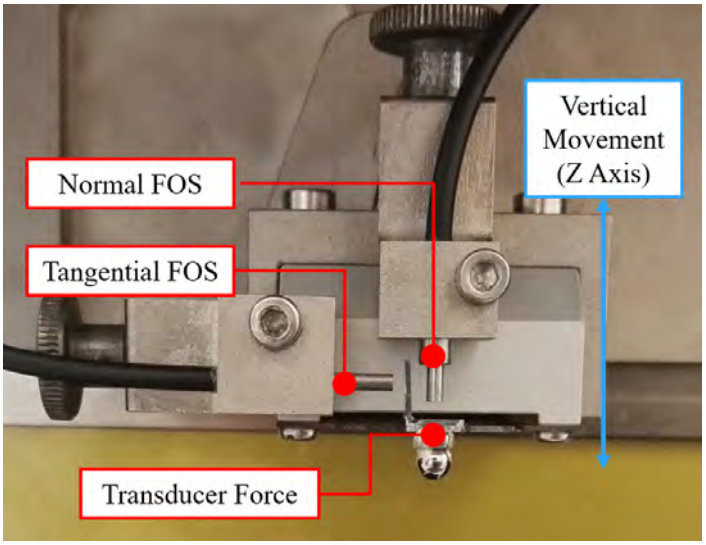

Figure 1.26: The header of the tribometer, which performs the vertical movement and includes the fiber optic sensors (FOS) as well as the transducer force.

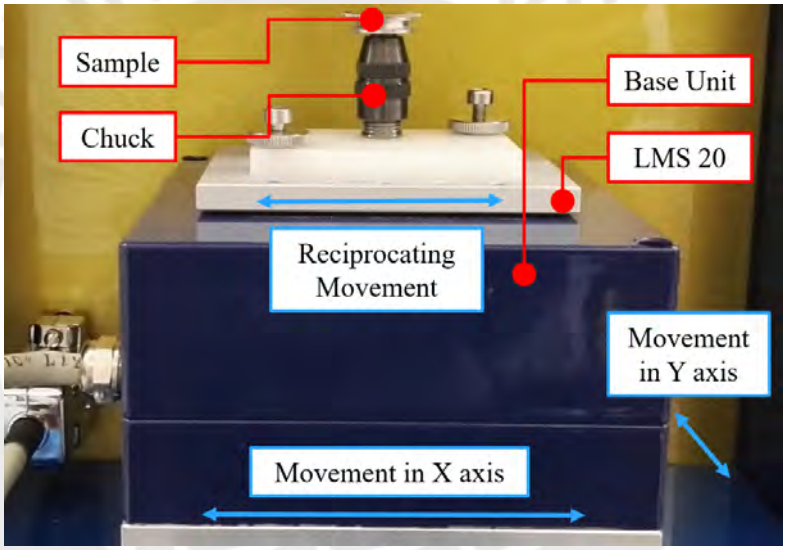

Figure 1.27: The base unit of the tribometer, which performs the movements in X and Y axis. It contains the LMS 20, which performs a reciprocating movement during the test, and the chuck, where the material is placed to be tested.

Table 1.3: Basalt Technical Specifications (ref [20])

X-Y positioning unit	drive type	stepper motor driven threaded spindle
	positioning range	20 mm x 20 mm
	positioning resolution	1 μm
	positioning accuracy	20 μm
	blocking force	>30 N
	maximum speed	2 mm/s
Z positioning unit	drive type	stepper motor driven threaded spindle
	positioning range	50 mm
	positioning resolution	1 μm
	positioning accuracy	20 μm
	blocking force	>30 N
	maximum speed	2 mm/s
Z fine positioning	drive type	piezo stack
	positioning range	40 μm (approx.)
	positioning resolution	0.25 μm
	positioning accuracy	1 μm
	blocking force	>30 N
	position measurement	Optical incremental encoder with a resolution of 50 nm
Control unit	embedded Linux PC	
Power supply	12 V DC, 8 A	
Housing dimensions	204 mm x 356 mm x 259 mm (W x H x D)	

The transducer force is composed by a cantilever with one bending element (spring) which deform itself in two directions: normal and tangential. The cantilever has two mirrors located in front of two fiber optic sensors (FOS), one is located on the normal axis and the second on the tangential axis. These sensors use laser to detect when the mirror attached to the cantilever approaches them. The sensor converts this information into a voltage differential. Then, the voltage read by these sensors are converted into a displacement equivalent (millimetres) of the cantilever on normal axis (d_n) and tangential axis (d_t). Next, the tribometer multiplies the displacement

values by the cantilever constants (Newtons/millimetres) in normal axis (Spr_n) and tangential axis (Spr_t). With these values, the forces are calculated by multiplying the deformation with the spring constant, i.e. the tangential force (F_t) and the normal force (F_n) are proportional to the spring constant for each direction.

$$F_n = d_n Spr_n \tag{1.38}$$

$$F_t = d_t Spr_t \tag{1.39}$$

Finally, the coefficient of friction (COF)(μ) is obtained by dividing the normal force between the tangential force. The main parts of the cantilever and the tangential and normal directions can be seen in Figure 1.28.

$$mu = \frac{F_n}{F_t} \tag{1.40}$$

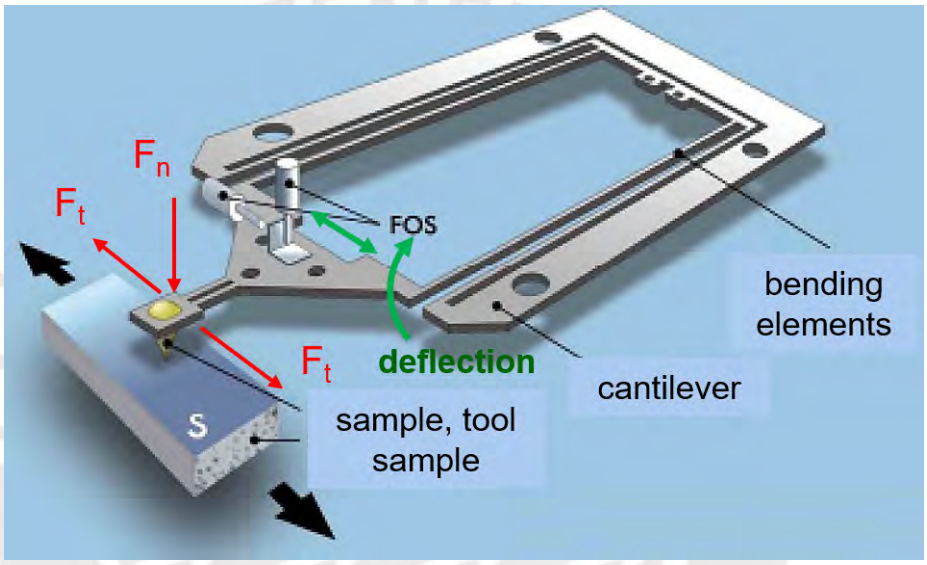

Figure 1.28: Principle elements of the cantilever located in the Basalt® MUST 2D-FM 1N. The normal direction is perpendicular to the reciprocating movement of the sample, whereas the tangential direction goes along this movement. Adapted from ref [20].

1.2.2 Keithley modules

The modules KEITHLEY Model 2400 Series Source Meter ® and the two KEITHLEY Model 2000 Multimeter were used to generate an analogue current (mA) and to acquire the analogue voltage (mV) and current (uA). Furthermore, these devices can communicate with any computer via Ethernet or GPIB (ref [3] and ref [4]). The modules can be seen in Figure 1.29 and Figure 1.30. (ref [3])

Figure 1.29: The frontal panel of the Sourcemeter Model 2400. Adapted from ref [4].

Figure 1.30: The frontal panel of the Multimeter Model 2000. Adapted from ref [3].

Also, a similar method to the four point probe measurement method (four wire sensing) was used to record the voltage and the current of the sample during the experiment. This method was employed to use higher current values than commercially available tribometers. Communication between the Keithley modules and the computer was carried by GPIB bus communication. The electrical connection diagram between the Keithley modules and the sample is shown in the Figure 1.31.

1.2.3 Previous program and Graphic user interface

In the previous work, a triboelectrical workstation was implemented, which used a tribometer and the same Keithley modules described earlier (ref [5]). The tribometer and the Keithley modules were connected to a computer and were controlled by a LabVIEW program. The tribological and the electrical properties were not stored in the same program, therefore the data was recorded by two differents programs in different experiments (ref [5]). Additionally, each program had a graphical user interface (GUI) to guide the user in data collection.. The graphical user interface used for the previous tribological section can be seen in Figure 1.32 and in Figure 1.33. The previous GUI of the electrical part can be seen in Figure 1.34.

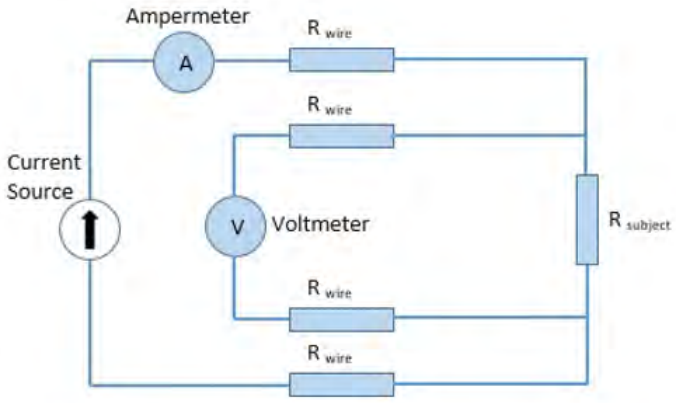

Figure 1.31: Diagram of the four wire sensing method. Extracted from ref [5].

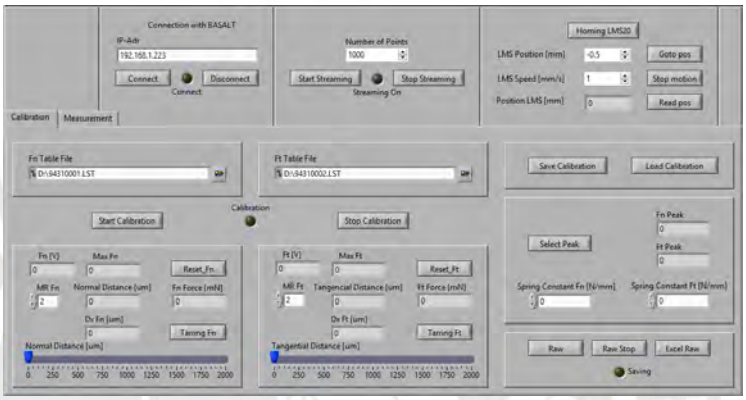

Figure 1.32: Previous user interface of the tribological section in LabVIEW (Calibration tab). Extracted from ref [5].

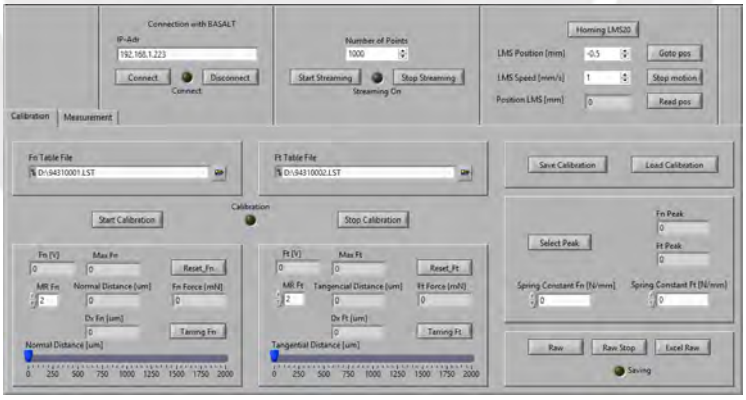

Figure 1.33: Previous user interface of the tribological section in LabVIEW (testing tab). Extracted from ref [5].

In the tribological GUI, the main objective was to obtain the coefficient of friction (COF) of the sample. The results obtained by this program are shown in the Figure 1.35 and Figure 1.36.

Figure 1.34: Previous user interface of the electrical section in LabVIEW. Extracted from ref [5].

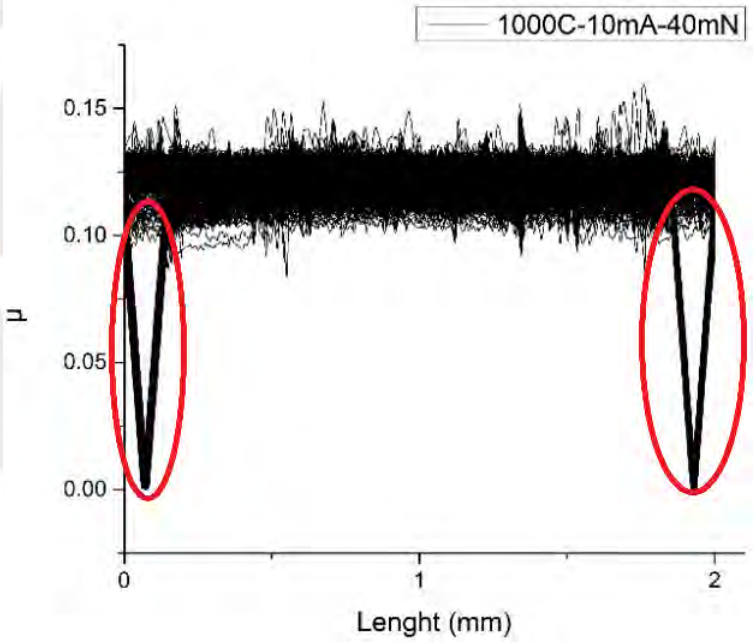

Figure 1.35: Coefficient of friction for each half cycle obtained with the previous program. The valleys, located at the beginning and at the end of each half cycle surrounded by a red circle, represent the data stored during the change of direction in the tribological test. Experiment performed at 10 mA during 1000 cycles with a set force of 40 mN conducted by E. Yupanqui (ref [5]).

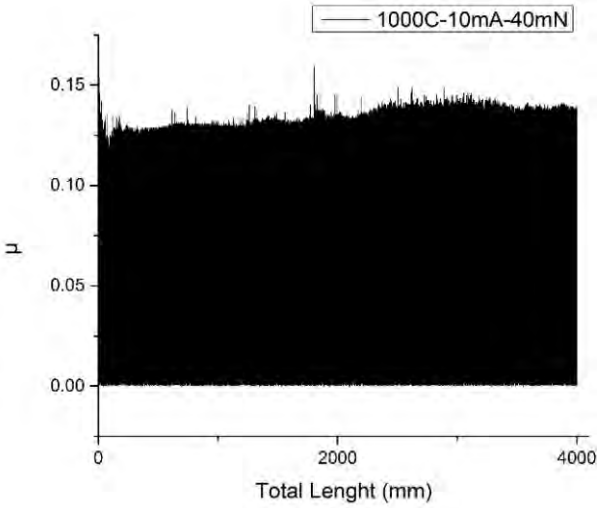

Figure 1.36: Variation of the coefficient of friction along the total length obtained with the previous program. The black spot is caused by the presence of the valleys. Experiment performed at 10 mA during 1000 cycles for a set force of 40 mN conducted by E. Yupanqui (ref [5]).

As shown in Figure 1.35 the valleys delimited by a red circle represent the data recorded during the direction change in the tribological test. The data recorded in these borders provide useful information about the COF. In the Figure 1.36 the effect of the valleys creates more issues because they give the illusion that the value of the COF value throughout the test is between 0 and 0.16 when the useful data is actually between 0.14 and 0.16.
Additionally, the normal force set in the program differs from the values recorded by the sensors after the tribological test. In the Figure 1.37 the desired normal force was 40 mN, while the normal force ranged from 40.3 mN and 40.8 mN. This program needs to be improved to achieve the desired normal force during the tribological test.

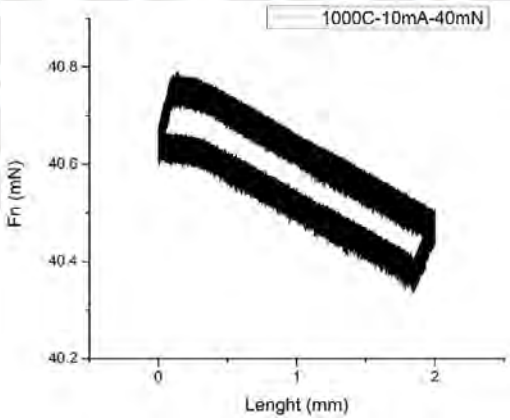

Figure 1.37: Normal force for each half cycle obtained with previous GUI. Experiment performed at 10 mA during 1000 cycles for a set force of 40 mN conducted by E. Yupanqui (ref [5]).

On the other hand, the main objective of the electrical program was to analyse the

electrical resistance of the test material throughout the entire test. The electrical resistance was calculated by dividing the voltage by the current. The voltage and the current were recorded with multimeters. The results obtained for this program are shown in the Figure 1.38, Figure 1.39 and Figure 1.40.

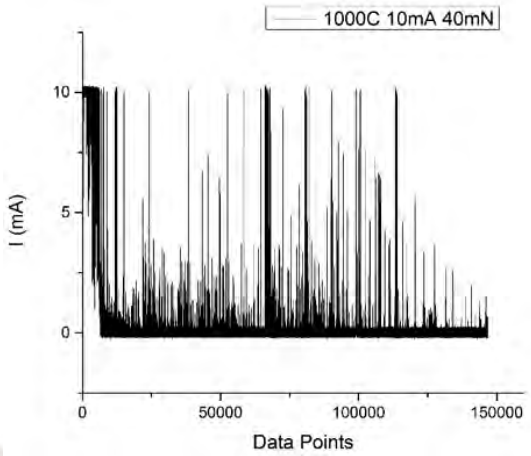

Figure 1.38: Current registered over all the test. Many values are close to zero, this means the presence of some mistake during the test or the program. Experiment performed at 10 mA during 1000 cycles for a set force of 40 mN conducted by E. Yupanqui (ref [5]).

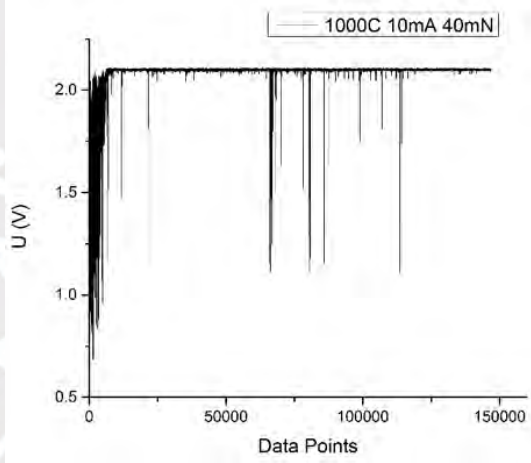

Figure 1.39: Voltage resistance registered over all the test. Many values are constant when the current values where close to zero, this means the presence of some mistake during the test or the program. Experiment performed at 10 mA during 1000 cycles for a set force of 40 mN conducted by E. Yupanqui (ref [5]).

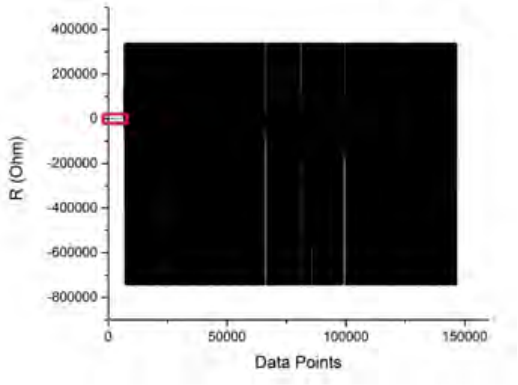

Figure 1.40: Electrical resistance registered over all the test. Only the red squard market show the behavior of the electrical resistence during the firsts cycles. Experiment performed at 10 mA during 1000 cycles for a set force of 40 mN conducted by E. Yupanqui (ref [5]).

As seen in Figure 1.38, the current values are acceptable at first. However, after some time, some the values drop to zero. The cause could be the lost of contact between the spherical indenter and the sample. Therefore, the current should not flow between the two objects and a voltage differential should be generated between them. This hypothesis is supported by the Figure 1.39 where the voltage values were high after a short time. Therefore, the electrical resistance values in the Figure 1.40 were not useful data to analyse actual electrical resistance of the sample during the test. The solution to this inconvenient is to ensure the contact between both objects throughout the entire test. In summary, two LabVIEW programs were developed for the analysis of thin films. The first program controlled the tribometer and recorded its tribological properties, with the tribometer being connected to an external computer via Ethernet. The second program managed the Keithley modules and recorded their electrical properties. All three devices were interfaced with the external computer via GPIB, using a USB-to-GPIB adapter for parallel communication (ref [5]). However, the USB-to-GPIB adapter requires that all Keithley modules be connected prior to data transmission, which introduces a limitation for real-time data acquisition. Specifically, the adapter waits for the data transfer from one module to be completed before proceeding to the next, making it unsuitable for applications requiring continuous data collection (ref [18]).

1.2.4 Experimental results on thin films

To validate the results obtained in this thesis, a review of previous experiments conducted on thin films was carried out. The article titled Tribological behavior of selected Mn + 1AXn phase thin films on silicon substrates by Hopfeld was chosen as the primary source for comparing experimental results and verifying the accuracy of the experiments conducted in this work. This study focuses on the tribological behavior of thin films of Ti_3SiC_2, Ti_2AlN, and Cr_2AlC phases, deposited by magnetron sputtering of elemental multilayers and rapid thermal annealing synthesis. The results

reveal that the tribological behavior of these MAX phases against a reference bearing steel 1.3505 shows an adhesive wear mechanism for Cr_2AlC and Ti_2AlN, with friction coefficients in the range of 0.30 to 0.70 and 0.15 to 0.50, respectively. The best friction and wear performance was observed for Ti_3SiC_2, with a friction coefficient in the range of 0.15 to 0.25. Furthermore, hypotheses regarding the wear mechanisms of all MAX phases analyzed are formulated. The following figures presents the tribological results for the Cr_2AlC material, with the first figure showing the initial data and the second illustrating how these results change with a temperature variation. Figure 1.41 displays the tribological analysis of the Cr_2AlC material. Different traces are marked by the corresponding colored numbers. The experiments were conducted under two distinct velocities (0.05 mm/s and 0.08 mm/s) and two different loads (50 mN and 125 mN). These parameters allow for a detailed assessment of the material's behavior under various conditions. Figure 1.42 shows the same tribological analysis of Cr_2AlC, but this time under elevated temperature conditions. This figure emphasizes how the material's friction and wear characteristics evolve as a result of increased temperature. These results will be compared with the experiments conducted in this thesis to assess the consistency and validity of the obtained data. (ref [27])

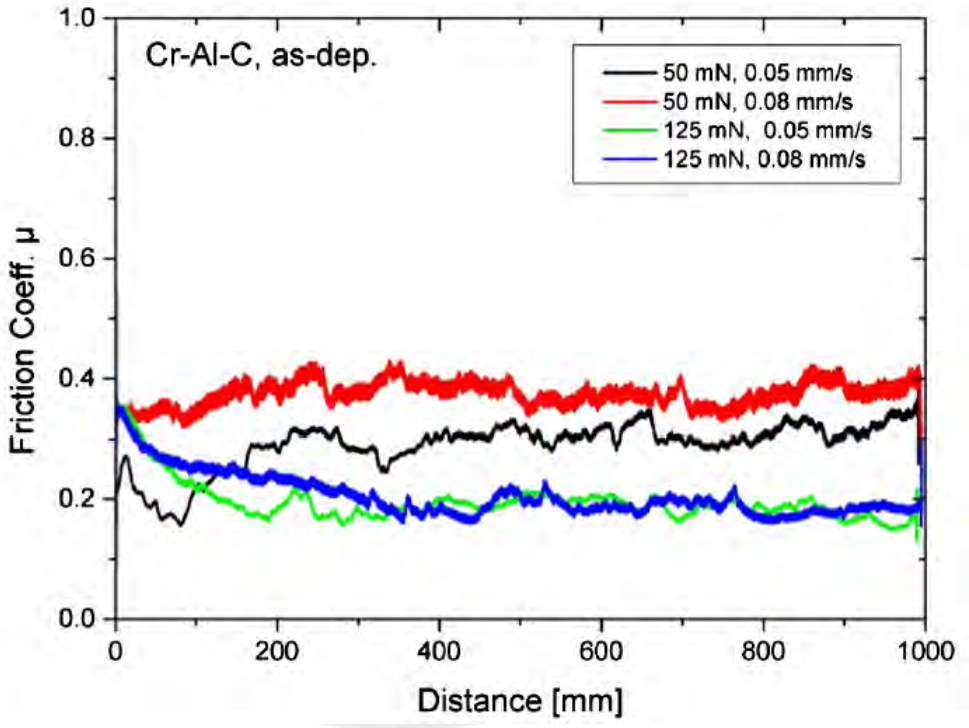

Figure 1.41: Evolution of the friction coefficient. Extracted from Hopfeld (ref [27]).

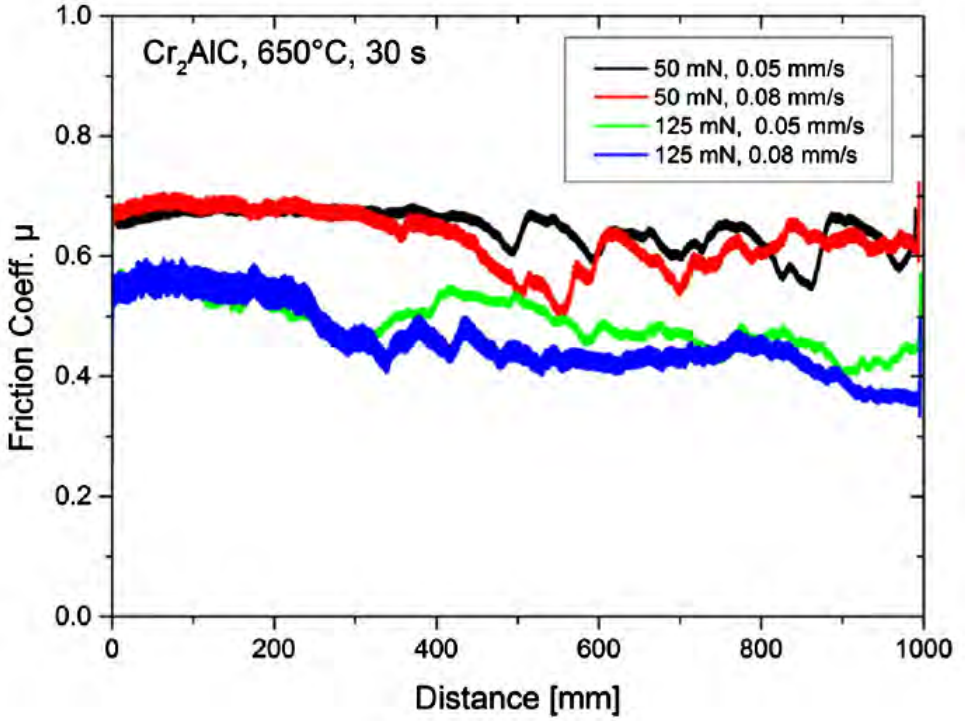

Figure 1.42: Evolution of the friction coefficient with 650°C. Extracted from Hopfeld (ref [27]).

CHAPTER 2

Process of development of the triboelectrical workstation

2.1 System Requirements

The system designed for this work consists of a tribological station to obtain the coefficient of friction, and Keithley modules used to analyze the electrical data of the sample. All of this is controlled by a LabVIEW program running on a portable workstation. Communication between the workstation and the tribological station is performed via Ethernet, while communication of the workstation with the Keithley modules is carried out through GPIB (at a speed of 1.5 Mbytes/s using the KUSB-488B) and RS232 serial (at 19200 baud). In this system, the sampling frequency is defined by the tribological station. Typically, the slowest component of the system dictates the sampling frequency (in this case, the serial communication at 19200 bps); however, software adjustments were made to interpolate current and voltage values. This way, data were acquired at the sampling rate of the tribological station. The tribological test employs 202 working cycles, of which the first two are excluded from the calculations since the experiment requires time to stabilize. Therefore, data from 200 cycles are recorded, with 1000 samples per cycle and a total distance traveled of 1000 millimeters. At the beginning of the experiment, both the tribometer speed and the applied normal force are defined. The resolution of the electrical data depends on the Keithley modules used in the system. For instance, the Model 2000 can measure voltages ranging from 0.1 µV to 1000 V (DC) and from 0.1 µV to 750 V RMS (AC). Additionally, it can measure direct current (DCI) from 10 nA to 3 A and alternating current (ACI) from 1 µA to 3 A RMS (ref [4]). To calculate the precision of the coefficient of friction, it is necessary to analyze the minimum forces that the tribometer can register. As explained in previous chapters, forces are calculated based on the minimum movement of the tribometer and the cantilever factor used. Table 1.3 shows that the minimum movement of the

tribometer is 1 µm in both directions. For this system, cantilevers with a normal axis of 1.9086 mN/µm and a spring constant of 4.0283 mN/µm in the tangential axis were employed. Therefore, the precision of the normal and tangential forces is 1.9086 mN in the normal axis and 4.0283 mN in the tangential axis, respectively. The experiments conducted allow for the verification of both the accuracy and precision of the equipment by comparing the obtained results with previous studies conducted on the same material under similar conditions. As a reference, the study by Hopfeld (ref [27]) is used to validate and confirm the reliability of the data obtained in this work.

2.2 Configuration and connection between devices

2.2.1 Physical connection between hardware

One of the objectives of this thesis is to control the tribometer and Keithley modules through a LabVIEW-based interface. To achieve this, a National Instruments (NI) portable workstation was selected to control the system. The portable workstation includes a NI PXI-1042 as a cage and a NI PXI-8105 embedded computer. This workstation is equipped with an Intel®Core™Duo processor T2500 (2.0 Ghz dual core processor), standard input/output interfaces, and a 30 GB hard drive. It also features 10 Mbit, 100 Mbit, or 1000 Mbit Ethernet interfaces, GPIB connector, and an RS232 serial port (ref [21], ref [22]). In summary, the workstation offers a powerful processor and multiple high-speed data transmission ports.
The device uses Windows XP® as a operative system and the LabVIEW 2008 version. The device has a RS-232 serial port, an Ethernet connection, four USB ports and GPIB controller (ref [22]). These ports are necessary for communication with the tribometer (Ethernet port) and the Keithley modules (RS-232 serial port and USB port). One KUSB-488B USB to GPIB adapter is used to connect the KEITHLEY Model 2400 Series Source Meter ® and one of the KEITHLEY Model 2000 Multimeter to the portable NI workstation. The connection diagram of the system is shown in the Figure 2.1.

The KEITHLEY Model 2400 Series Source Meter is configured as a current source, one KEITHLEY Model 2000 Multimeter is configured as a ammeter and the other multimeter is configured as a voltmeter. The current source and the ammeter are connected with the portable NI workstation by the KUSB-488B USB to GPIB adapter with a transfer speed of 1.5 Mbytes/s ([23]) and the voltmeter is connected by the RS-232 serial port at 19200 bauds per second ([24]).
The connections between the sample, the Keithley modules and the tribometer are similar to the previous work (ref [5]). The four-wire resistance method is used to make the electrical connections. The other method mentioned before were not used because the user has access to the sample, and with the four-wire method, the noise in the wires is nullified. In Figure 2.2 and Figure 2.3, the physical connection according to the four-wire resistance measurement configuration is shown in Figure 1.25.

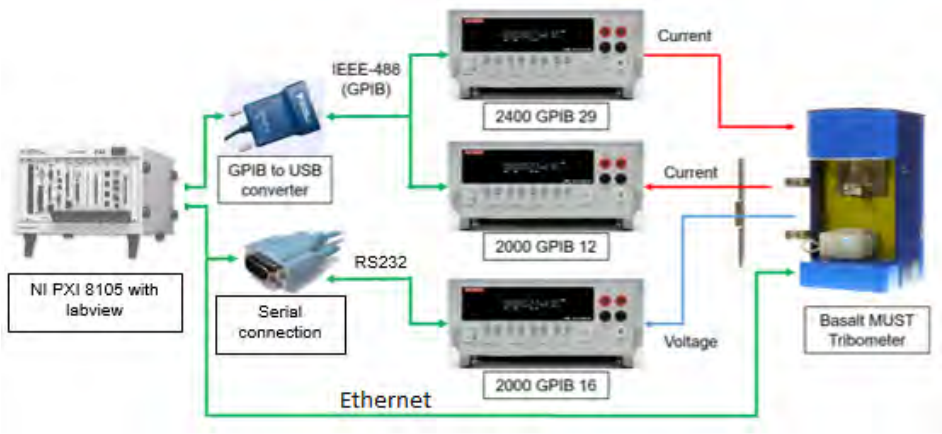

Figure 2.1: Connection diagram of the system. The KEITHLEY Model 2400 Series Source Meter is configured as a current source, one KEITHLEY Model 2000 Multimeter is configured as a ammeter and the other multimeter is configured as a voltmeter.

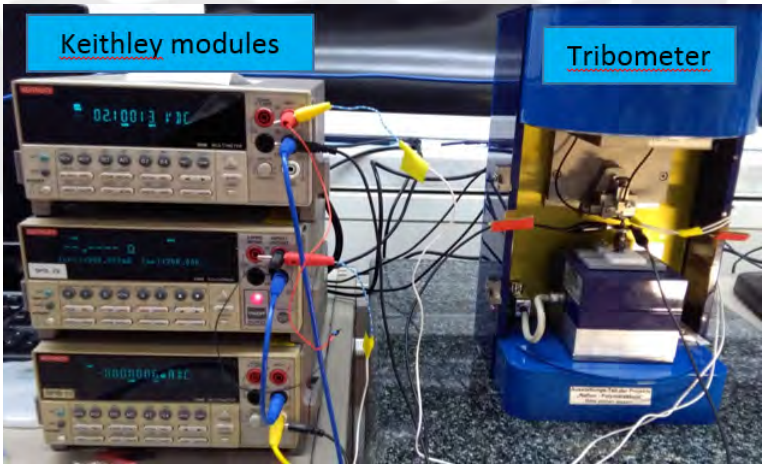

Figure 2.2: Overview of the electrical connections between the tribometer, the sample and the Keithley modules.

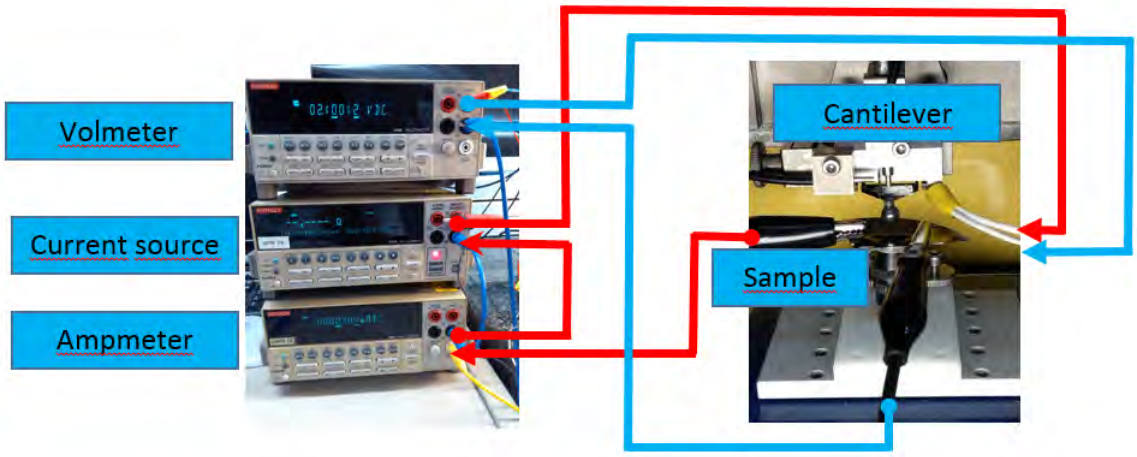

Figure 2.3: Diagram of physical connections between the tribometer, the sample and the Keithley modules based on the four wire resistance method.

2.2.2 Software Configuration

In order to synchronize the tribological experiment with the electrical measurement the following manual configurations were performed in the Keithley modules:

- The KEITHLEY Model 2400 Series Source Meter must be manually configured to remote mode via GPIB bus communication with primary address number 29. (following the indication in ref [4]). It is essential to correctly assign the address number and communication type otherwise the program will not be able to read data from the Keithley modulus.
- The KEITHLEY Model 2000 Multimeter must be manually configured to remote mode via GPIB bus communication with primary address number 16 (follow the indication in ref [3]). It is essential to correctly assign the address number and communication type or the program could not read the information of the Keithley modulus.
- The KEITHLEY Model 2000 Multimeter must be manually configured to remote mode via RS-232 serial communication with a baud rate of 9600, Xon/Xoff flow control, CR terminator, no parity and one stop bit (following the indication in ref [3]). It is important use this configuration as it provides the best range of values (with less noise) and a fast data transmission rate (This was the result of experimentation).

On the other hand, the following manual configurations were performed in the portable NI workstation to ensure the communication:

- The RS-232 serial port on the portable NI workstation must be manually configured with the same values as the voltmeter.
- The KI 488 driver must be installed on the portable NI workstation to use the KUSB-488B USB to GPIB adapter (ref [23]). If the workstation already has one

driver for GPIB bus communication, it must be replaced with the KI 488 driver. Otherwise, the program will not read the data from the GPIB adapter.

- The Ethernet settings must be manually configured for the communication with the tribometer. Use an IP address similar to the tribometer's, but change the last number to generate a second user on the subnet , allowing it to function as both a receiver and transmitter. Additionally, enter the tribometer's IP address as the default gateway. Finally, change the default subnet mask to 255.255.1.0, as the first subnet is used by the USB port (ref [22]).

2.3 Improvement of the Tribology Program and Data

2.3.1 Maintaining constant the normal force during the test

First, the results of normal force obtained from the previous tribological program was analysed. Figure 2.4 shows that for a desired normal force of 40 mN, this value may not be reached during the entire experiment.

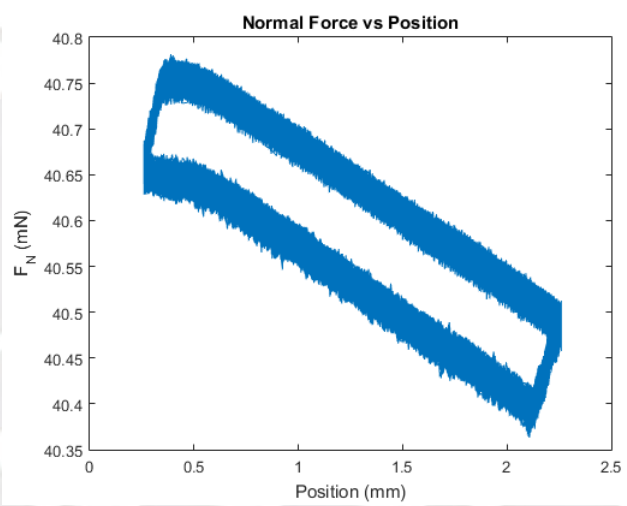

Figure 2.4: Variation of the normal force versus position obtained from the initial program. The normal force measured in the experiment was higher than the desired value (40 mN). Experiment executed at 10 mA, during 100 cycles for a desired normal force of 40 mN conducted by E. Yupanqui (ref [5]).

Possible causes of this behavior are the following:

- The presence of surface irregularities, such as roughness, on the material after manufacturing.
- The sample is attached to the chuck using a special adhesive. This may cause an inclination angle in the sample.
- Noise from the system itself, such as from the tribometer's servomotors.

- An incorrect algorithm in the program for setting the initial normal force, that is, when the sphere comes into contact with the material's surface before starting the experiment.
- Loss of contact with the surface due to deterioration of the sample during the experiment.

The first cause is inherent to the material and therefore cannot be improved through software. The second depends on the user's skill when placing the sample in the tribometer. The third is corrected after data recording. Finally, the fourth and fifth causes were addressed in a previous work as a Project Seminar (ref [25]) and adapted to the new program of this Master's thesis. The new algorithms are explained in the following section.

2.3.1.1 Updated algorithm for setting initial normal force

The program allows the user to set the desired normal force value. Then, the program increases the displacement in z-axis on a constant value of 0.2 mm until normal force read by the cantilever in real time is equal or close to the previously established desired normal force value (ref [5]).

The first algorithm developed in the previous Project Seminar (ref [25]) and improved in this master thesis is shown in Algorithm 1. The position of the Basalt MUST 2D-FM 1N in z-axis is increased or decreased depending on the value of the normal force after each movement. First, the sphere approaches to the sample at 0.2 mm per cycle until the value of the normal force read is less than one-third of the desired force. This value was selected to avoid excessive displacement along the z-axis. Once the force value exceeds this initial limit, the approach is of 0.02 mm per cycle. Finally, the module retracts by 0.001 mm per cycle if the normal force exceeds the range of desired force values. This range is calculated based on the minimum sensor accuracy and is explained in the following section. The values to move the z-axis in the tribometer were calculated based on experiments, the value of spring constant and the limits of the Basalt module (ref [25]).

According to the supplier, the movement precision in the z axis of the module is 20 µm and the minimum movement amount in this axis is 1 µm. The algorithm uses the difference between the current position measured by the sensor and the initial relative position. Hence, the algorithm uses the minimum value that the module can move as a limit to define the minimum force precision recorded by the sensor (F_{mina}). The minimum force accuracy achieved by the sensor is calculated using the minimum motion value of the module (Mov_{min}) and spring value on the normal axis (Spr_n). The value F_{mina} is calculated in the following operation:

$$F_{mina} = Mov_{min} \cdot Spr_n \tag{2.1}$$

The program developed in the present thesis allows the user to employs higher forces to perform the tribological test than the previous through the change of cantilever in the tribometer. As explained previously, the value F_{mina} depends on the Mov_{min} (1 µm

according ref [20]) and the value of Spr_n.

Therefore, the normal force accuracy (F_{nac}) of the algorithm will change depending on the cantilever used to perform the test. The possibles cantilevers had the value of the spring constant in normal axis of 0.043 mN/µm and the value of the spring constant in normal axis of 1.9086 mN/µm. In the following equation the values of F_{mina} that could be used are calculated:

$$F_{nac} = 1\,\mu\text{m} \cdot 0.043\,\text{mN}/\mu\text{m} = 0.043\,\text{mN} \tag{2.2}$$

$$F_{nac} = 1\,\mu\text{m} \cdot 1.9086\,\text{mN}/\mu\text{m} = 1.9086\,\text{mN} \tag{2.3}$$

According to the previous calculation, the normal force accuracy (F_{nac}) of the algorithm chosen is 0.05 mN or 2.00 mN depending on the cantilever installed in the tribometer. The range of acceptable values is based on F_{nac} and the new program calculate this during the calibration of the tribometer (shown in the Appendix 1.1).

The values chosen for the approach in the z-axis were 0.2 mm, 0.02 mm and 0.001 mm respectively. This values were chosen by experimentation in the project seminar (ref [25]). In the new program, the relation of this values with the normal force accuracy is maintained, except the regression value that was chose for tribometer physical limit (1.2). The entire the algorithm was implemented in the event Z Position as it was in the project seminar. The new program place the initial normal force faster and more accurate than the tribological program made in ref [5]. The events of this algorithm in the new program are shown in Appendix 1.2.

Algorithm 1 Increase accuracy to place initial normal force

Requirement: Read the vertical position of the BASALT MUST 2D-FM 1N and adjust the header to achieve the desired normal force (F_{n_d}). This algorithm employs the value of normal force accuracy (F_{nac}).
Guarantee: Obtain normal force values with an accuracy of 0.05 mN(Spring constant in normal axis of the cantilever is 0.043 mN/µm).
Calculate the acceptable limits of the normal force (F_{n_l} and F_{n_h}).
$F_{n_l} = F_{n_d}$ - F_{nac} (mN)
$F_{n_h} = F_{n_d} + F_{nac}$ (mN)
Show the actual vertical position of the BASALT (Pos_z).
Calculate the actual normal force (F_{n_a}) in base of the vertical position read for the sensor FOS in real time ($Dist_s$), the normal spring constant (Spr_n) and the zero normal distance (Z_n) calculated previously in the calibration part.
$F_{n_a} = Spr_n$ (Z_n - $Dist_s$) (mN).
Compare the actual normal force with the acceptable limits of the normal force and change Pos_z.
while end = FALSE **do**
    if $F_{n_a} < F_{n_l}$ **then**
        if $Fn_a < Fn_d/3$ **then**
            $a = 0.2$ (mm)
        else
            $a = 0.02$ (mm)
        end if
        $Pos_z = a + Pos_z$
    else
        if $F_{n_a} > F_{n_h}$ **then**
            $a = 0.001$ (mm)
            $Pos_z = Pos_z$ - a
        else
            end = TRUE
        end if
    end if
end while
Send a completion message.
Execute a new tarring for zero tangential distance.

2.3.1.2 Constant Normal Force Algorithm

As it was mentioned in section 2.3.1, there is a loss of contact surface due to deterioration of the sample during the experiment. The previous work has not developed any algorithm to solve this issue .The second program offers a solution to this problem and was developed in this master thesis, the details can be seen in Algorithm 2. This algorithm compares the normal force value during the tribological test with the previously set desired normal force value. After comparing the values, the algorithm moves the measurement head (spherical indenter) of the tribometer to adjust the normal force.

This algorithm calculates the value of F_{n_ac} and includes a control mechanism to make adjustments on the measurement head of the tribometer based on the value of F_{n_ac}. This operation is necessary because the tribometer can now use different cantilevers, which changes the acceptable range of normal force values. On the other hand, when the user performs the test with a high normal force, contact between the sphere and the sample is maintained. However, the noise increases when the user employs a cantilever with a high spring constant in z axis. Finally, the Algorithm 2 solve these issues.
In the new program, this algorithm is located in the event "Timeout", in the phase of "Testing" outside of the data recording loop as well as in the project seminar program. The new algorithm is shown in Appendix 1.3.

Algorithm 2 Maintain the normal force constant during experiment

Requirement: Monitor the normal force throughout the experiment (F_{n_r}) and adjust the position of the Basalt MUST 2D-FM 1N in z axis (Pos_z) until the desired normal force (F_{n_d}) is achieved. The value of the spring constant in z axis (Spr_n) and the F_{nac} depend on the cantilever used. Moreover, if the correction value ($Correc_z$) is less than 0.001 (minimal movement), change it to 0.
Guarantee: Maintain the normal force value with an accuracy of 0.05 mN
Calculate the acceptable limits of the normal force (F_{n_l} and F_{n_h}).
$F_{n_l} = F_{n_d}$ - F_{nac} mN.
$F_{n_h} = F_{n_d} + F_{nac}$ mN.
Compare the value of the actual normal force read(F_{n_r}) with the limits and change Pos_z. Also, multiple Spr_n by 1000 to equilibrate the units and divide F_{n_d} - F_{n_r} by 2 to reduce the displacement of $Correc_z$.
if $F_{n_r} < F_{n_l}$ **then**
    $Correc_z = (F_{n_d}$ - $F_{n_r})/(2000(Spr_n))$ mm
    if $Correc_z < 0.001$ **then**
        $Correc_z = 0$
    else
        $Correc_z = Correc_z$
    end if
    $Pos_z = Pos_z + Correc_z$
end if
if $F_{n_r} > F_{n_h}$ **then**
    $Correc_z = (F_{n_r}$ - $F_{n_d})/(2000(Spr_n))$ (mm)
    if $Correc_z < 0.001$ **then**
        $Correc_z = 0$
    else
        $Correc_z = Correc_z$
    end if
    $Pos_z = Pos_z$ - $Correc_z$
end if

2.3.2 Analysis and cleaning of tribological data after the test

In the preivous work (ref [5]), the tribological data recorded by the LabVIEW program was stored in an Excel file without a post-processing. Subsequently, during the project seminar, a post-processing program was developed (ref [25]) and the data were stored in a text file (.txt).In this master's thesis, two MATLAB programs were used for analizyng the tribological data. The first program focuses on converting the tribological data from the txt file to variables in MATLAB. The second program focuses on performing the analysis, along with the filtering and cleaning process.

In the new LabVIEW based program, both the tribological and the electrical data are stored in a text file (.txt). However, the user must erase certain lines and replace the commas with periods in the text file before importing it into MATLAB(See Appendix 3). The two MATLAB program, derived from the previous ones developed during the project seminar, have been updated in this master's thesis.
The first program uses the MATLAB commands to import the data from the text file into a main matrix (R). This matrix contains essential information from the original file necessary for identifying the tribological and electrical properties of the material, including the position on X axis (mm, absolute), normal force (mN), tangential force (mN), friction coefficient, voltage (mV) and current (uA).

The second program uses the MATLAB commands to analyse the valleys mentioned in the section 1.2.3. This new program follows the same procedure as the one developed during the project seminar, which is explained in the following paragraph. Additionally, the valley data shown in Figure 2.5 correspond to the constant slope zone depicted the Figure 2.6.

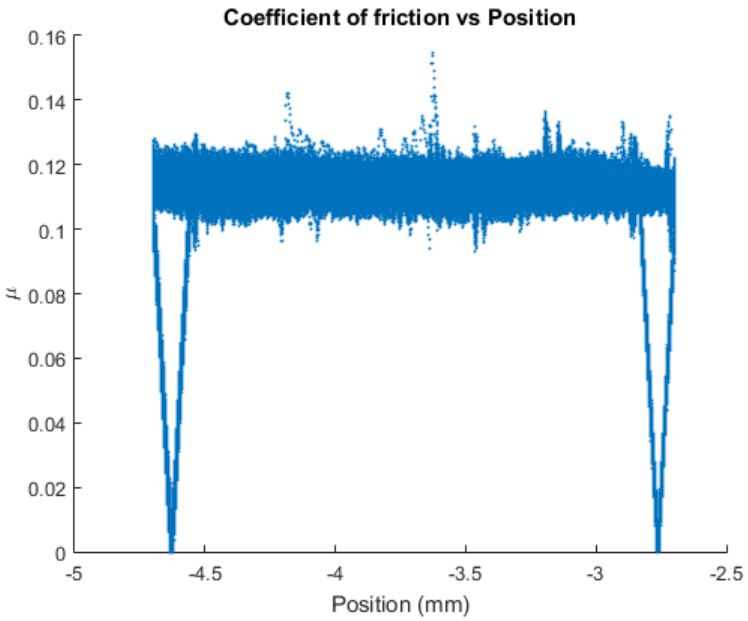

Figure 2.5: Variation of the coefficient of friction. Experiment performed at 0 mA during 1000 cycles for a set force of 40 mN conducted by E. Yupanqui (ref [5]).

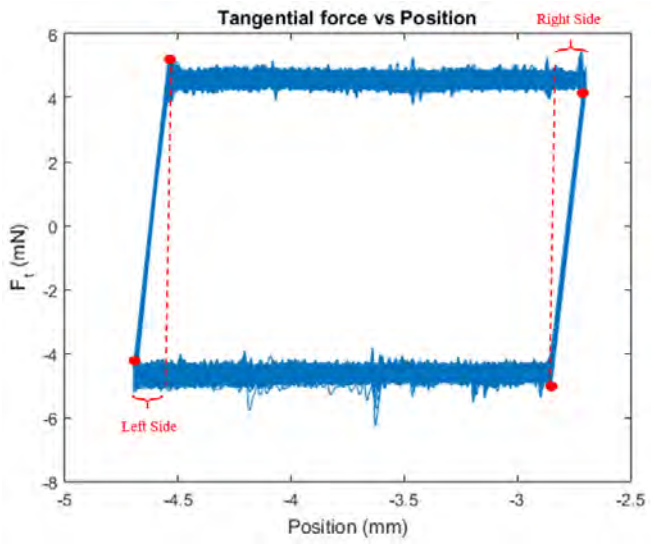

Figure 2.6: Variation of the tangential force. Red points indicate the coordinates where the constant slope zones begin and end. Experiment performed at 0 mA during 1000 cycles for a set force of 40 mN conducted by E. Yupanqui (ref [5]).

Algorithm 3 describes this first part of the second tribology program. The algorithm analyses a data set ($Ndata$) to identify the areas with constant slope, highlighted in red in Figure 2.6.
First, the program determinates the position of the maximum and the minimum value of the tangential force using MATLAB commands. Then, it evaluates the values near these two points using the same procedure as in the project seminar to identify the desired zones by analysing the slope (ref [25]). The procedure involves evaluating a set of data N_{data} around the point of the maximum tangential force ($P_F max$) and the point of the minimum tangential force ($P_F min$). After experimentation, the staring value for testing N_{data} was determined to be 8000.
For each data set, the program calculates the slope between two consecutive points and compares with the maximum angle deviation (d_p). This process is repeated for all data in the group to identify points where the slope is steep. The stored points correspond to areas where the normal force is zero. However, the change of cantilever introduced additional noise in the Ft(t) values, necessitating updates to the original program, specifically changes to the filter values. The MATLAB program is shown in the Appendix 3).

Second, due to the previous process, the vector $F_t1(t)$ will contain repeated data from the the tangential force versus position plot points. Once these data are removed, the results from the previous two parts in a test with a high initial normal force are shown in Figure 2.7. The points in the middle were added incorrectly due to the increased noise. This noise will appear when the tribometer uses a cantilever with a high spring constant. However, this can be filtered out in the next step.

Algorithm 3 Offline debugging algorithm - Analysing slope

Requirement: Read values of tangential force (F_t), LMS20 position (x), group of elements to analyse (n_e), the point of the maximum tangential force ($P_F max$),the point of the minimum value of the tangential force ($P_F min$), group of data (N_{data}) and maximum angle deviation (d_p)
Guarantee: Identify the data located in the constant slope zones on the left and ride sides
Identification of the initial point on the nearby of the $P_F max$ and the $P_F min$
$ini_a = P_F max - \frac{N_{data}}{2}$
$ini_b = P_F min - \frac{N_{data}}{2}$
Analysing the first zone. In $\alpha(j)$ is recorded the slope between two points with the arc tangent (the operation atan). At the same time, the values in α are operated and stored in *deviation* for a posterior analysis with d_p
for $i \leftarrow ini_a$ to $N_{data} + ini_a$ **do**
    for $j \leftarrow 1$ to n_e **do**
        $\alpha(j) = atan\left(\frac{F_t(i+j) - F_t(i)}{x(i+j) - x(i)}\right)$
        $deviation(j) = \frac{\alpha(j) - \alpha(1)}{\alpha(1)}$
        $j = j + 1$
    end for
    Count quantity of elements of *deviation* lower than d_p and store it in variable *pos* ▷ Done with MATLAB commands
    if $pos = n_e - 1$ **then**
        Store vector $F_t1(i + j)$
    end if
    $i = i + 1$
end for
Analysing the second zone
for $i \leftarrow ini_b$ to $N_{data} + ini_b$ **do**
    for $j \leftarrow 1$ to n_e **do**
        $\alpha(j) = atan\left(\frac{F_t(i+j) - F_t(i)}{x(i+j) - x(i)}\right)$
        $deviation(j) = \frac{\alpha(j) - \alpha(1)}{\alpha(1)}$
        $j = j + 1$
    end for
    Count quantity of elements of *deviation* lower than d_p and store it in variable *pos* ▷ Done with MATLAB commands
    if $pos = n_e - 1$ **then**
        Store vector $F_t1(i + j)$
    end if
    $i = i + 1$
end for
Eliminate repeated values ▷ Done with MATLAB commands

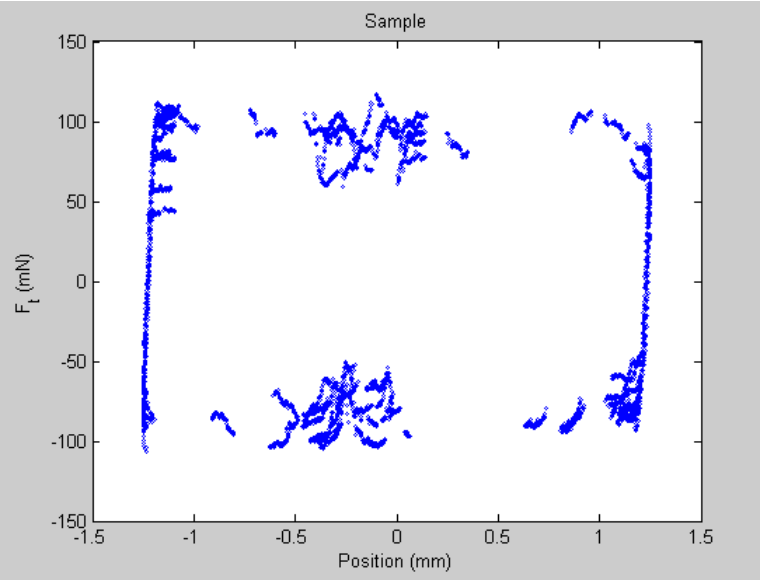

Figure 2.7: Data extracted from the original test. The points in the middle were added wrongly due the increased of the noise.

The third part of the program involves filtering the data shown in Figure 2.7. The total length of the position (pos_{tot}) and the middle point of the position (pos_mid) are identified. The data are then divided into left and right segments based on the value of pos_{mid}. The program applies a limit to the left segment, defined by the position of the tangential force (lim_l), and uses the MATLAB max command to find the point where the tangential force is maximum (Pft_{maxl}). Subsequently, the program generates a regression line based on of $Pft_{maxl}$and calculates the points that fall below this line, representing the values on the left side. This is feasible because the desired data are always located at the edges. Next, the algorithm applies the same logic to the right side. In this case, the program establishes another boundary (lim_r), finds the point where the tangential force is minimum (Pft_{mimr}) and generates a corresponding linear equation. This logic is described in Algorithm 4 and the result of the vectors containing the unwanted data stored are shown in the Figure 2.8. Next, the new program removes the unwanted data from the original dataset and creates a new vector containing only the desired data. Finally, the program uses the filter process and repeats all the previous algorithms to enhance data quality and eliminated any values that were not previously removed. The MATLAB program is presented in Appendix 3).

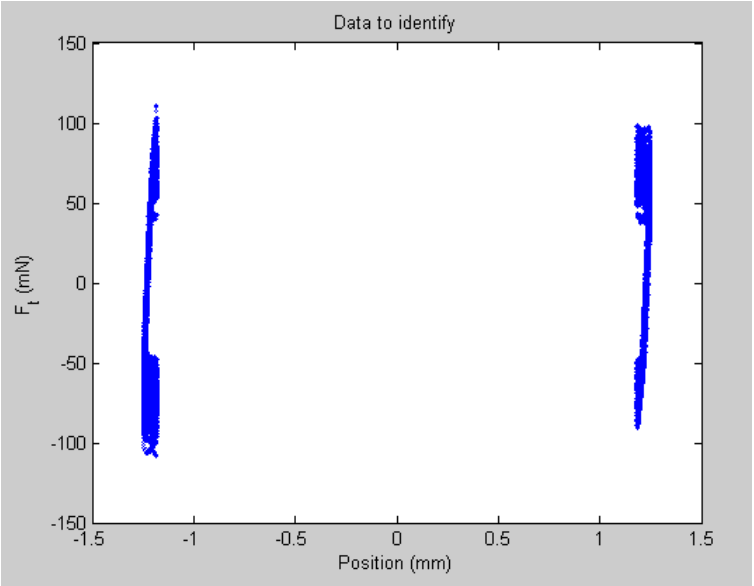

Figure 2.8: Data extracted from the original data. The points in the middle were filtered.

Algorithm 4 Offline debugging algorithm - Identifying edges

Requirement: Read values of tangential force (F_{t1}) and the LMS20 position (x_d) shown in Figure 2.7.
Guarantee: Identify the data located in the constant slope zones on the left and ride sides
Identified total length of the position (pos_tot), the middle point of the position (pos_{mid}) and the total of tangential force points ($point_tot$). ▷ Done with MATLAB commands
Generate two arrays with the left and the right zone on each one.
for $i \leftarrow 1$ to $point_{tot}$ **do**
    if $x_d < pos_{mid}$ **then**
        Store tangential force in vector $F_{tl}(i)$
        Store position in vector $p_l(i)$
    end if
    if $x_d > pos_{mid}$ **then**
        Store tangential force in vector $F_{tr}(i)$
        Store position in vector $p_r(i)$
    end if
end for
The limits for both zones were generated. The value of 0.03 was obtain through experimentation and is used to prevent having the same point in lim_l and lim_r. There is not issue,as the values not analysed where located in the middle.
$lim_l = 0.03pos_{tot} - \frac{pos_{tot}}{2}$
$lim_r = -(0.03pos_{tot} - \frac{pos_{tot}}{2})$
Search the maximum tangential force value in the left zone (Pft_{maxl}) limited by the value of lim_r. ▷ Done with MATLAB comands
Search the minimum tangential force value in the right zone (Pft_{mimr}) limited by the value of lim_r. ▷ Done with MATLAB commands
Analysed the left and the right zone with the values of Pft_{mimr} and Pft_{maxl}
if $F_{tl} < Pft_{maxl}$ **then**
    Store tangential force in vector F_{t1}
    Store position in vector $p1$
end if
if $F_{tr} > Pft_{mimr}$ **then**
    Store tangential force in vector F_{t1}
    Store position in vector $p1$
end if

2.4 Improvement of the electrical program and the electrical data

After establishing the physical connection and configuring the software for communication between the Keithley modules, the tribometer and the portable NI workstation mentioned in Section 2.2, the system is controlled by a LabVIEW program. The enhancements on the tribological program from the project seminar (ref [25]) are detailed in Section 2.3.1. Additionally, the new program incorporates events, which are necessary for controlling the electrical components, it was based on the electrical program developed by Edson Yunpaqui (ref [5]).

The first events added were those for connecting and disconnecting the Keithley modules with the NI portable workstation. The main difference lies in the VISA address. Figure 2.9 displays the code for remotely configuring the Keithley modules, and additional information in the Appendix 2.1.

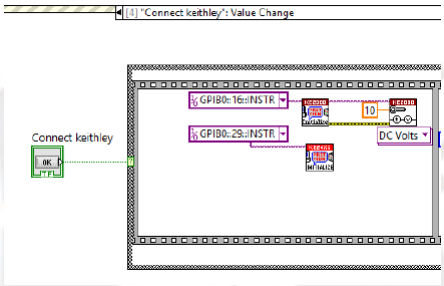

Figure 2.9: In the New event Connect Keithley, the communication configuration between the Keithley modules and the workstation utilizes different blocks to record electrical data and the tribological data simultaneously.

An electrical time interval was calculated to synchronize the electrical data with the tribological data during data recording. The new program computes the electrical interval in the Start Streaming event. This interval is determined based on the Stream Interval of the tribometer and the limits of the Keithley modules. These modules store a minimum of five electrical data points for each half cycle performed by the tribometer (data obtained through experimentation). However, the duration of the electrical interval is constrained by the minimum operational time of the LabVIEW program commands (1 ms). The components of the event program are illustrated in Figure 2.10,with further details provided in Appendix 2.2

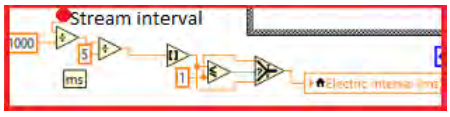

Figure 2.10: In the Start Stream event the value of the electrical interval is calculated based on the Stream Interval of the tribometer and the limits of the hardware.

Before starting the tribological test, the user must configure the Keithley 2400 as a current source with the specified value. According to the Keithley 2400 user manual (ref [4]), the user must set a measurement range and a maximum voltage compliance value when the module is remote configured as a current source. However, the default Keithley libraries in LabVIEW only configure the measure range (compliance level). To complete the configuration process, a subVI based on SCPI commands was developed in this thesis. SCPI commands in LabVIEW allow for sensor control without the need for a specific driver. This subVI sets the measurement range, also referred to as compliance level (Com_{lev}) to establish the maximum compliance value (Com_{max}).
The sub-program utilizes the recommended Com_{max} values mentioned in the user manual to create a relation between the measurement range and compliance level. This relation was developed for a theoretical maximum electrical resistance value of 10 Ohm for the sample (see Table 2.1). By establishing this ratio, the Keithley modules are saved from high of voltage or current pecks during the test.

Table 2.1: Relation between compliance level (Com_{lev}) and the maximum compliance value ($Com_{ma}x$) for a maximum electrcail resistance value of 10 Ohm ($Theo_{res}$). Values based on the user manual of the Keithley 2400 (ref [4]).

Current set by the user	**Compliance level**	**Maximum compliance value**
0 mA	0 V	0 V
10 mA	2 V	2.1 V
100 mA	20 V	21 V
1 A	200 V	210 V

The subprogram requires the VISA address to specify which Keithley module will supply power. Additionally, the program includes an error input and an error output to indicate any errors that may occur during this process, as described in Algorithm 5. Unfortunately, the compliance value must be set on the SourceMeter Keithley each time the Modulus is configured in remote mode. There is currently no option to set the compliance value in the module as a preset, unlike the actions described in Section 2.2.

Algorithm 5 Configure Output - Maximum Compliance Value

1: **Requirement:** Read values of compliance level (Com_{lev}), the VISA address and the previous error value in the error input.
2: **Guarantee:** Configure the maximum compliance value (Commax) voltage for the Keithley 2400 set as a current source in remote mode, and indicate if an error occurs during the process.
3: Read the Com_{lev} value.
4: Compare this value with the values shown in the Table 2.1.
5: **if** $Com_{lev} == 2$ **then**
6: $\quad Com_{max} = 2.1$
7: **end if**
8: **if** $Com_{lev} == 20$ **then**
9: $\quad Com_{max} = 21$
10: **end if**
11: **if** $Com_{lev} == 200$ **then**
12: $\quad Com_{max} = 210$
13: **end if**
14: Use the VISA address to configure the Com_{max} in the Keithley 2400
15: Analyse the present of a error during this process.

In the "Turn on the power source" event, the program configures the Keithley 2400 as a current source with the value specified by the user in mA. Additionally, the program calculates the compliance level based on the values in Table 2.1. This event and the subprogram "Configure Output - Maximum Compliance Value" are shown in the Figure 2.11,while the application ID shown in Figure 2.12. More information can be found in Appendix 2.3.

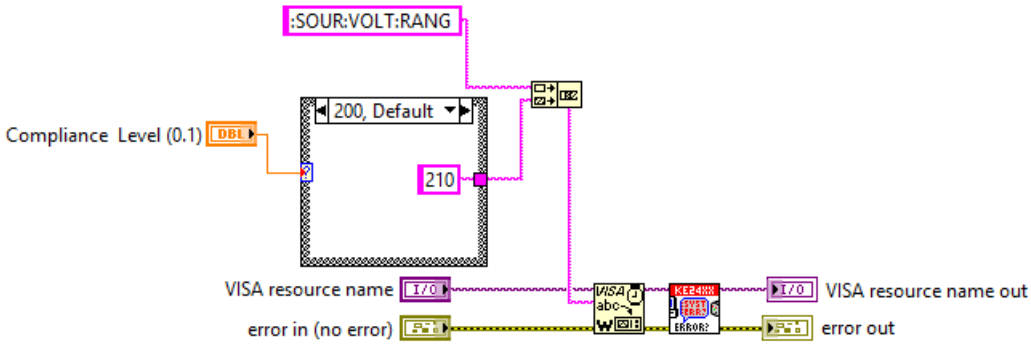

Figure 2.11: This Sub VI performs the configuration of the maximum compliance value in the Keithley 2400 after this module has been configured as a current source. The current value supplied by module is set by the user for each test.

To switch off the Keithleys modules when an error occur or when the user decides to stop the test, several events were modified in the new program. These changes include

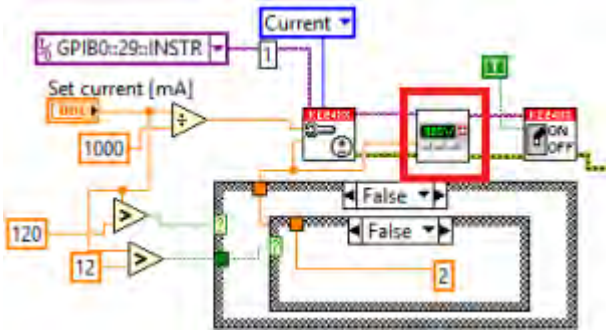

Figure 2.12: The SubVI in the Figure 2.11 is located within the red square. This event is shows the assignation of compliance value according to Table 2.1 .

the initialization of indicators, a new method to shut down the workstation at specified time intervals , and the display of messages, as shown in Appendix 2.4.The shutdown sequence follows this order: first, the current source; then, the Keithley modules; and finally, the tribometer.

The algorithm located in the "Timeout" event during the "Testing" phase has been updated to stored electrical data simultaneously with the tribological data. The new program utilizes a LabVIEW timer to evaluate the time in milliseconds for recording the electrical data. It then employs the previously calculated electrical interval value to store this data.
Since the communication speed between the workstation and the tribometer is faster than that between the Keithley modules, the program allows the previously recorded current and recorded voltage to be stored alongside the new tribological data until the Keithley modules measure the new data. The electrical interval determines the timing for recording the electrical data. This code is presented in Appendix 2.5.

The obtained electrical data require an brief analysis and cleaning process after the test is performed. Since the test was conducted with a current upper an 100 pA there are no issues with the electrical values (ref [19]). The voltage and current data were recorded simultaneously with the tribological data in the MATLAB program. However, the previous MATLAB program removes some irrelevant data points from the tribological values. Consequently, this program uses these filtered data points to eliminate unnecessary electrical data, ensuring that both datasets contain the same number of values for consistent plotting. For instance, electrical values corresponding to positions where the normal force was zero were deleted. Finally, only the tribological data and electrical data located in the center of the normal force versus position plot were retained for further analysis.

2.5 New user interface

The new user interface is shown in the Figure 2.13, with more details provided in Appendix 2. The interface is divided into three parts: Setup, Calibration and Testing, indicates by a red circle in Figure 2.13. These sections follow the necessary steps to run a test. The interface includes specific areas for controls and indicators. Additionally, it informs to the user about the characteristics of each control and indicator through text message, labels and a system of locked buttons.
The new GUI program has incorporated the necessary input to control the Keithley modules and the tribometer simultaneously. In the Setup section, the user must connect the workstation to the Keithley modules and the tribometer and configure them. The Calibration section is only unlocked when all previous Setup steps have been successfully completed. In the Calibration section, the user must manually calibrate the FOS sensors and prepare the numerical variable for testing (see Figure 2.14). The Testing section allows the user to set all the tribological and electrical values for the test in the correct order. It also enable the user to start the test, record the results, and stop the test when requested (see Figure 2.15). A step-by-step guide for using the new graphical user interface is provided in Appendix 3.

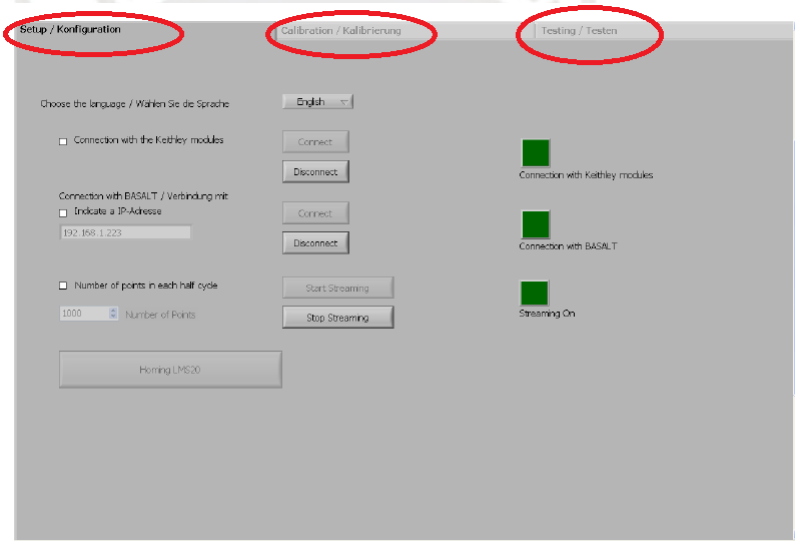

Figure 2.13: The Setup guides the user in establishing communication between the tribometer,the Keithley modules, and the workstation. The Calibration tab will only be unlocked once the entire Setup section has been successfully completed.

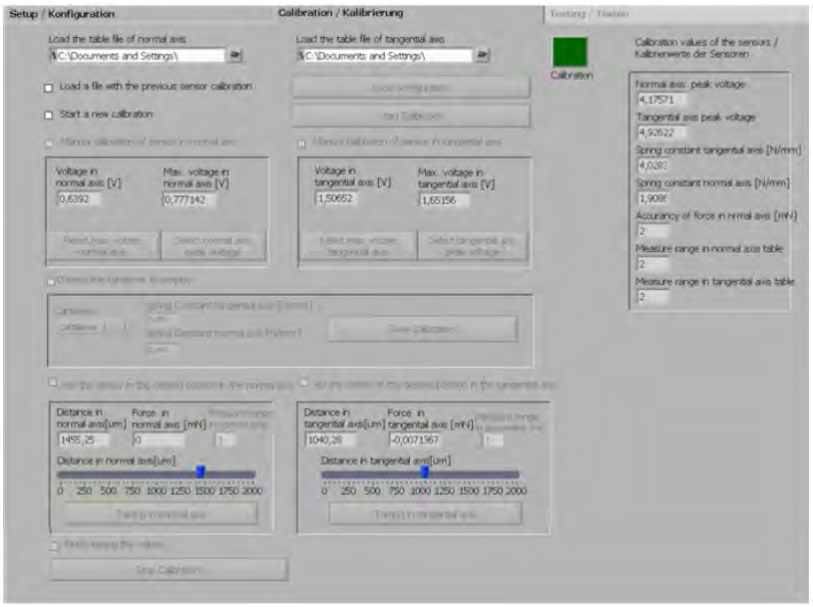

Figure 2.14: The Calibrate guides the user in calibrating the sensors on the FOS and others variables. The Testing tap will only be unlocked once all calibrations have been completed.

Figure 2.15: The Testing guides the user in setting the tribological and electrical parameters for the test. it then assists the user in establishing the initial normal force, making contact with the sample, setting the current, starting the test, recording the test and stopping the test upon user request.

Additionally, the failed experiment restart and user communication algorithms develop in ref [25] will continue to be utilized in the new program. The emergency stop, stop button, and safety algorithms from ref [25] have also been enhanced to control the Keithley modules and the tribometer. Figure 2.16 shown the event Stop Test and the sequence for shutting down the system. Current is the most critical property to shut down, as it poses the greatest danger in the system. Therefore, the program must wait for a period before losing contact between surfaces, as any residual electricity could create a voltage differential. Once the electrical hazard is addressed, the program proceeds with the shutdown sequence.

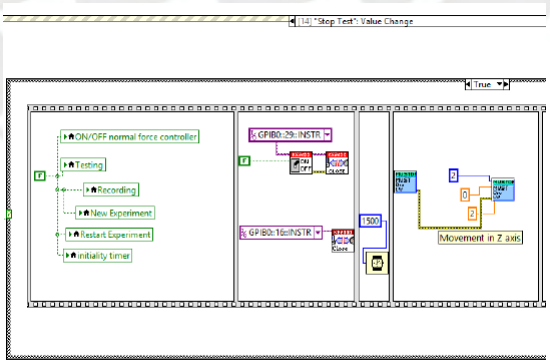

Figure 2.16: The Turn off sequence in the Stop Test event is as follows: first turn off the logical variable; then, disable the Keithley modules. After 1.5 seconds, move the indenter along the z-axis to separate it, followed by the other step outlined in Appendix 2.4

The others safety algorithms are included in the main event. The first is the emergency button located in the Testing section for emergency during operation, and the second is the ESCAPE key on the keyboard, serving as a physical button. Figure 2.17 shown both algorithms, similar to the previous one. However, the speed of the shutdown sequence in case of an emergency is faster because these algorithms are integrated into the main program. The complete events can be found in Appendix 2.4).

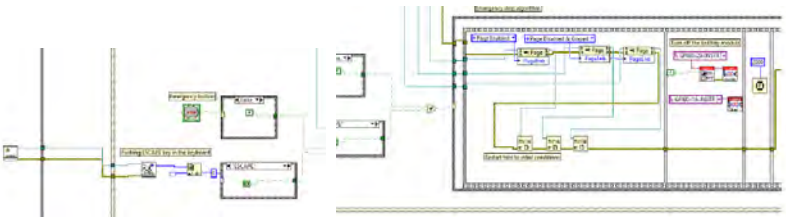

(a) (b)

Figure 2.17: The shutdown sequence in the main Event utilizes the same algorithms for both scenarios, as the electrical hazard is the most dangerous.

CHAPTER 3

Experiments

Tests were conducted to verify the response of the programs developed in this master thesis. The behavior of the tribological data obtained using the new program should closely resemble that obtained during the project seminar (ref [25]) when the applied current is zero. Since the method for obtaining the tribological data is the same in both cases, a similar behavior of the results will confirm that the new program is capable of acquiring tribological data as effectively as the previous program. Additionally, Holfeld's work will be used to corroborate the coefficient of friction values in the experiments with Cr2AlC thin films
The program should display changes in the coefficient of friction resulting from the effect of current flow in the sample. As mentioned in Section 1.1.2, the current flow accelerates the electrons in the thin film (ref [17]). Consequently, according to the theory presented in Section 1.1.1.5, an increase in the temperature of the thin film raises the value of the friction coefficient (ref [7] and ref [9]).

The material provided as sample was an $Cr_2AlC - MAX - Phase$ material. MAX-phase material are composed of a transition metal M (for example Ti, Cr or Nb); an element from group A of the periodic table (for example Al,Si,Ge or Sn) and an element X, which can be either N or C (ref [26]). Most MAX-phase material exhibit characteristics of both metallic and ceramic materials. They possess good electrical conductivity and demonstrate a linear relationship between temperature and electrical resistance (ref [26]). Another notable property of MAX-phase materials is their non-linear elastic behavior against cycling loading, similar to the methods used by the tribometer. Therefore, the tribological data is expected to exhibit hysteresis due to the material composition. Furthermore, the theoretical elastic modulus of $Cr_2AlC - MAX - Phase$ is higher that the experimentally elastic modulus (ref [2]). This abnormality increase the interest in study the mechanical properties of this material. This discrepancy increases interest in studying the mechanical properties of this material, and the system

developed in this master's thesis will aid in collecting more data on this phenomenon. The parameters of the experiments performed are shown in Table 3.1. The variables modified during the experiments include the set normal force, the LMS 20 velocity, and the amount of current applied to the probe surface. According to the theory, increasing the force F would enhance the sample penetration distance d (see in equation 1.7). Additionally, increasing the contact radius α results in a larger contact area between the spherical penetrator and the sample. This larger contact surface reduces the inherent errors caused by the materials roughness (ref 1.1.1). The velocity of the LMS20 also influences friction; an increase in sliding speed typically reduces the coefficient of friction (ref [9]). Therefore, a lower sliding velocity produces a more stable coefficient of friction. Finally, an increase in current flow is expected to raise friction levels, as explained in the previous section (see 1.1.1.5).

However, all the experiment were conducted with the same measurement length of the LMS20 (2.5 mm), the same recording two cycles, and the same number of cycles (202), resulting in a total length of (1000 mm). A piece of paper towel soaked in alcohol was used to clean the sample and the tribometer sphere prior to testing. This ensured that the surfaces were free of dust and other contaminants, and that they were devoid of any lubrication once the alcohol had evaporated. It is important to note that all tests were performed using a cantilever with a tangential spring constant of 4.0283 mN/um and a normal spring constant of 1.9086 mN/um.

Table 3.1: Tests conducted with the new program in LabVIEW.

N°	**Force (mN)**	**Velocity (mm/s)**	**Current (mA)**	**Total length (mm)**
Test 1	150	0.5	0	1000
Test 2	50	0.5	0	1000
Test 3	150	1	0	1000
Test 4	50	1	0	1000
Test 5	50	1	100	1000
Test 6	150	1	100	1000
Test 7	150	0.5	100	1000

The results obtained in the Test 1,Test 2, Test 3 and Test 4, conducted without electric current, exhibit behavior similar to the observed in the project seminar (ref [25]). The noise in the results of the tests is higher than the obtained in the project seminar; however, this is attributed to the greater force set on them, which is influenced by the higher elastic constant of the new cantilever. According to theory, an increase in noise was anticipated following the application of a higher force.

The tribological results obtained from Test 1 using LabVIEW and MATLAB programs are displayed in Figure 3.1, Figure 3.2 and Figure 3.3. The values recorded by LabVIEW are presented on the left side of Figure 3.1, while the values obtained after using MATLAB are displayed on the right side of the same figure.

Test 1 Parameters: Set Force=150 mN, Velocity=0.5 mm/s, Total Length = 1000 mm

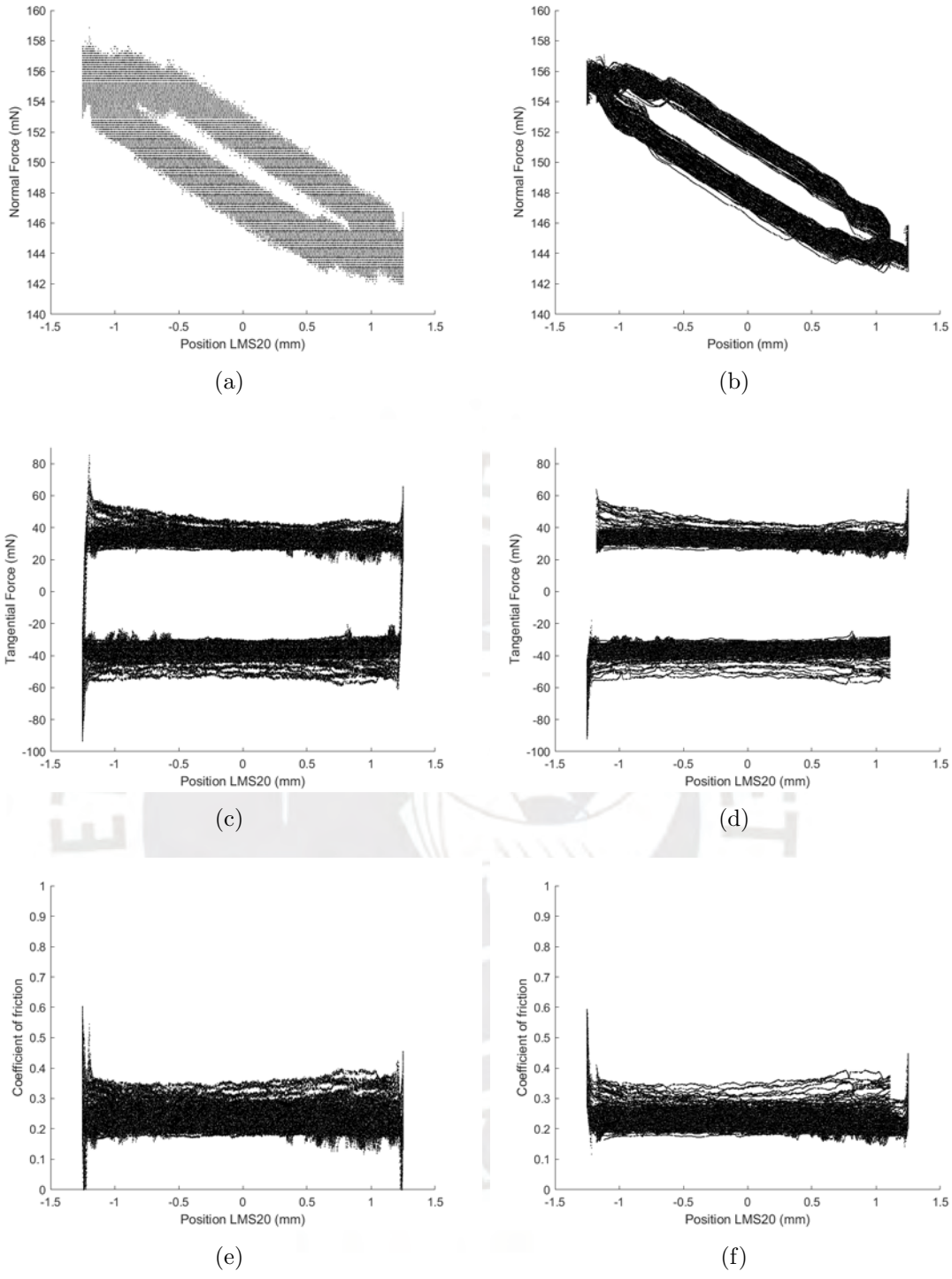

Figure 3.1: Results obtained after applying the new program to the data recorded with the LabVIEW and MATLAB programs: (a) Normal force recorded by the LabVIEW program, (b) Normal force after processing with the MATLAB program, (c) Tangential force recorded by the LabVIEW program, (d) Tangential force after processing with the MATLAB program, (e) Coefficient of friction (COF) calculated by the LabVIEW program, (f) COF after processing with the MATLAB program.

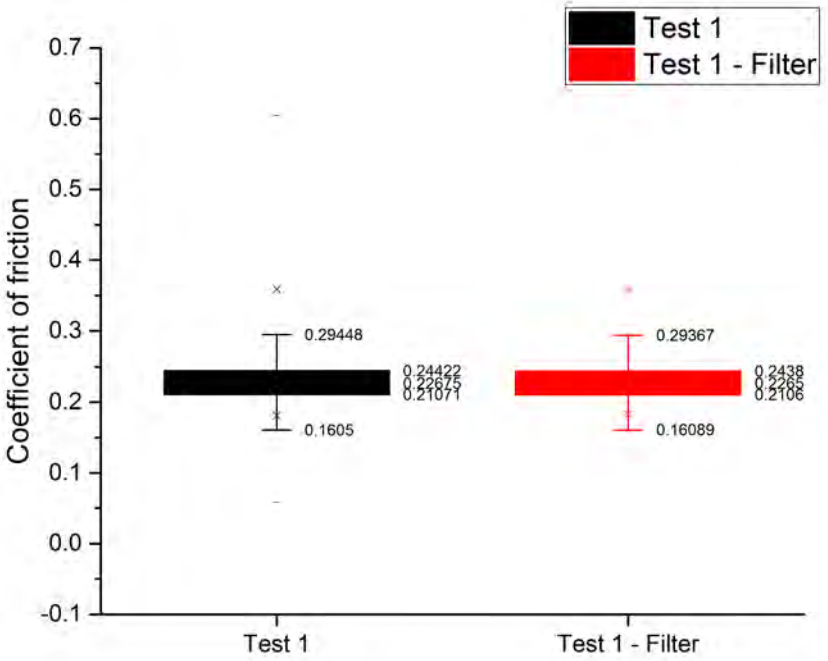

Figure 3.2: Test 1: Analysis on the effect of the new process in the updated MATLAB program. The left side displays the values without applying the new process,while the right side shows the values after the new process has been applied.

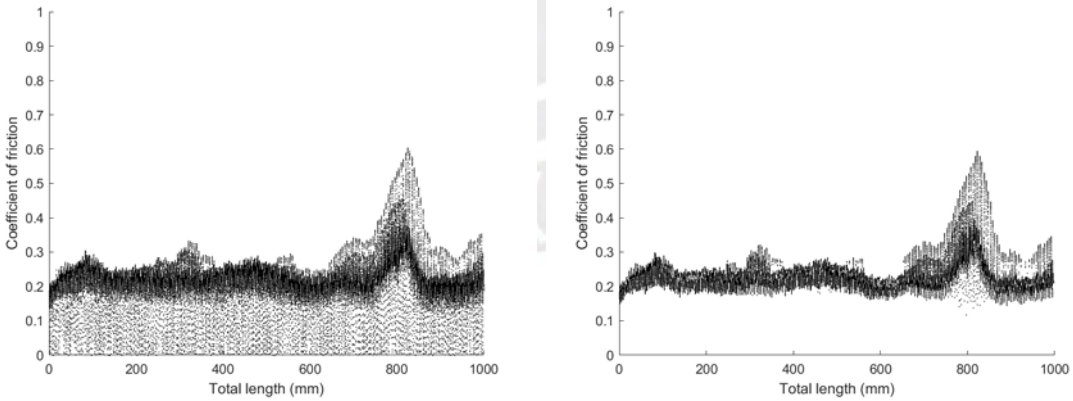

(a) (b)

Figure 3.3: Test 1: (a) COF versus total length without applying the MATLAB program. (b) COF versus the total length after applying the MATLAB program.

In Figures 3.1 (a) and Figure 3.1 (b), the values of the normal force are plotted. The hysteresis observed during the process may be associated with the nonlinear elastic behavior of MAX-phase materials, as previously explained. Thus, this hysteresis is an inherent property of the material, and the MATLAB program cannot eliminate it. In Figure 3.1 (c) and Figure 3.1(d),the transition zones in the tangential force were identified and removed after applying the MATLAB program. Similarly, the valleys of the friction coefficient shown in Figure 3.1 (e) were erased in Figure 3.1 (f), consistent with the approach taken in the project seminar.

Figure 3.2 illustrates the effect of the new process implemented in the updated MATLAB program. As previously mentioned, this process includes a new filter for experimentally calculated values and a second application of the algorithm to identify unusual data (see Section 2.3). The data on the left display coefficient of friction (COF) without the new process, while the middle values represent the mean COF (0.22675) along with its variance, with the maximum and minimum COF values at the extremes. The data on the right present the mean COF (0.2265), its variance values, and the maximum and minimum values after the new process. With this data, we can assert that the new algorithm reduces the data dispersion when calculating the friction coefficient.

Figure 3.3 shows the final result of COF versus total length after applying the MATLAB program. The values obtained for the coefficient of friction, ranging from 0.16059 to 0.29367, along with the behavior observed in this first experiment, exhibit a remarkable similarity to the results presented by Hopfeld et al. (Figure 1.41, green line)(ref [27]). The slight variations in the behaviors can be attributed to the differences in the sliding velocities applied in both experiments.

Figures 3.4, Figure 3.5, and Figure 3.6 present the tribological results of Test 2, Test 3, and Test 4. These results are consistent with those shown in the project seminar, with the exception of Test 2. Figures 3.8 and Figure 3.9 illustrate the cleaning of unwanted data in the calculation of the coefficient of friction, similar to Figure 3.3.

Test 2 Parameters: Set Force=50 mN, Velocity=0.5 mm/s, Total Length = 1000 mm

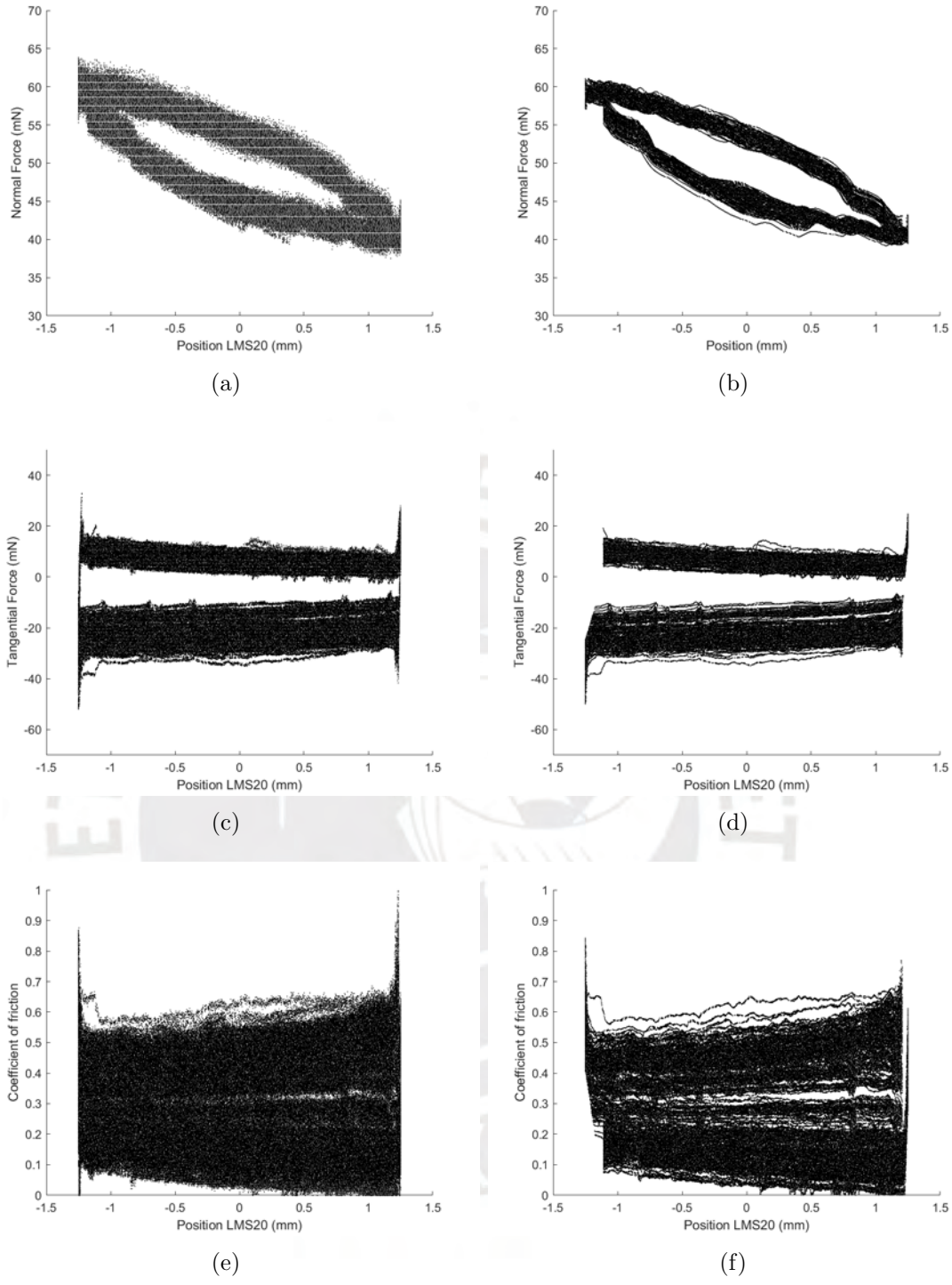

Figure 3.4: Results obtained after applying the new program to the data recorded with the LabVIEW and MATLAB programs: (a) Normal force recorded by the LabVIEW program, (b) Normal force after processing with the MATLAB program, (c) Tangential force recorded by the LabVIEW program, (d) Tangential force after processing with the MATLAB program, (e) Coefficient of friction (COF) calculated by the LabVIEW program, (f) COF after processing with the MATLAB program.

Test 3 Parameters: Set Force=150 mN, Velocity=1 mm/s, Total Length = 1000 mm

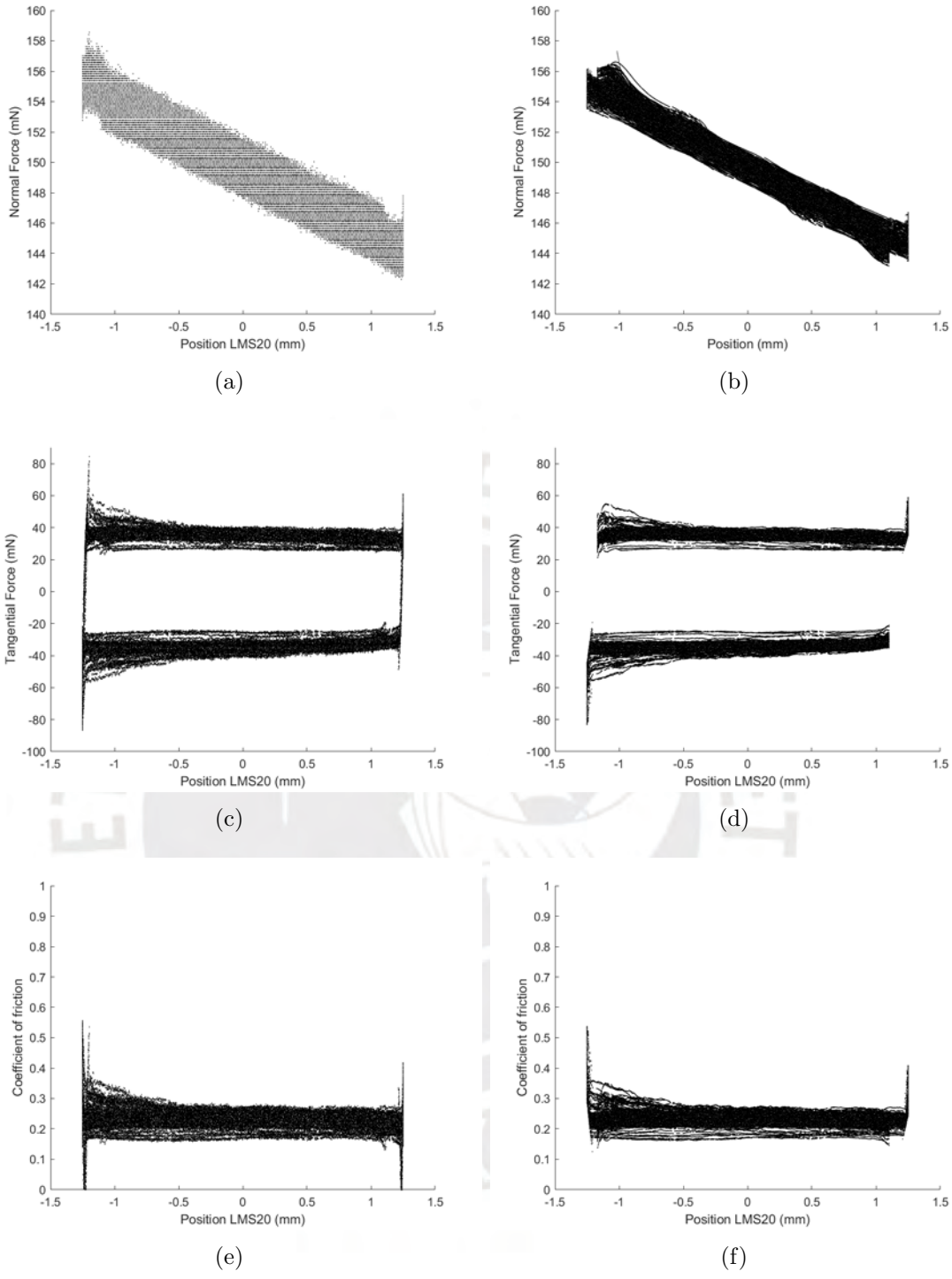

Figure 3.5: Results obtained after applying the new program to the data recorded with the LabVIEW and MATLAB programs: (a) Normal force recorded by the LabVIEW program, (b) Normal force after processing with the MATLAB program, (c) Tangential force recorded by the LabVIEW program, (d) Tangential force after processing with the MATLAB program, (e) Coefficient of friction (COF) calculated by the LabVIEW program, (f) COF after processing with the MATLAB program.

Test 4 Parameters: Set Force=50 mN, Velocity=1 mm/s, Total Length = 1000 mm

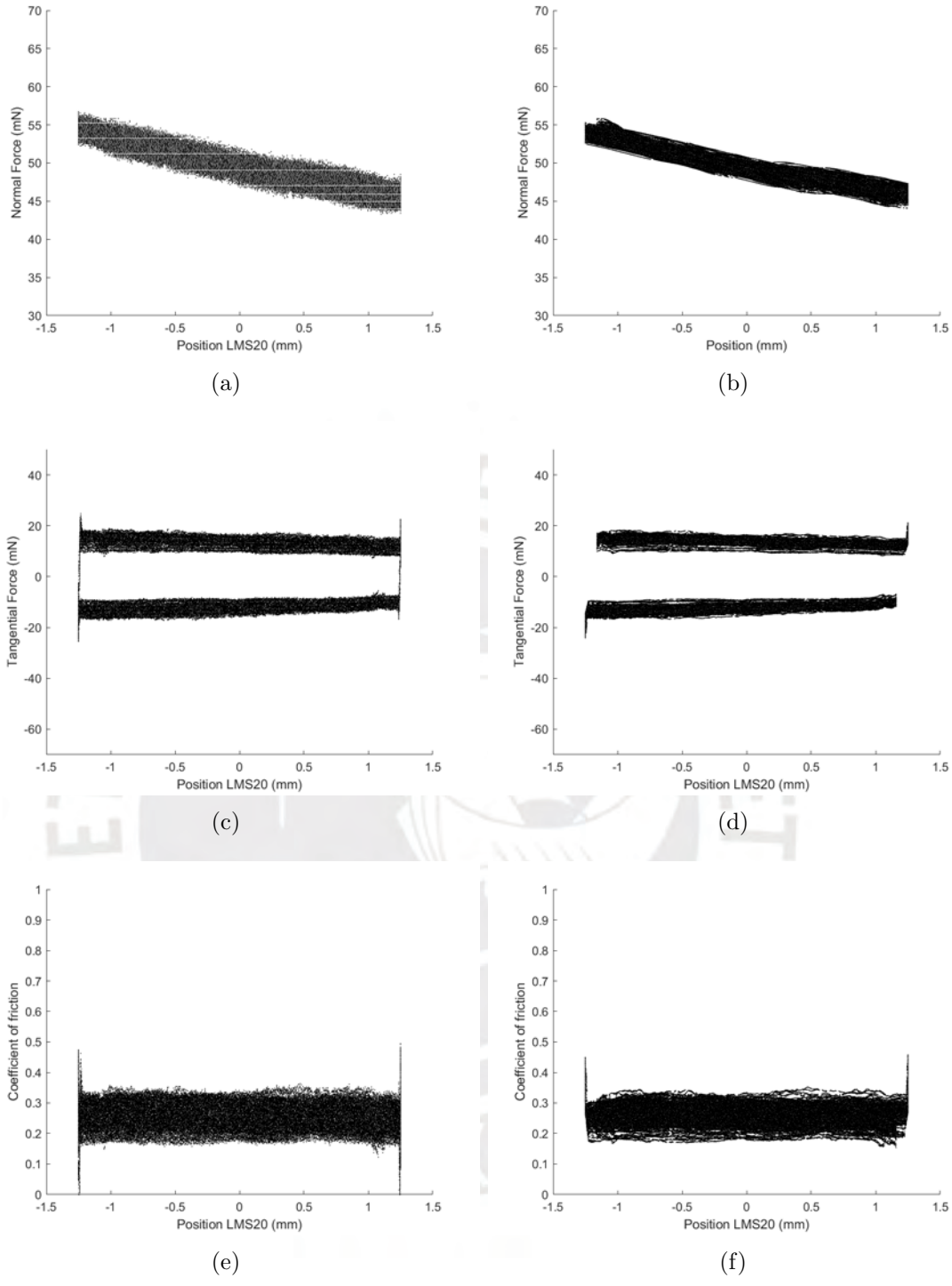

Figure 3.6: Results obtained after applying the new program to the data recorded with the LabVIEW and MATLAB programs: (a) Normal force recorded by the LabVIEW program, (b) Normal force after processing with the MATLAB program, (c) Tangential force recorded by the LabVIEW program, (d) Tangential force after processing with the MATLAB program, (e) Coefficient of friction (COF) calculated by the LabVIEW program, (f) COF after processing with the MATLAB program.

Figure 3.7, Figure 3.8 and Figure 3.9 present the COF versus total length after applying the MATLAB program in Test 2, Test 3 and Test 4. Figure 3.10 presents a comparative analysis of the coefficient of friction for Test 1, Test 3, and Test 4. It is evident that the data dispersion has been significantly reduced, and the obtained values align with those reported by Hosted (ref [27]).

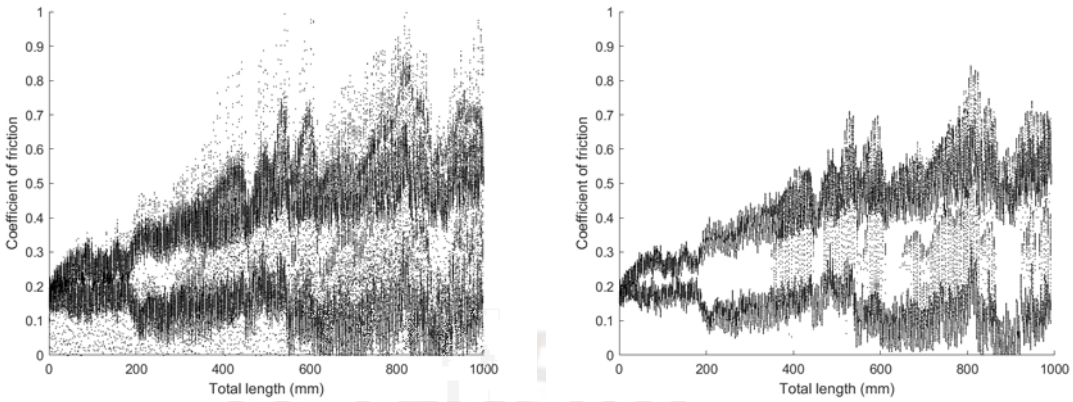

(a) (b)

Figure 3.7: Test 2: (a) COF versus total length without applying the MATLAB program. (b) COF versus the total length after applying the MATLAB program.

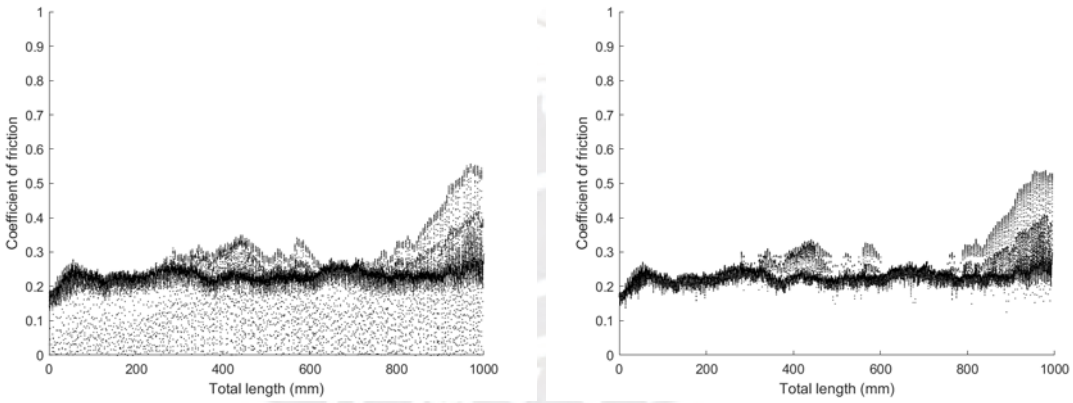

(a) (b)

Figure 3.8: Test 3: (a) COF versus total length without applying the MATLAB program. (b) COF versus the total length after applying the MATLAB program.

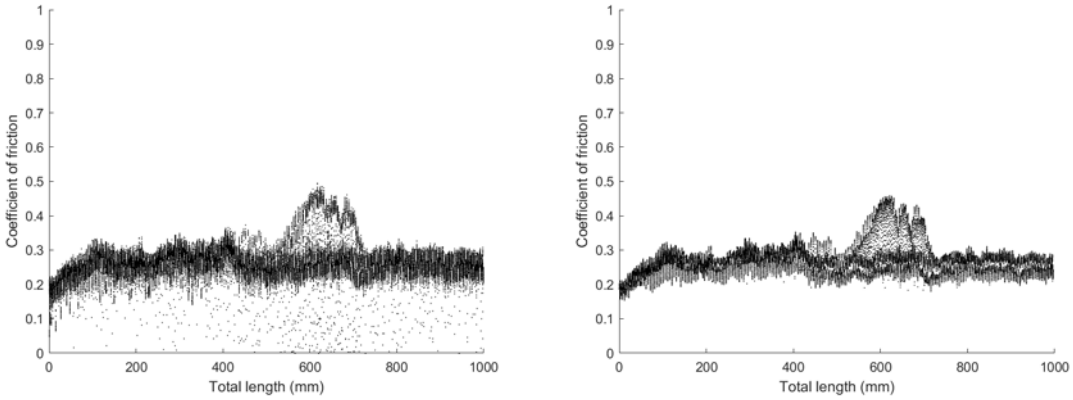

(a) (b)

Figure 3.9: Test 4: (a) COF versus total length without applying the MATLAB program. (b) COF versus the total length after applying the MATLAB program.

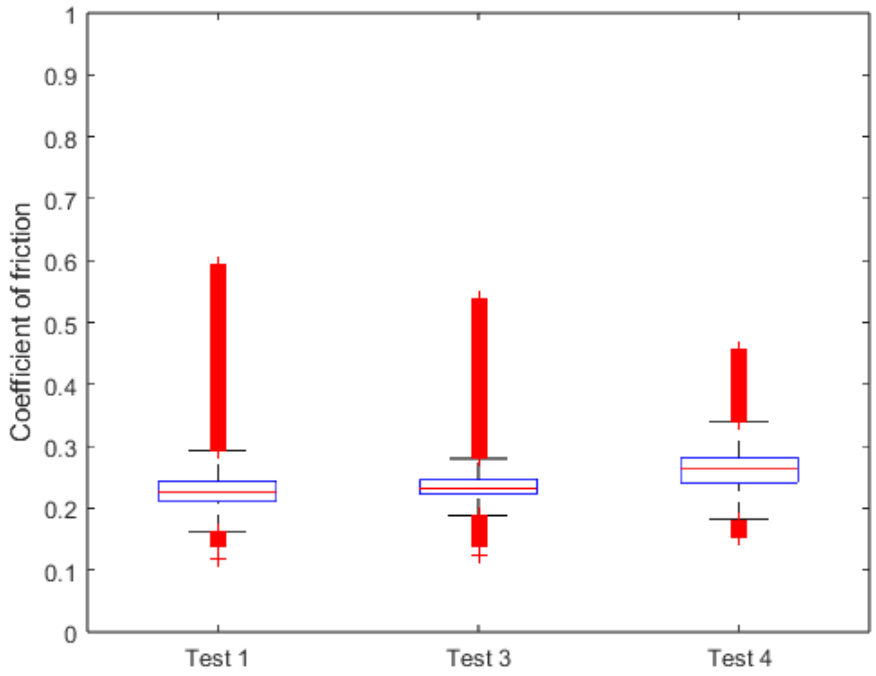

Figure 3.10: Comparative analysis of the coefficient of friction for Tests 1, Test 3, and Test 4.

Based on these results, we can conclude that the enhancements in the programs have maintained and improved the collection of tribological data for higher forces compared to the work presented in the project seminar. In addition, the ranges of friction coefficient values shown in Figure 3.10 agree with those presented by Hopfeld et al. (Figure 1.41)(ref [27]). The observed data scatter can be attributed to differences in sliding velocities and cantilever characteristics, since our experiment was performed at a higher

velocity.

Figures 3.11, Figure 3.12, and Figure 3.13 present the tribological results of Test 5, Test 6, and Test 7, respectively. As explained in the theory above, the coefficient of friction increased due to the influence of the current on the sample during the tests. Additionally, the algorithm consistently filters out extraneous data.

Test 5 Parameters: Set Force=50 mN, Velocity=1 mm/s, Total Length = 1000 mm, Current = 100 mA

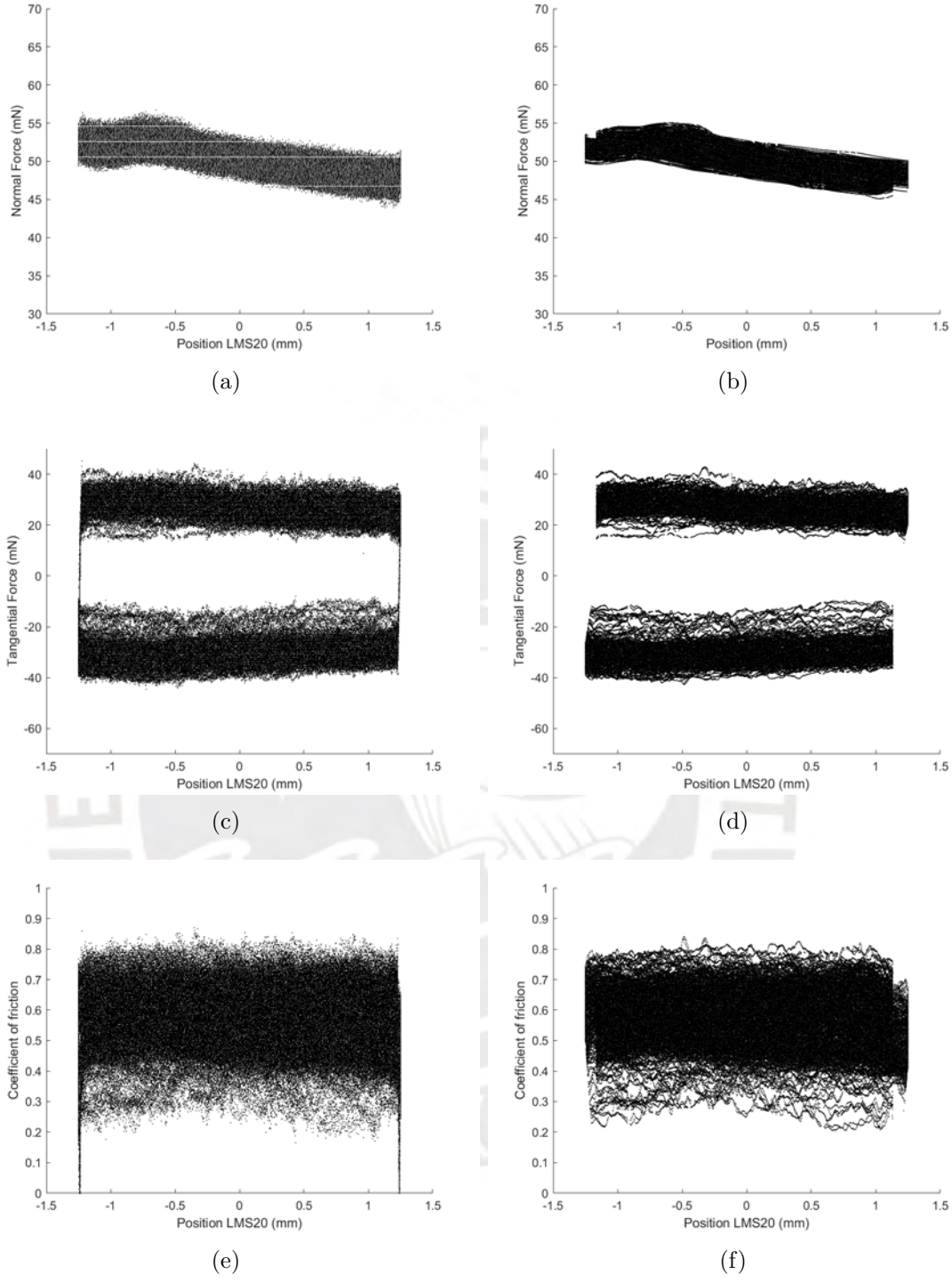

Figure 3.11: Results obtained after applying the new program to the data recorded with the LabVIEW and MATLAB programs: (a) Normal force recorded by the LabVIEW program, (b) Normal force after processing with the MATLAB program, (c) Tangential force recorded by the LabVIEW program, (d) Tangential force after processing with the MATLAB program, (e) Coefficient of friction (COF) calculated by the LabVIEW program, (f) COF after processing with the MATLAB program.

Test 6 Parameters: Set Force=150 mN, Velocity=1 mm/s, Total Length = 1000 mm, Current = 100 mA

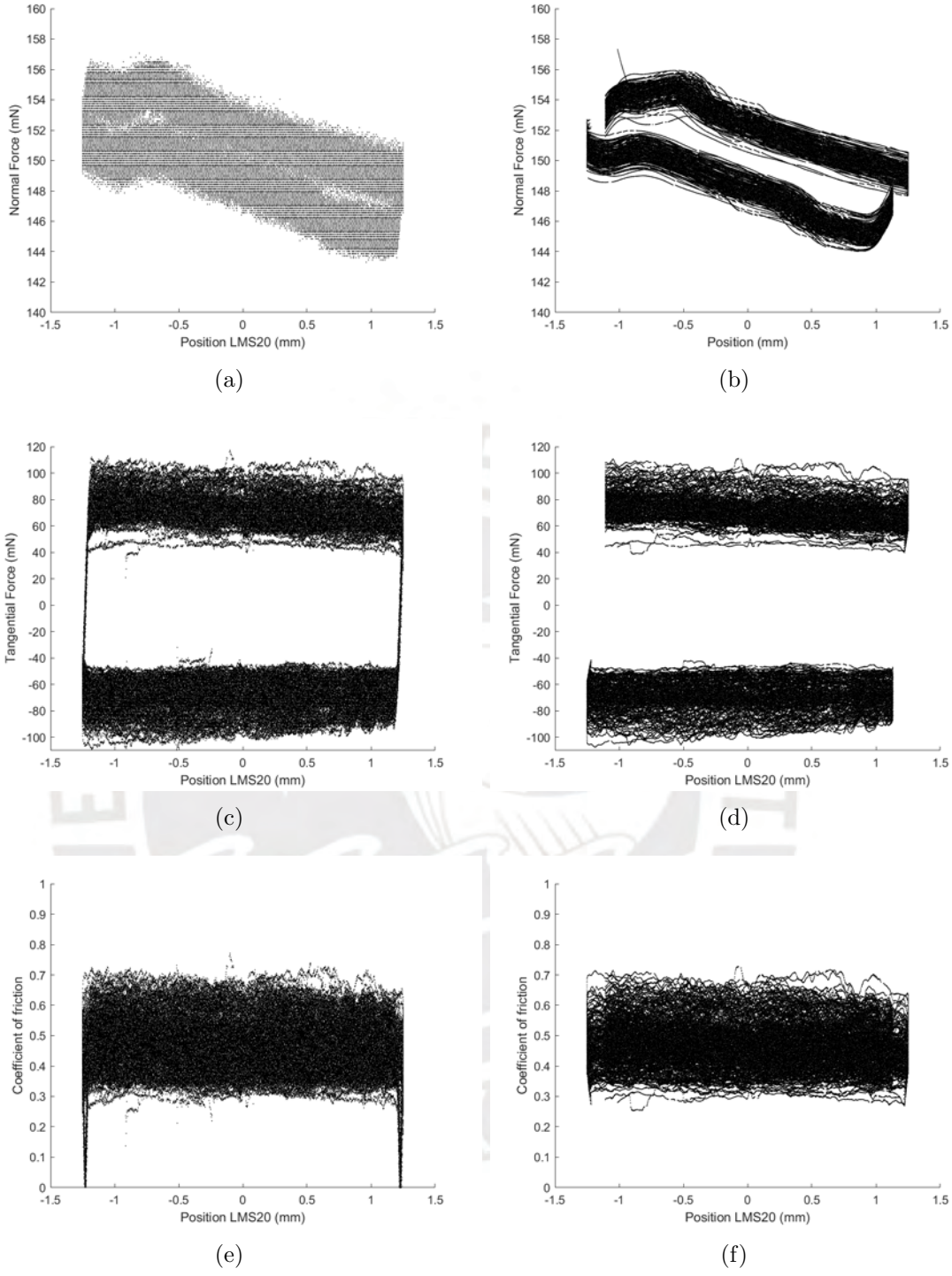

Figure 3.12: Results obtained after applying the new program to the data recorded with the LabVIEW and MATLAB programs: (a) Normal force recorded by the LabVIEW program, (b) Normal force after processing with the MATLAB program, (c) Tangential force recorded by the LabVIEW program, (d) Tangential force after processing with the MATLAB program, (e) Coefficient of friction (COF) calculated by the LabVIEW program, (f) COF after processing with the MATLAB program.

Test 7 Parameters: Set Force=150 mN, Velocity=0.5 mm/s, Total Length=1000 mm, Current=100 mA

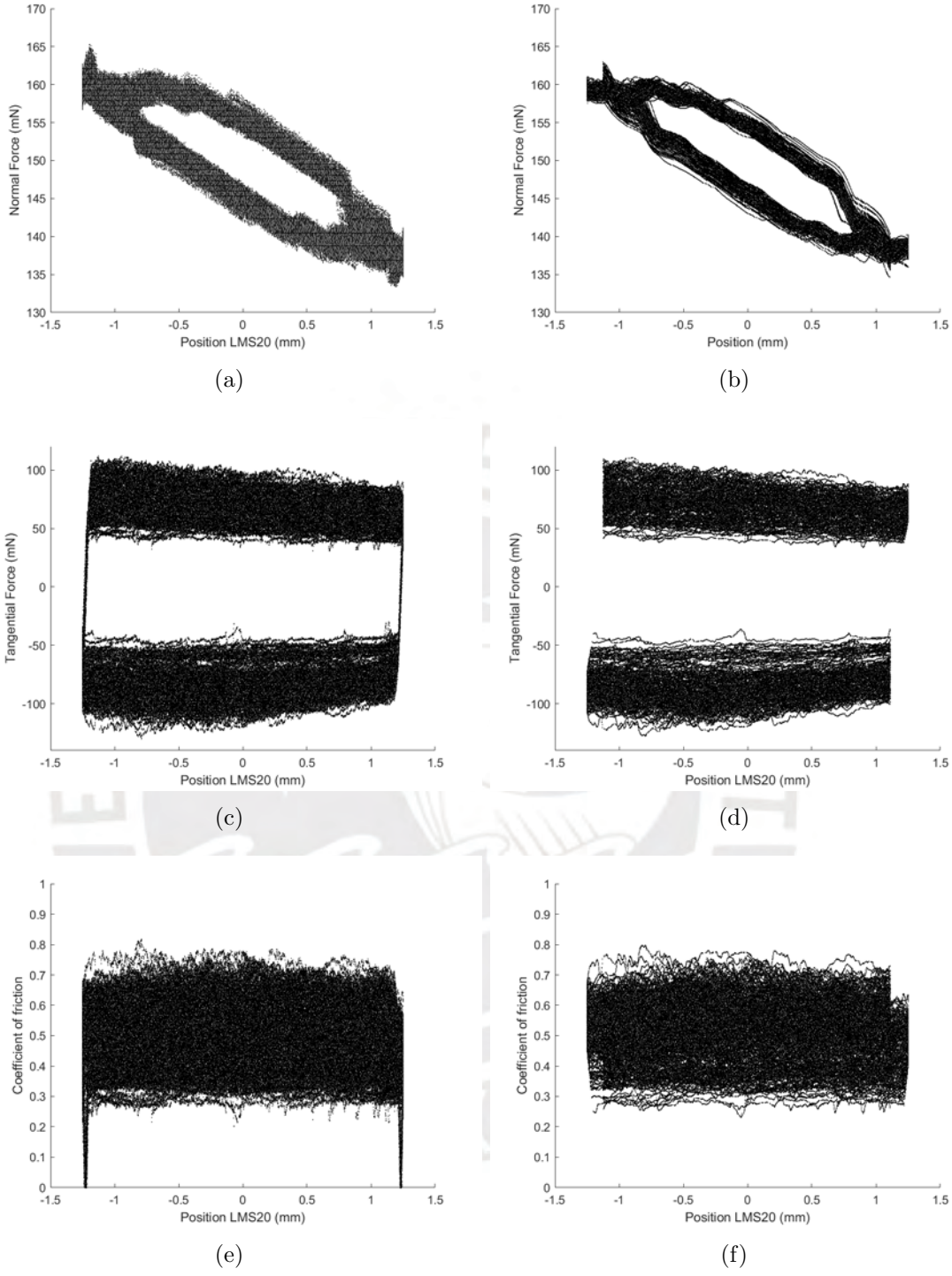

Figure 3.13: Results obtained after applying the new program to the data recorded with the LabVIEW and MATLAB programs: (a) Normal force recorded by the LabVIEW program, (b) Normal force after processing with the MATLAB program, (c) Tangential force recorded by the LabVIEW program, (d) Tangential force after processing with the MATLAB program, (e) Coefficient of friction (COF) calculated by the LabVIEW program, (f) COF after processing with the MATLAB program.

Figure 3.14, Figure 3.15 and Figure 3.16 present the COF versus total length after applying the MAT-LAB program in Test 5, Test 6 and Test 7. Figure 3.17 presents a comparative analysis of the coefficient of friction for Test 5, Test 6, and Test 7. The algorithm consistently filters out extraneous data, leading to a significant reduction in data dispersion. Additionally, the coefficient of friction values have increased with the application of current

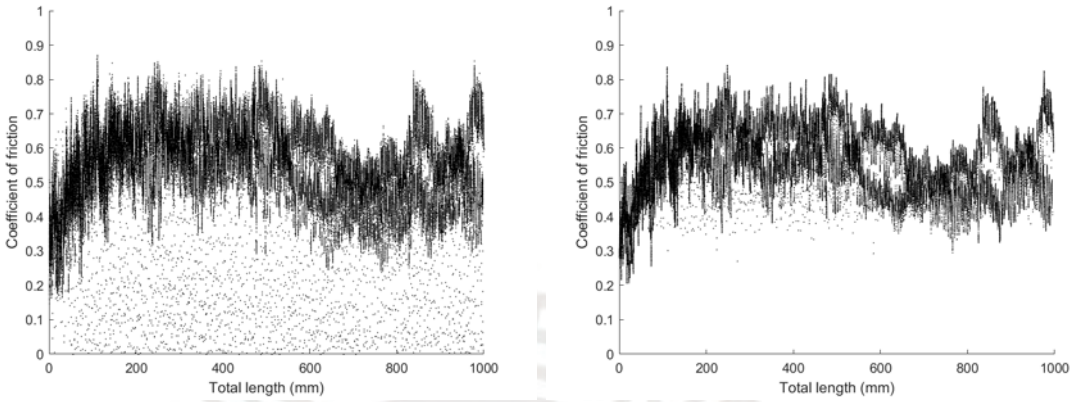

(a) (b)

Figure 3.14: Test 5: (a) COF versus total length without applying the MATLAB program. (b) COF versus the total length after applying the MATLAB program.

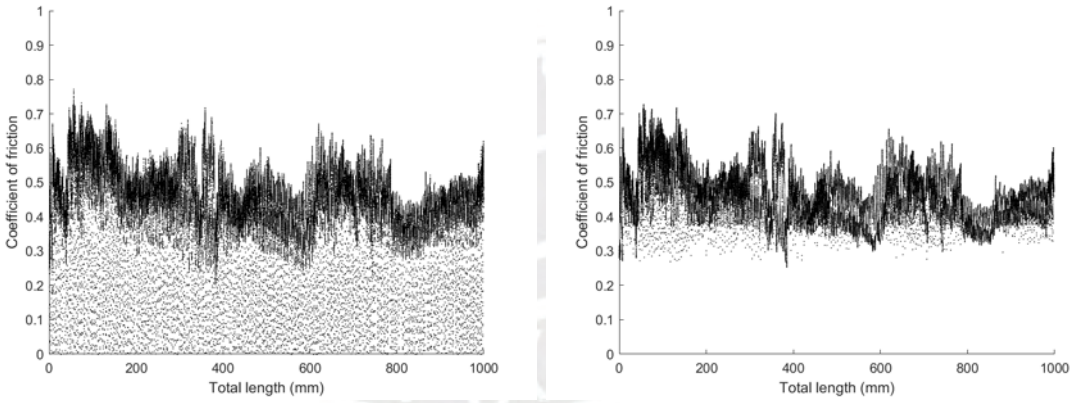

(a) (b)

Figure 3.15: Test 6: (a) COF versus total length without applying the MATLAB program. (b) COF versus the total length after applying the MATLAB program.

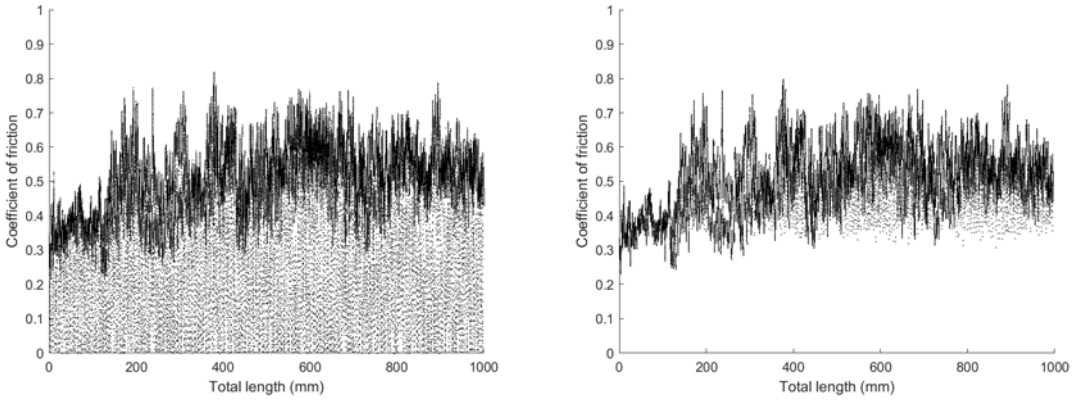

(a) (b)

Figure 3.16: Test 7: (a) COF versus total length without applying the MATLAB program. (b) COF versus the total length after applying the MATLAB program.

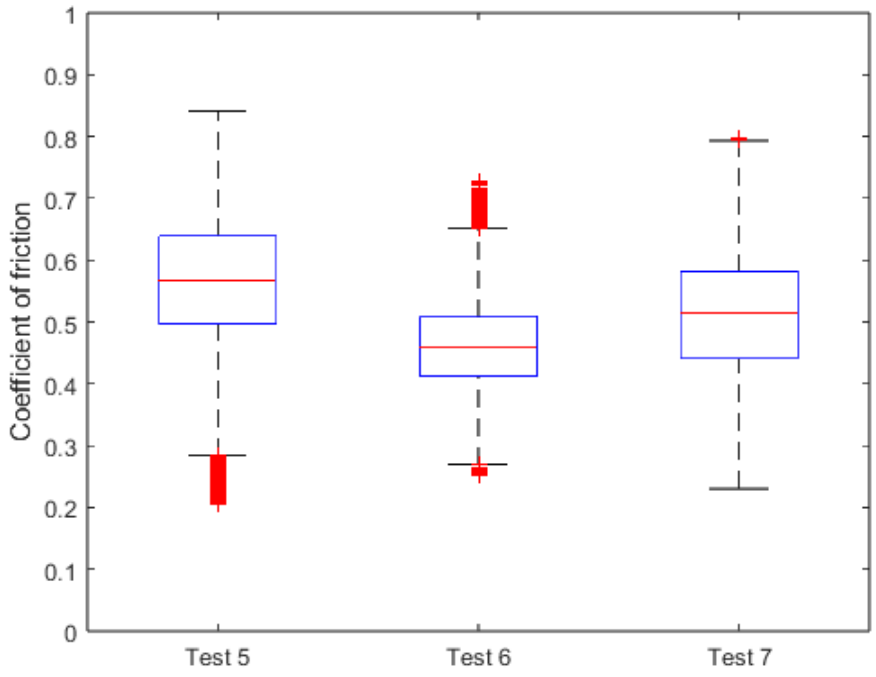

Figure 3.17: Comparative analysis of the coefficient of friction for Tests 5, Test 6, and Test 7.

Based on these results, the ranges of friction coefficient values shown in Figure 3.17 agree with those presented by Hopfeld et al. (Figure 1.41)(ref [27]). The observed data scatter can be attributed to differences in sliding velocities and cantilever characteristics, since our experiment was performed at a higher velocity.

Figure 3.18, Figure 3.19 and Figure 3.20 present the COF versus total length after

applying the MAT-LAB program , along with the behavior of the electrical properties for Test 5, Test 6 and Test 7. Figure 3.21 provides a comparative analysis of the electrical resistance for Test 5, Test 6, and Test 7. Test 5 and Test 7 exhibit similar results in the calculation of electrical resistance. The differences observed in Test 6 will be further discussed in the conclusions

Test 5 Parameters: Set Force=50 mN, Velocity=1 mm/s, Total Length = 1000 mm, Current = 100 mA

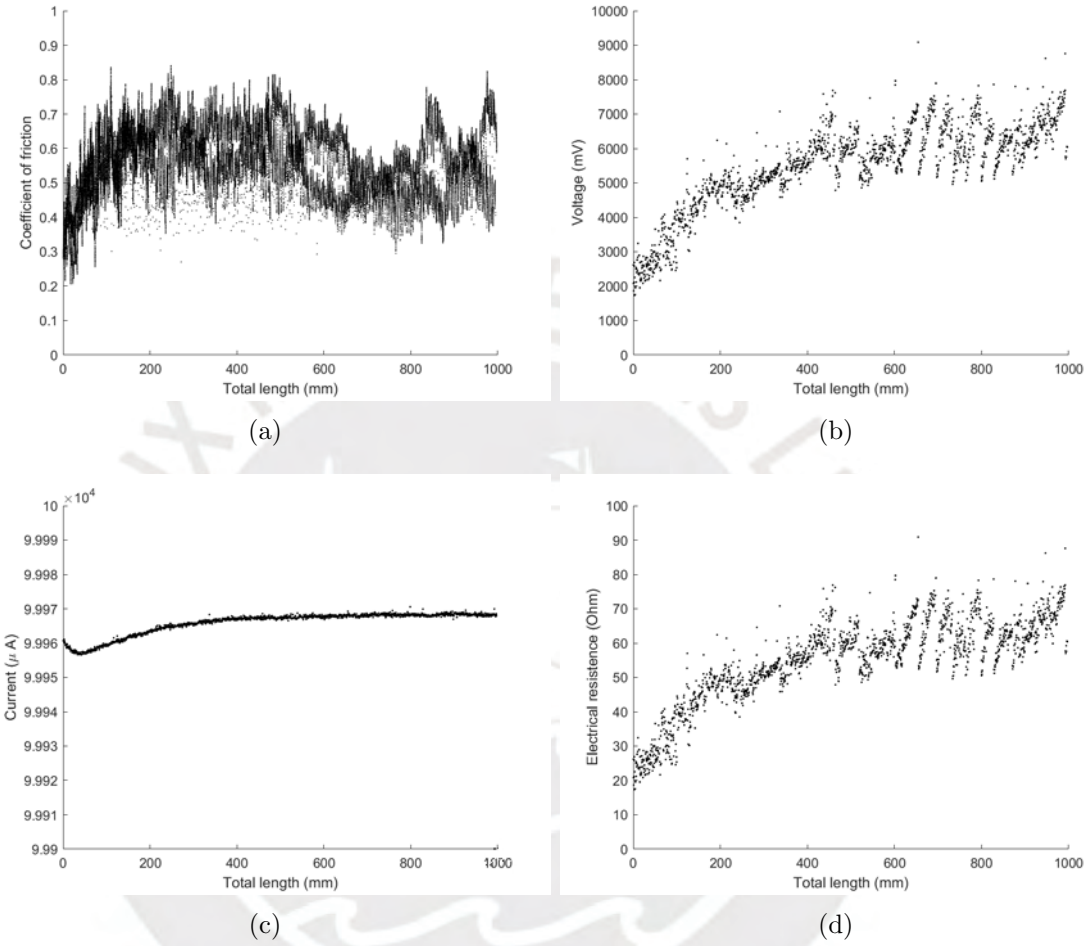

Figure 3.18: Results obtained after applying the MATLAB program to the data recorded by the LabVIEW program: (a) COF against the total length after applying the MATLAB program; (b) Voltage versus total length after applying the MATLAB program; (c) Current versus total length after applying the MATLAB program; (d) Electrical resistance versus total length after applying the MATLAB program.

Test 6 Parameters: Set Force=150 mN, Velocity=1 mm/s, Total Length = 1000 mm, Current = 100 mA

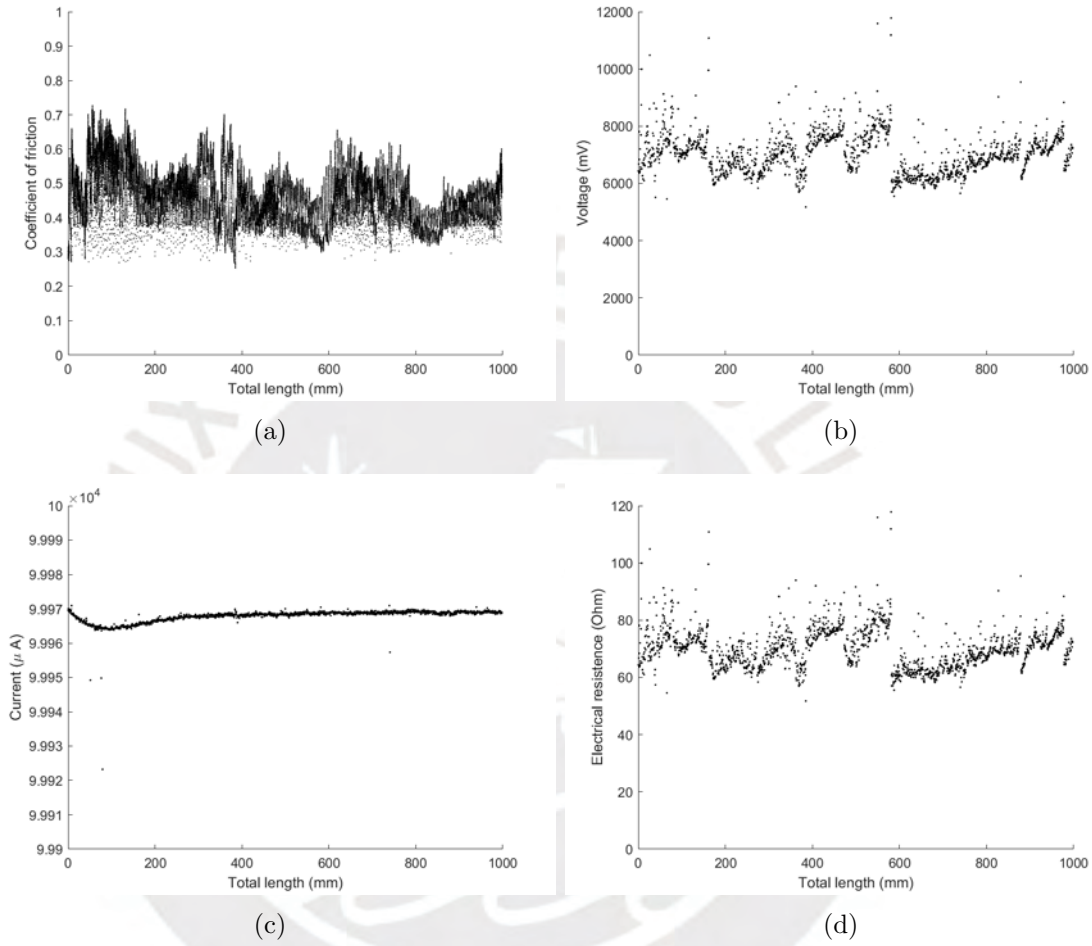

Figure 3.19: Results obtained after applying the MATLAB program to the data recorded by the LabVIEW program: (a) COF against the total length after applying the MATLAB program; (b) Voltage versus total length after applying the MATLAB program; (c) Current versus total length after applying the MATLAB program; (d) Electrical resistance versus total length after applying the MATLAB program.

Test 7 Parameters: Set Force=150 mN, Velocity=0.5 mm/s, Total Length = 1000 mm, Current = 100 mA

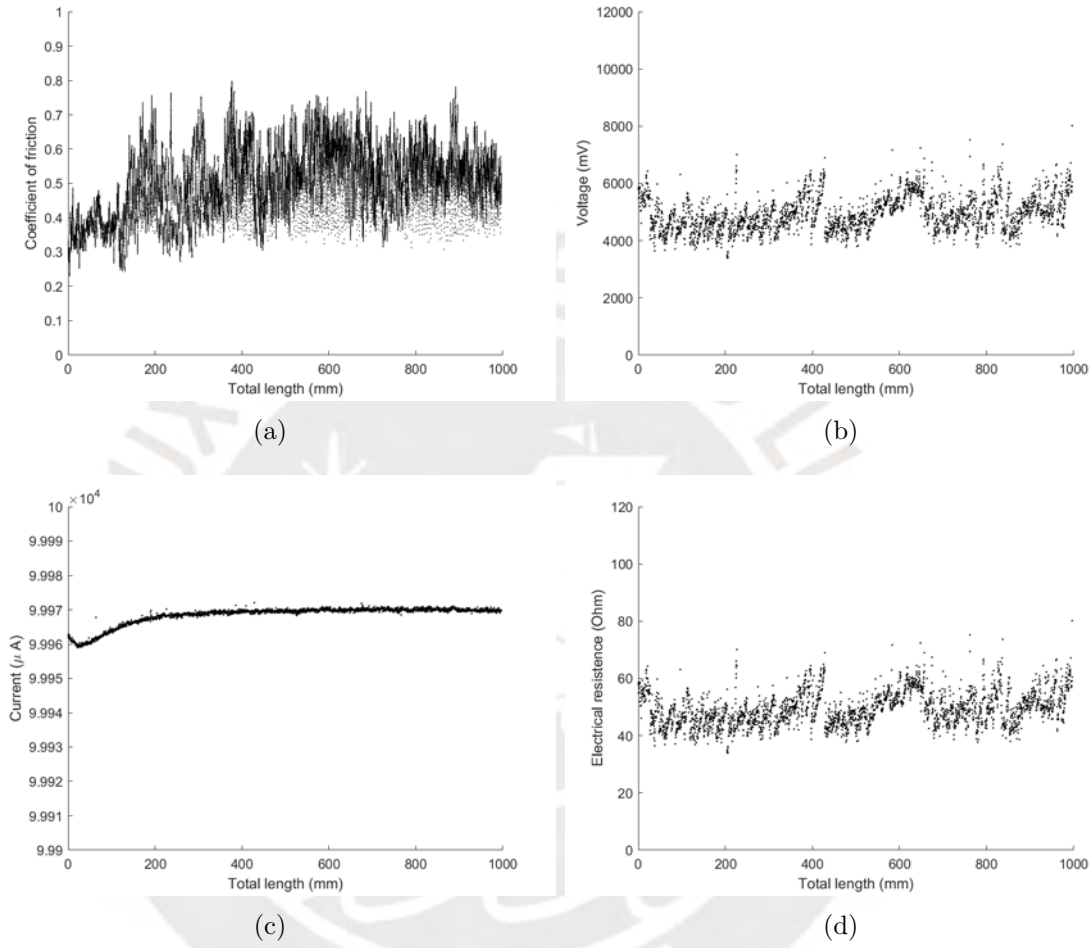

Figure 3.20: Results obtained after applying the MATLAB program to the data recorded by the LabVIEW program: (a) COF against the total length after applying the MATLAB program; (b) Voltage versus total length after applying the MATLAB program; (c) Current versus total length after applying the MATLAB program; (d) Electrical resistance versus total length after applying the MATLAB program.

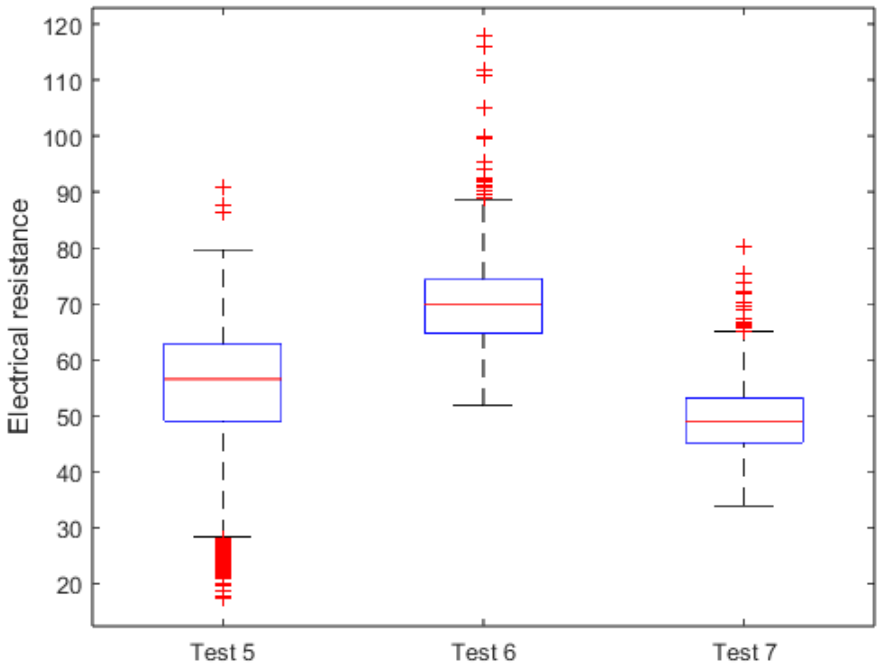

Figure 3.21: Comparative analysis of the electrical resistance for Test 5, Test 6, and Test 7.

The results presented in Figure 3.17 show a variation in the coefficient of friction ranging from 0.4 to 0.65. As theorized at the beginning of this section, the increase in current would elevate the temperature of the samples, which, in turn, would lead to an increase in the coefficient of friction. This observed trend in the coefficient of friction is consistent with the findings reported by Hopfeld et al. (Figure 1.42)(ref [27]), who also considered the temperature factor in their experiments. The variations observed in the data can be attributed to the fact that the experiments were conducted at different temperatures, which directly affects the tribological behavior of the material under investigation.

The information obtained from tests Test 1, Test 2, Test 3, Test 4, Test 5, Test 6 and Test7 is summarized in Table 3.2 and Table 3.3. The workstation recorded electrical noise in Test 1, Test 2, Test 3 and Test 4 because no electric current was applied during these tests. The table present the expected results.

Table 3.2: Results of the Test1, Test2, Test3 and Test4 performed with the workstation and the post process program based in LabVIEW.

N°	Average normal force (mN)	Average tangential force (mN)	Average COF	Variance of the COF
Test1	149.702	34.763	0.22653	0.001325
Test2	49.466	14.666	0.287792	0.026237
Test3	149.712	35.724	0.238479	0.001266
Test4	49.665	13.145	0.264472	0.001288

Table 3.3: Results of the Test5, Test6 and Test7 performed with the workstation and the post process program based in LabVIEW.

N°	Average normal force (mN)	Average tangential force (mN)	Average COF	Variance of the COF	Average Voltage (mV)	Average Current (uA)	Average electrical resistance (Ohm)	Variance of the electrical resistance
Test5	50.314	28.474	0.56616	0.00895	5481.21	99965.82	54.8305	146.101
Test6	150.130	69.921	0.46558	0.00532	7004.93	99958.53	70.0781	49.333
Test7	149.641	76.442	0.50999	0.00943	4950.05	99968.46	49.5161	34.572

First, the increase of the normal force in Test 1 and Test 3 corresponds to a reduction in the variance of the COF compared to Test 2 and Test 4, as anticipated from the error reduction. Second, the COF value decreased in Test4 compared to Test 2 due the increased in cycle speed. However, this effect diminishes with increasing sample normal force or temperature. The COF values in Test 5, Test 6 and Test 7 increased due the current flow compared with Test 4, Test 3 and Test 1.

Additionally, it is important to mention that the results in Test 2 and Test 6 exhibit irregularities. As illustrated in Figure 3.4d , the tangential force is not symmetrical, unlike the other tests. In Figure 3.4b, the effect of the correction algorithm is evident; however, it was insufficient to eliminate the presence of two distinct behaviors of the friction coefficient during the experiment, as shown in Figure 3.7. Among the possible causes of this error we can suppose an error in placing the sample in the system, the low force at which it performs the experiment or some deformity in the sample.

In Test 6, irregularities were observed in the voltage value, as shown in Figure 3.19b. Although there is a minimal change in the tribological properties, the change at the electrical level is considerable. After a detailed analysis of the experiments, the following hypothesis is proposed: Test 5 and Test 6 were conducted sequentially using the same sample but with different applied forces. It is suggested that in Test 5, the

electrical properties of the sample may have changed due to the action of the current or due to potential errors during the assembly of the experiment, which increased its electrical resistance by the end of the test. Notably, the electrical resistance value at the conclusion of Experiment 5 is very similar to that observed throughout Experiment 6. In Experiment 7, the sample was replaced, and the assembly was performed more meticulously, resulting in consistent behavior throughout the experiment and the smallest variation in the results (Table 3.3).

CHAPTER 4

Conclusions

The designed triboelectrical workstation has successfully met the objectives outlined for this thesis. The workstation employ a tribometer using a pin-on-disk procedure, along with Keithley modules utilizing the four points method, to record tribological and electrical data of a$Cr_2AlC - MAX - Phase$ thin Film sample in real time. One of the key challenges identified in previous work, synchronizing the tribometer with the Keithley modules, was effectively resolved by implementing advanced algorithms and refined experimental procedures.

1. **Improve the accuracy of the normal force control:**
   The LabVIEW program, which controls the entire system, demonstrated a significant improvement in the accuracy of normal force control. The program allows users to configure the modules and tribometer, calibrate sensors, set experimental parameters, and execute the experiment. The system successfully maintained accurate force control during both the initial approach and the ongoing experiment, which meets the objective of improving the accuracy of the normal force measurement.

2. **Address current fluctuations during the experiment:**
   The program designed in LABVIEW ensured that fluctuations in current were effectively minimized, guaranteeing relevant electrical data of the experiment. This stability was crucial for achieving accurate tribological measurements and meeting the goal of addressing current fluctuations during the experiments.

3. **Establish reliable communication between system components:**
   The system's design achieved communication between the Keithley modules, tribometer, and computer. Using LabVIEW, the system provided real-time control, which is essential for simultaneous and synchronized data acquisition.

4. **Improve the graphical user interface (GUI):**
   The graphical user interface (GUI) in LabVIEW was optimized, making it intuitive for users to navigate step by step through the testing process. The GUI provides users with full control over the experimental parameters, further enhancing the system's usability and meeting the objective of improving the user interface.

5. **Simultaneously record electrical and tribological data:**
   A key feature of the system was its ability to record both electrical and tribological data simultaneously during the experiment. This integrated data acquisition allowed for a comprehensive analysis of the sample's behavior under varying conditions, thus fulfilling the objective of simultaneous data recording.

6. **Develop a MATLAB-based post-processing tool to filter irrelevant data:**
   The MATLAB program developed as part of this thesis successfully filtered and processed the recorded data. Using specific algorithms and filters, irrelevant data points were removed, ensuring that only relevant test data were retained. This met the objective of developing a post-processing tool to clean the data before further analysis.

7. **Compare the experimental results with previous studies:**
   The experimental results obtained from this study were compared to results from previous research, particularly the work by Hopfeld et al. The data demonstrated consistency with established materials engineering theory, validating the effectiveness and reliability of the triboelectrical workstation. This comparison confirmed that the developed system successfully met the objective of benchmarking the experimental results against previous studies.

The values of the friction coefficients obtained in Test 1, Test 3, and Test 4 ranged from 0.2 to 0.3 (Figure 3.10), with a low variance (0.001, Table 3.2). The behavior of these coefficients throughout the experiments is shown in Figure 3.3, Figure 3.8 and Figure 3.9. Although the tests were performed under different force and velocity conditions, the results obtained, as well as the behavior of the friction coefficients during the experiments, are consistent with the findings reported by Hopfeld in his studies, cited in this document (Section 1.2.4).

In Test 5 and Test 7 the experiments were repeated, adding this time an electric current of 100 mA (Figure 3.11 and Figure 3.13). In these cases, the friction coefficient increased significantly, ranging from 0.4 to 0.65 (Figure 3.17), with a higher variance (0.009, Table 3.3) compared to the previous experiments. This trend was to be expected, since theory predicts that the inclusion of current in the process leads to an increase in sample temperature. In fact, as Holfeld's results show, the increase in temperature results in a significant increase in the coefficient of friction.

The calculated electrical resistance varied between 45 and 65 ohms (Figure 3.21, Table 3.3). This behavior can be attributed to the type of contact of the electrical connectors, as well as to the interpolation algorithm used to record the current and voltage during the tests.

Future work could focus on improving the sample clamping mechanism by employing a more effective sample holder for the tribometer. Additionally, conducting more

experiments with varying current levels would provide deeper insights into the material's tribological behavior under different electrical conditions. The incorporation of temperature recording would enhance the ability to compare the results obtained from this system with those from other studies, offering a more comprehensive analysis of the material's performance under controlled temperature variations.

Bibliography

[1] Nikolai Braunovic, Milenko and Konchits, Valery and Myshkin. *Electrical Contacts: Fundamentals, Applications and Technology*. 2007.

[2] Paul G. Slade. *Electrical Contacts: Principles and applications*, volume 158. 2 edition edition, 2003.

[3] Keithley Instruments. *Model 2000 Multimeter User's Manual*. Number August. 2010.

[4] Keithley Instruments. *Model 2400 Series SourceMeter User's Manual*. 2002.

[5] Edson Yupanqui. Implementation of a triboelectrical workstation for the investigation of the influence of electrical current on the tribological properties of thin films. 2016.

[6] A. Sethuramiah and Rajesh Kumar. Fundamental Approaches to Chemical Wear Modeling. *Modeling of Chemical Wear*, pages 105–128, 2016.

[7] Valentin L. Popov. *Kontaktmechanik und Reibung*, volume 53. 2013.

[8] Anthony C. Fischer-Cripps. *Introduction to Contact Mechanics*. 2006.

[9] Bharat Bhushan. *Introduction to Tribology, Second Edition*. 2013.

[10] A. Sethuramiah and Rajesh Kumar. Lubricants and Their Formulation. *Modeling of Chemical Wear*, pages 25–39, 2016.

[11] I.M. Hutchings. *Tribology : Friction and Wear of Engineering Materials*. 1992.

[12] Mohamed A. Hussein, Abdul Samad Mohammed, and Naser Al-Aqeeli. Wear characteristics of metallic biomaterials: A review. *Materials*, 8(5):2749–2768, 2015.

[13] J E Shigley and R G Budynas. *Mechanical Engineering Design*, volume New York,. 2015.

[14] C. Mathew Mate. *Tribology on the Small Scale*. Oxford University Press, 2008.

[15] Luis Fernández Ruiz-Morón. *Desarrollo De Un Procedimiento Para El Cálculo De La Fuerza De Fricción En Un Contacto Ehd. Validación Experimental Del Procedimiento*. PhD thesis, 2012.

[16] G Dyos. *The Handbook of Electrical Resistivity The Handbook of Electrical Resistivity*. 2012.

[17] P.L. Rossiter. The electrical resistivity of metals and alloys. 1987.

[18] John G. Webster and H. Eren. *Measurement, Instrumentation and Sensors. The Handbook*. 1999.

[19] Jerry Janesch. Two-Wire vs. Four-Wire Resistance Measurements: Which Configuration Makes sense for Your Application? (May):2–4, 2013.

[20] Tetra GmbH. System documentation BASALT®-MUST Precision Tester. page 67, 2004.

[21] National instruments. *NI PXI-1042 Series User Manual*. 2004.

[22] National instruments. *NI PXI-8105 User Manual*. 2007.

[23] Keithley Instruments Inc. *Model KUSB-488B USB to GPIB Converter Reference Manual*. Number March. 2010.

[24] Nestor Forero. Normas de Comunicación en Serie: RS-232, RS-422 y RS-485. page 67, 2012.

[25] José Carlos Macavilca and Diego Ricardo Cárdenas. Improvement of a triboelectrical workstation used to obtain the properties of thin films, 2016.

[26] Beatriz Nuñez. Procesamiento y caracterización de materiales porosos de fases MAX. page 304, 2018.

[27] Marcus Hopfeld, Rolf Grieseler, Anneka Vogel, Henry Romanus, and Peter Schaaf. Tribological behavior of selected mn+1axn phase thin films on silicon substrates. *Surface and Coatings Technology*, 257:286–294, 2014. 25 years of TiAlN hard coatings in research and industry.

User interface

1 Previous user interfaces

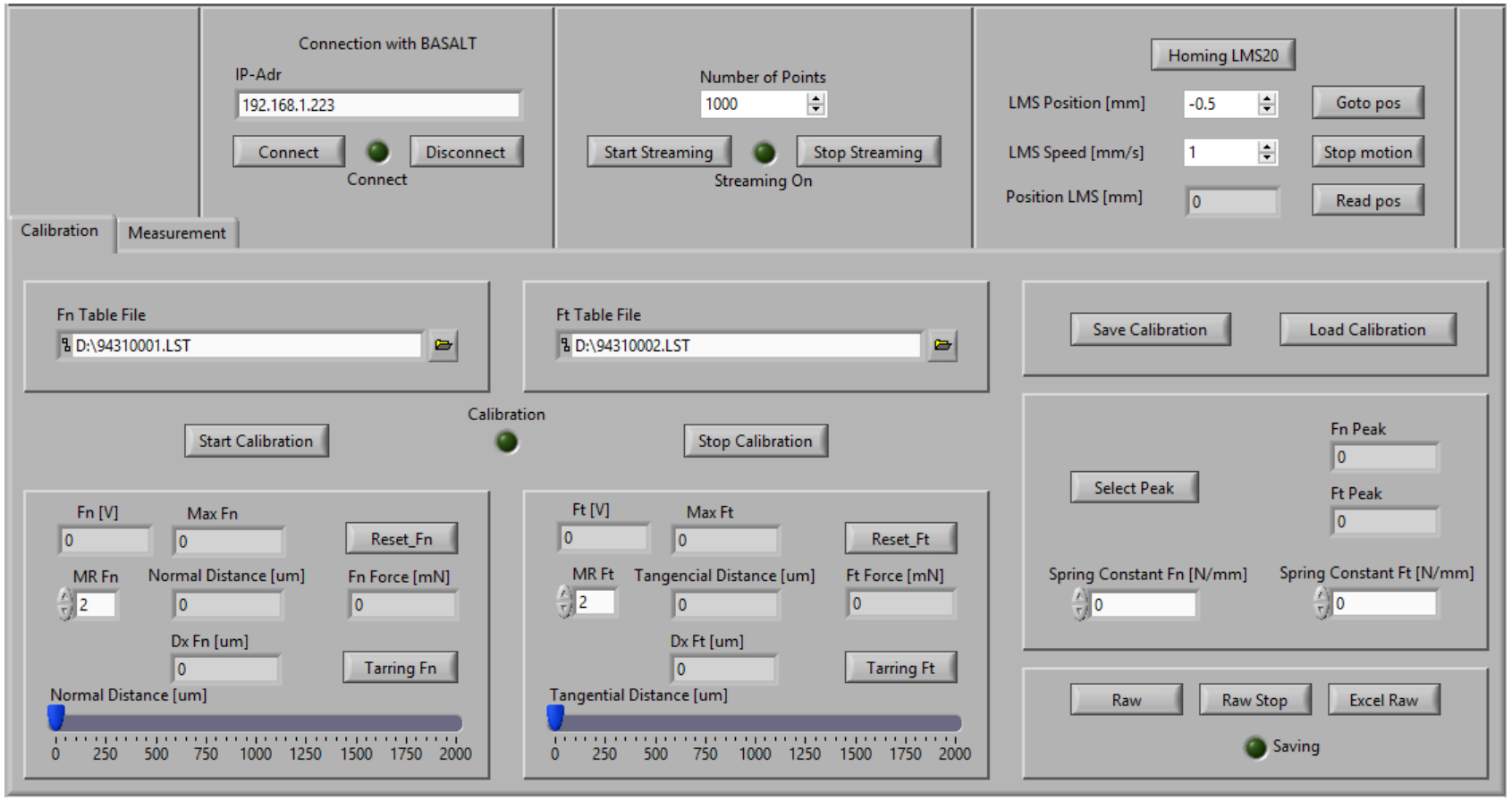

Figure 6.1: User interfaces of the previous work (calibration tab) .

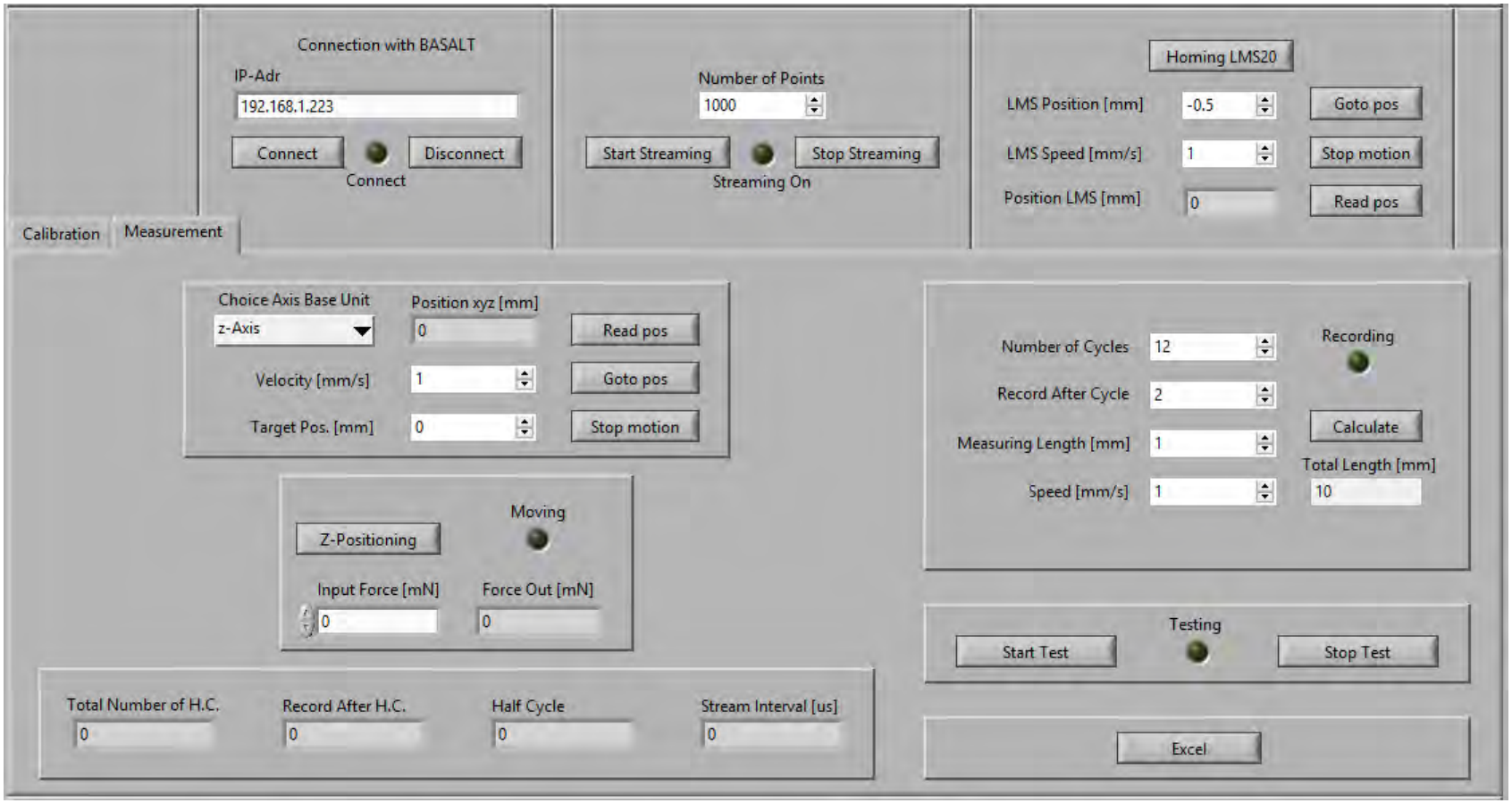

Figure 6.2: User interfaces of the previous work (Testing tab).

2 New user interfaces

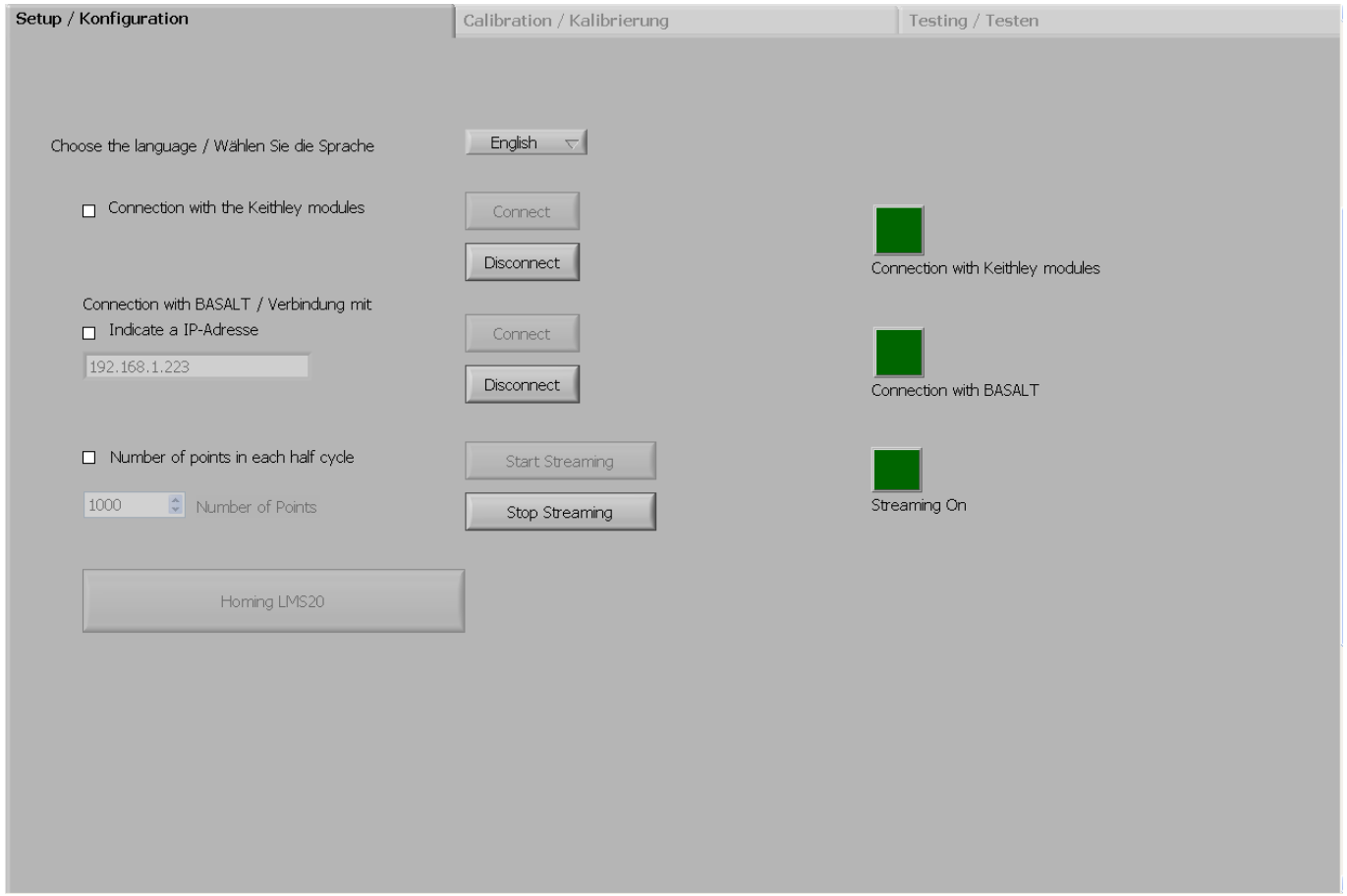

Figure 6.3: New user interfaces (Setup tab).

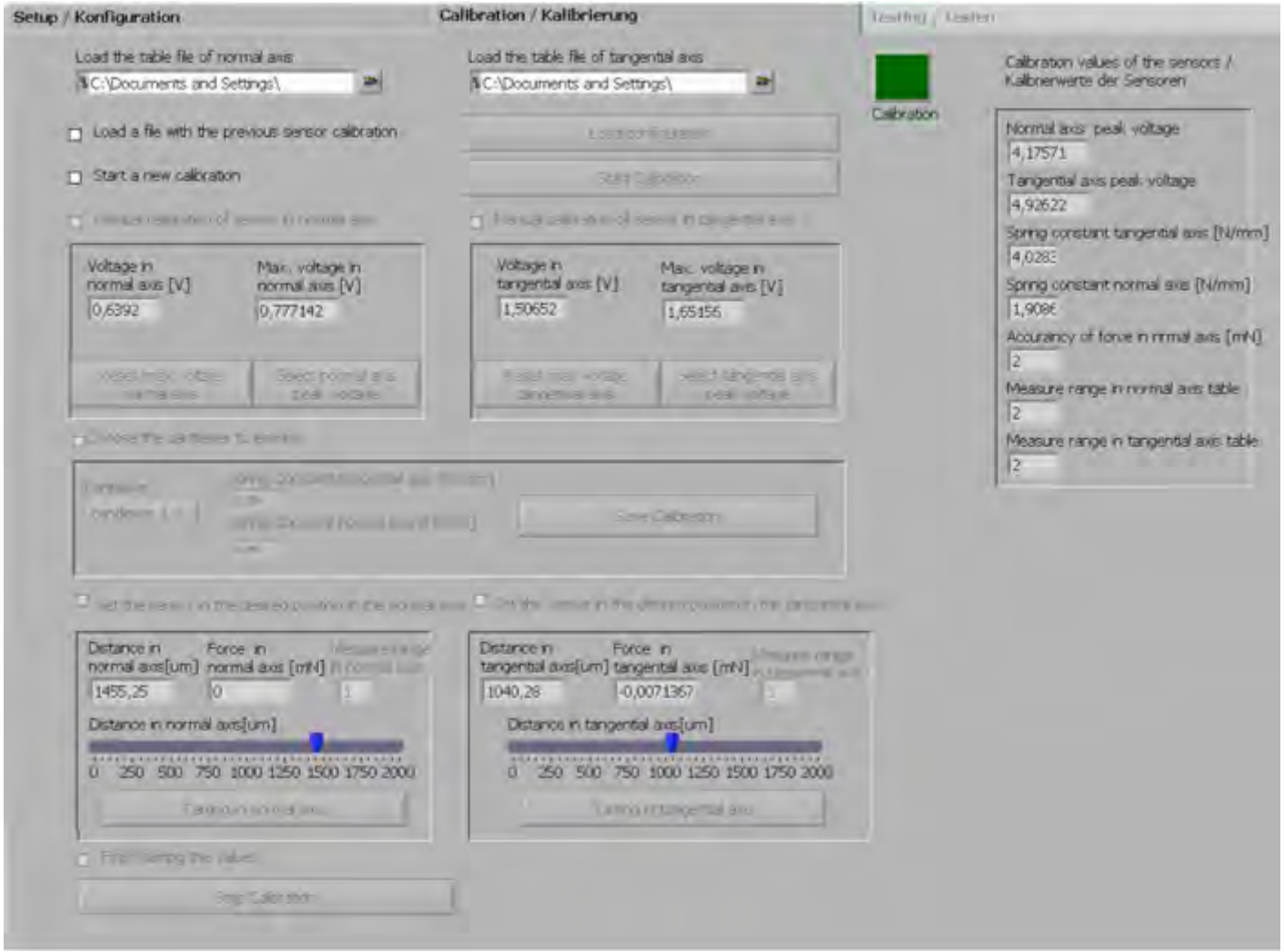

Figure 6.4: New user interfaces (Calibration tab).

Figure 6.5: New user interfaces(Testing tab).

Upgrades to the Labview Program

1 Enhancement in the Tribological Section

1.1 Calibration updates

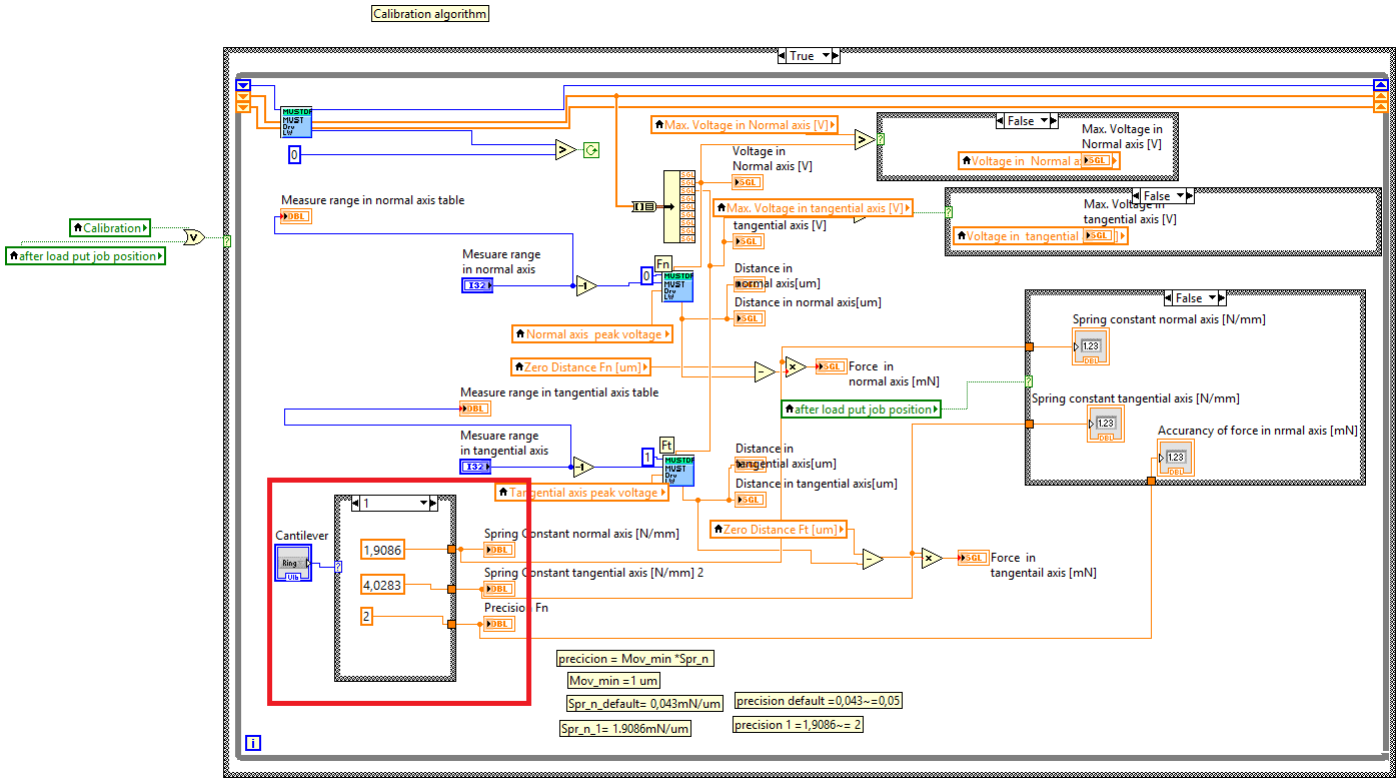

Figure 7.1: The new algorithm for calibrating the tribometer and setting the necessary values for the tribological experiment. The red square highlights the section that allows adjusting the normal force depending on the cantilever used

1.2 Updates to the algorithm for setting the initial normal force.

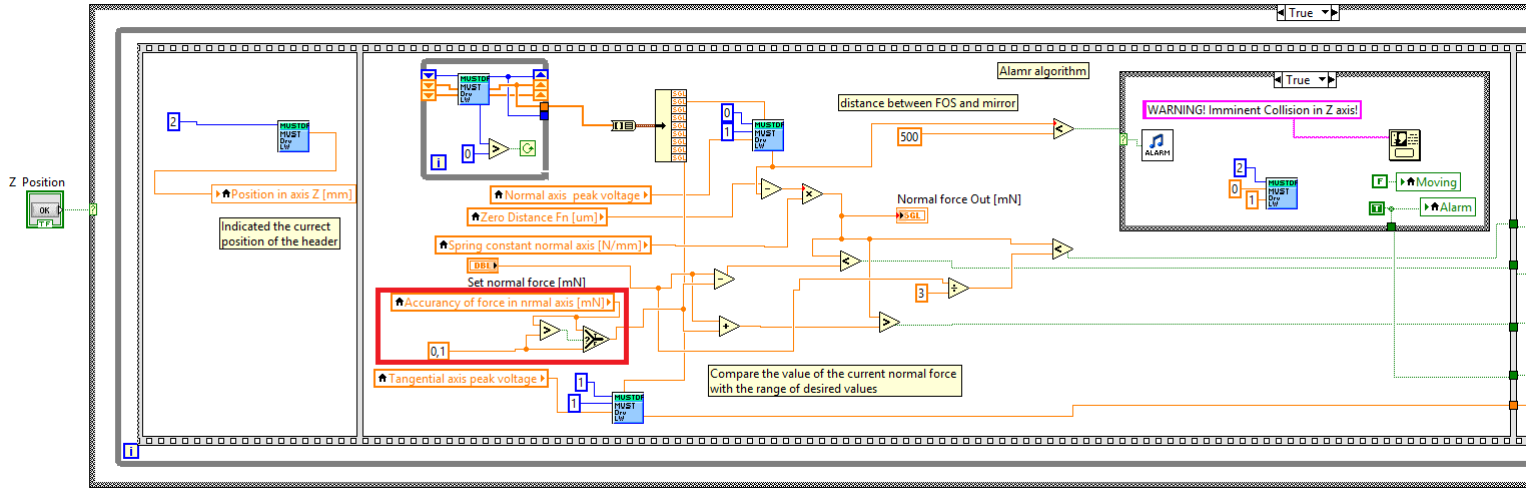

Figure 7.2: The new algorithm to increase the accuracy when setting the initial normal force. The red square shows the use of the precise normal force to calculate the acceptable limits(a)

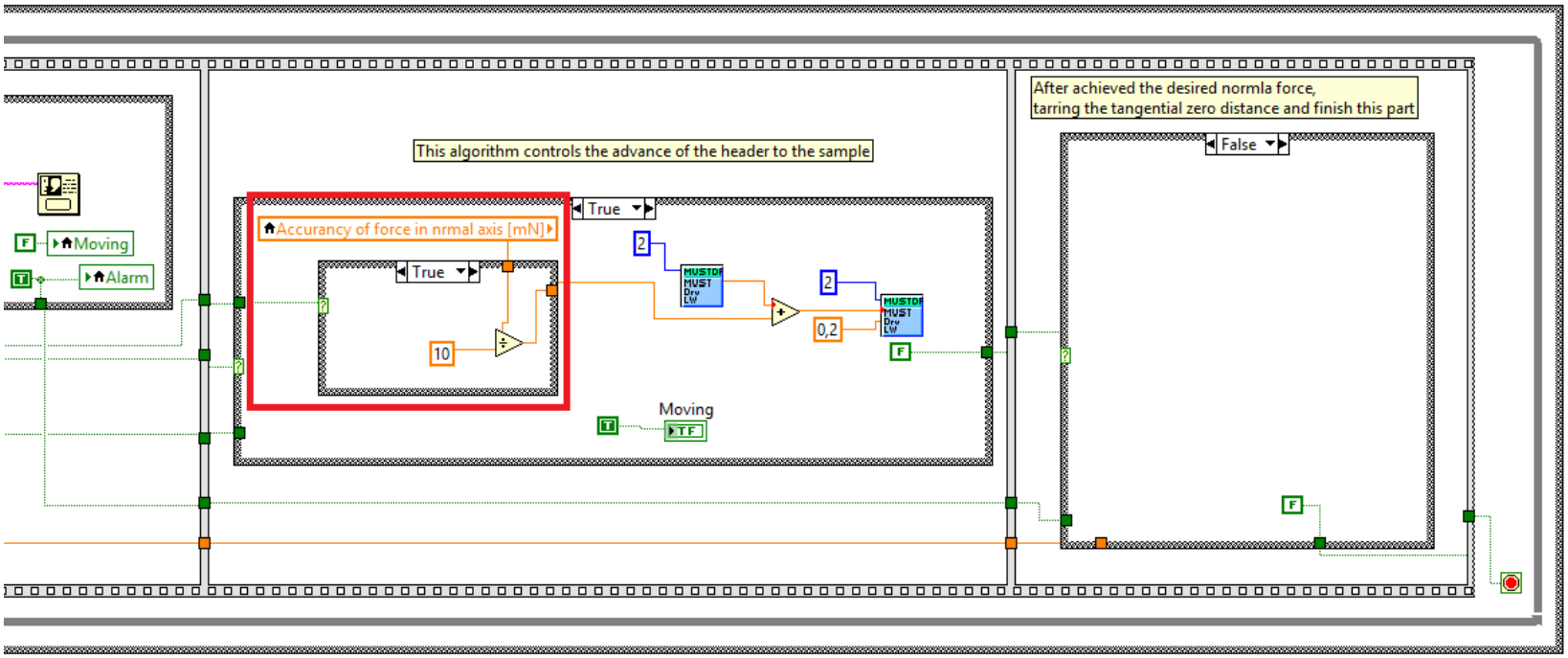

Figure 7.3: The new algorithm to increase the accuracy when setting the initial normal force. The red square shows that the first approximation depends on the accuracy of the normal force(b).

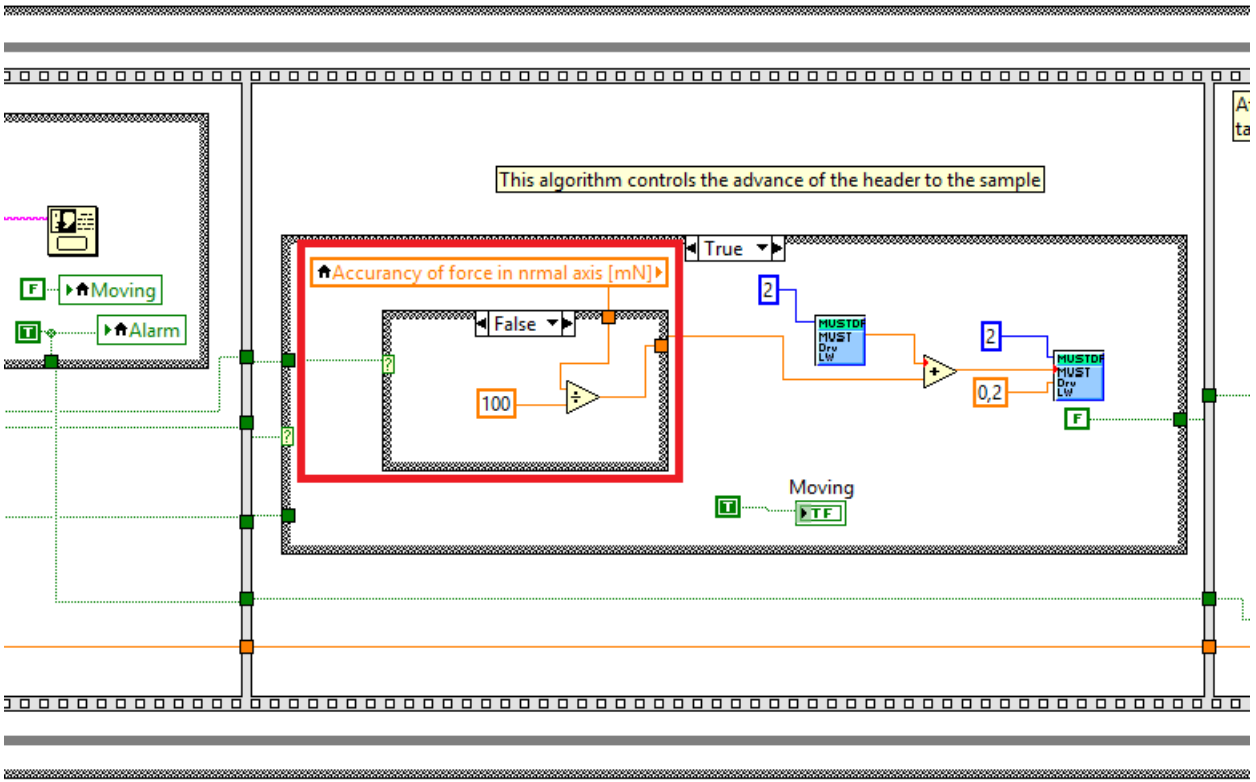

Figure 7.4: The new algorithm to increase the accuracy when setting the initial normal force. The red square shows that the second approximation depends on the accuracy of the normal force (c).

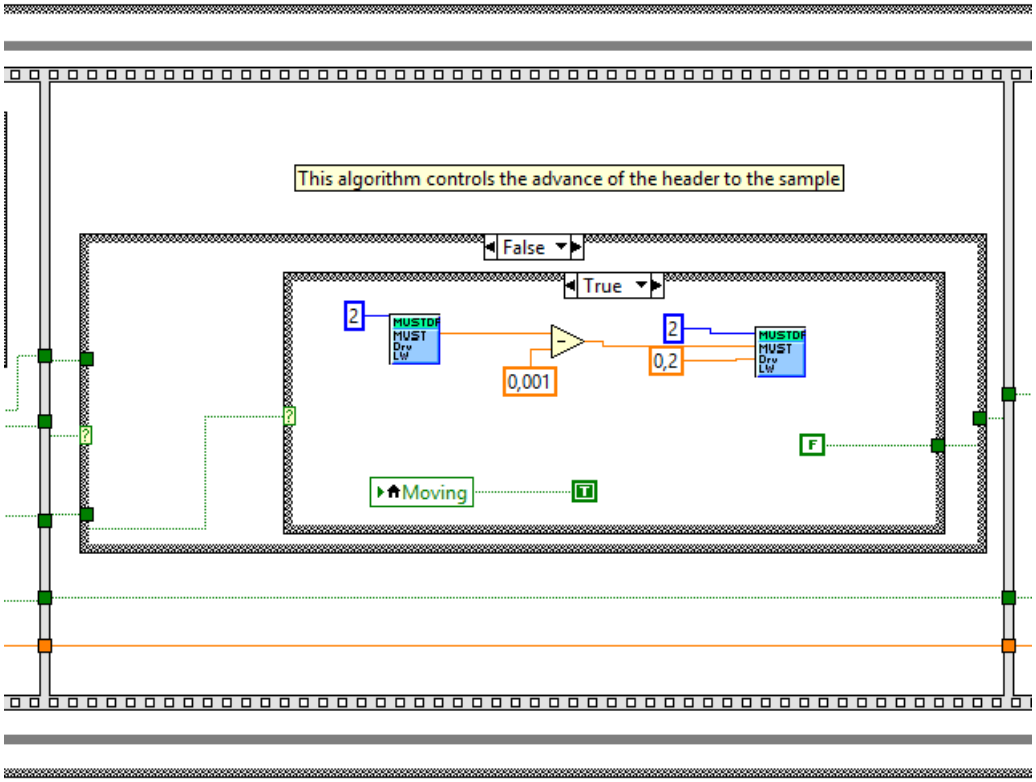

Figure 7.5: The new algorithm to increase the accuracy when setting initial normal force. The regression value is chosen due to the physical limits of the tribometer (d).

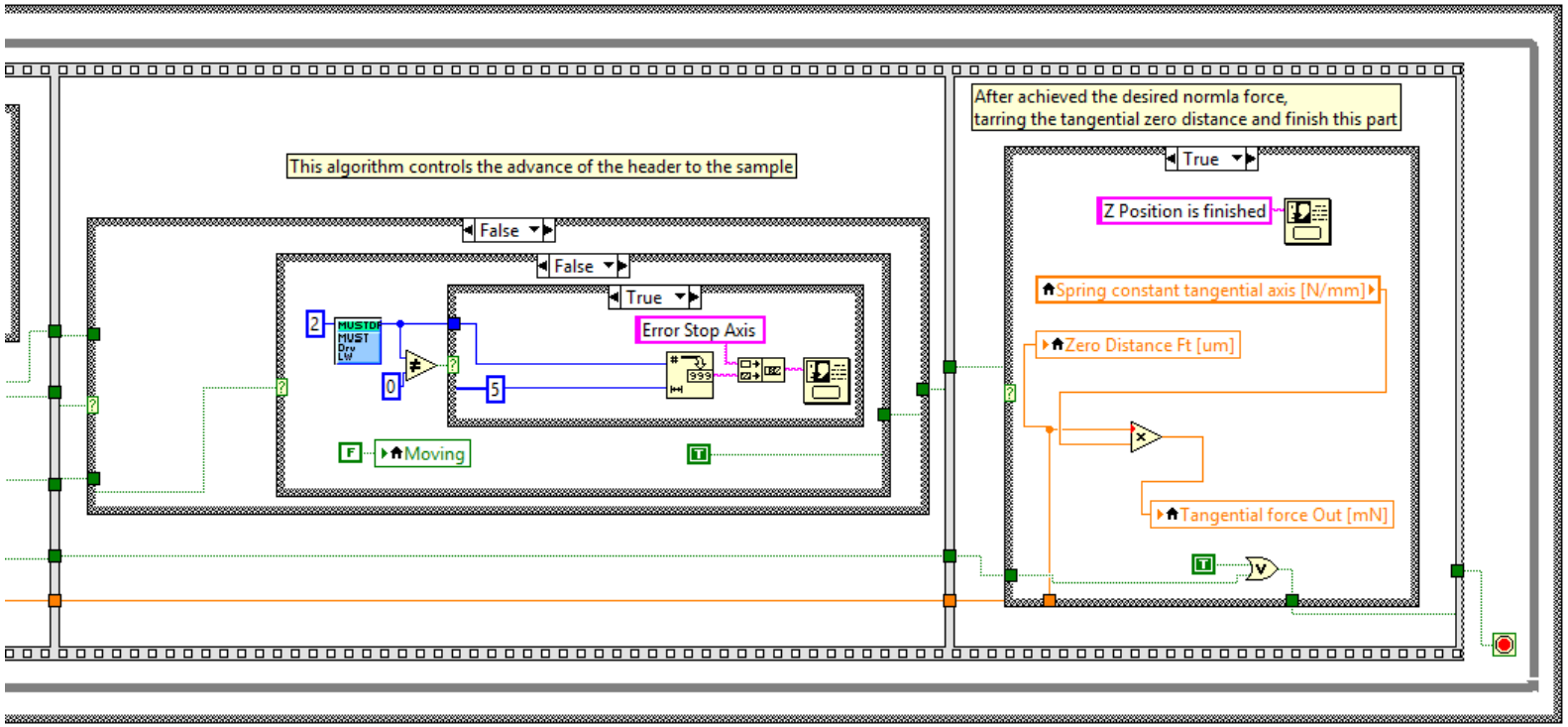

Figure 7.6: The new algorithm to increase the accuracy when setting the initial normal force. Finish process to set the initial normal force(e)

1.3 Updates to the algorithm for maintaining a constant normal force

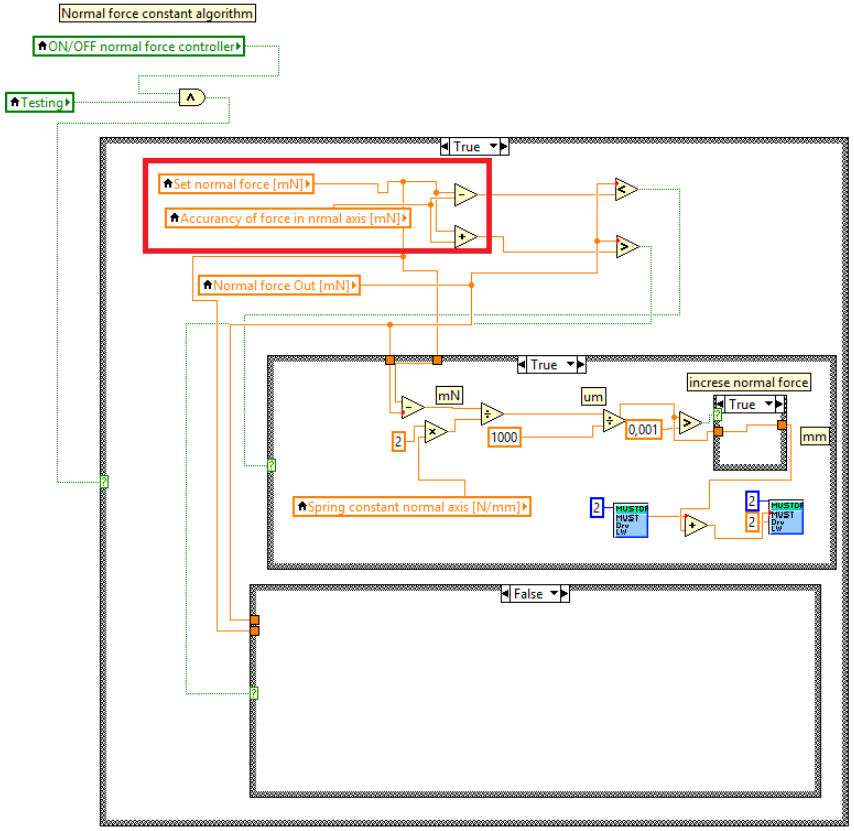

Figure 7.7: The new algorithm for maintaining the normal force within the desired range of values throughout the experiment. The red square shows the normal force and the maximum deviation to calculate the limits of the normal force (a).

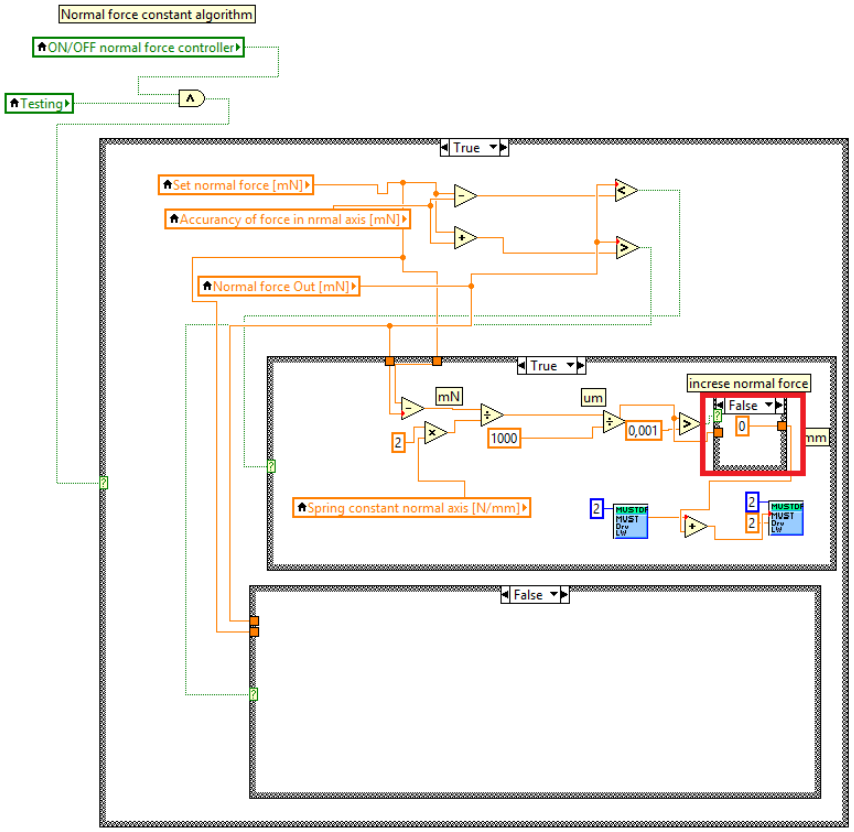

Figure 7.8: The new algorithm for maintaining the normal force in the desired range of values throughout the experiment. This case applies when the value of the normal force is less than the acceptable range. The red square shows the limit of the adjustment to be made by the algorithm (b).

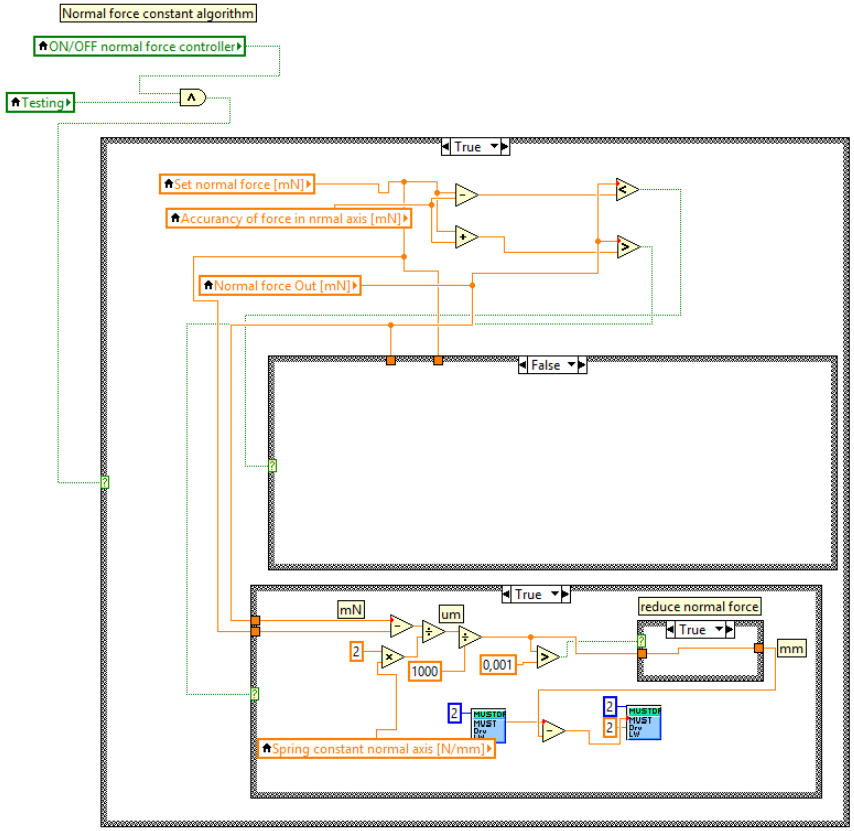

Figure 7.9: The new algorithm for maintaining the normal force within the desired range of values throughout the experiment. This case applies when the value of the normal force is greater than the acceptable range (c).

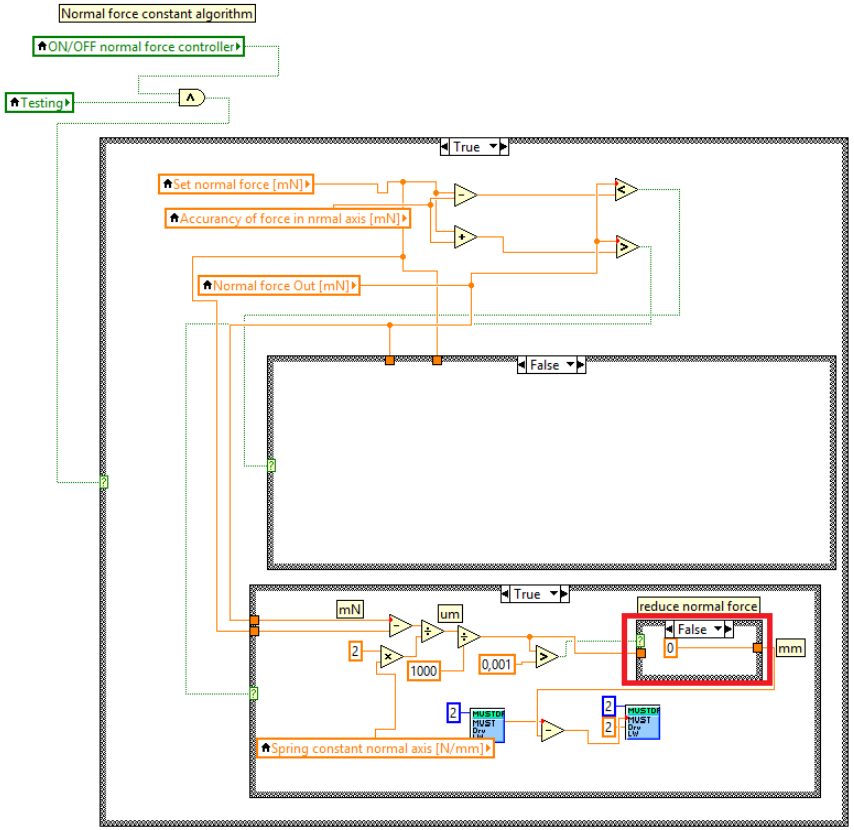

Figure 7.10: The new algorithm for maintaining the normal force within the desired range of values throughout the experiment. This case applies when the value of the normal force is greater than the acceptable range. The red squared shows the limit of the adjustment to be made in this part (d).

2 Enhancement in the electrical section

2.1 Connection and disconnection events

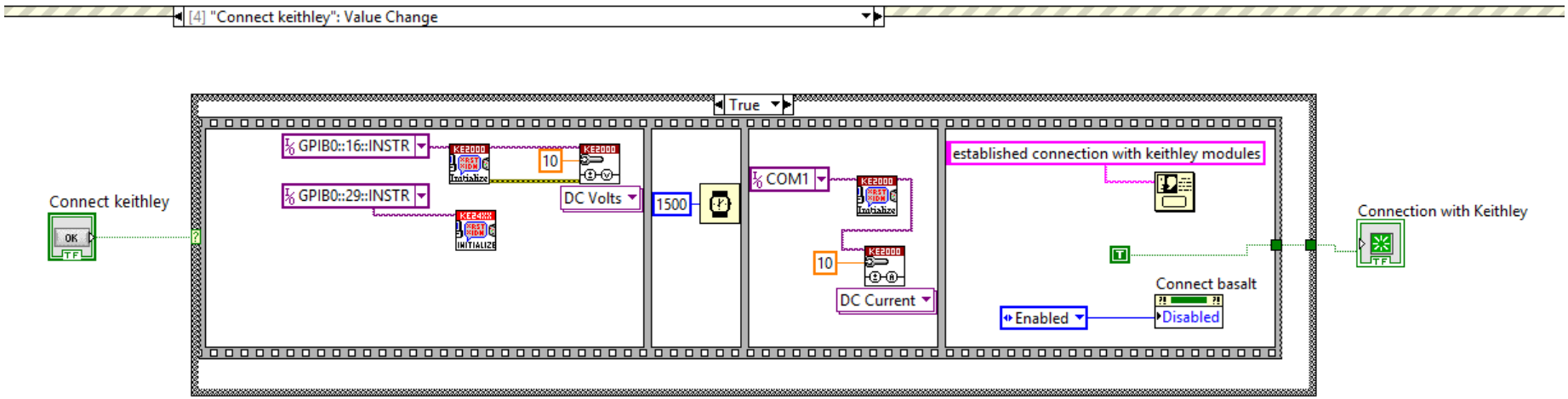

Figure 7.11: Event that shows the connection between the workstation and the keithley module (Ethernet or GPIB bus).

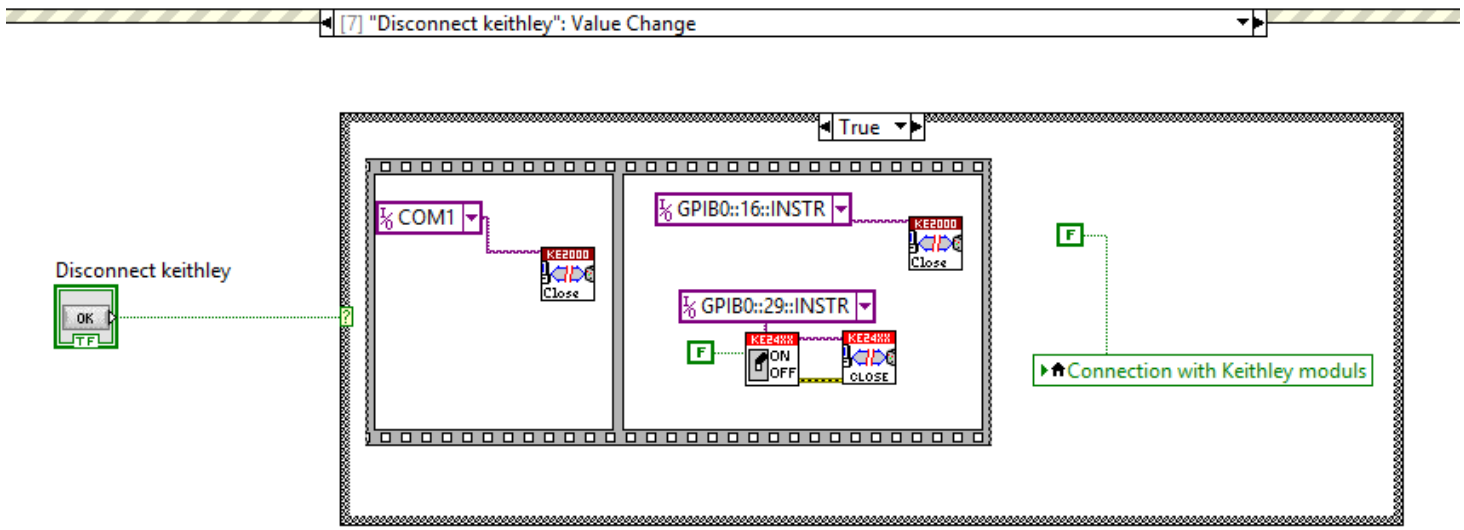

Figure 7.12: Event that shows the disconnection between the workstation and the keithley module (Ethernet or GPIB bus).

2.2 Streaming start event update

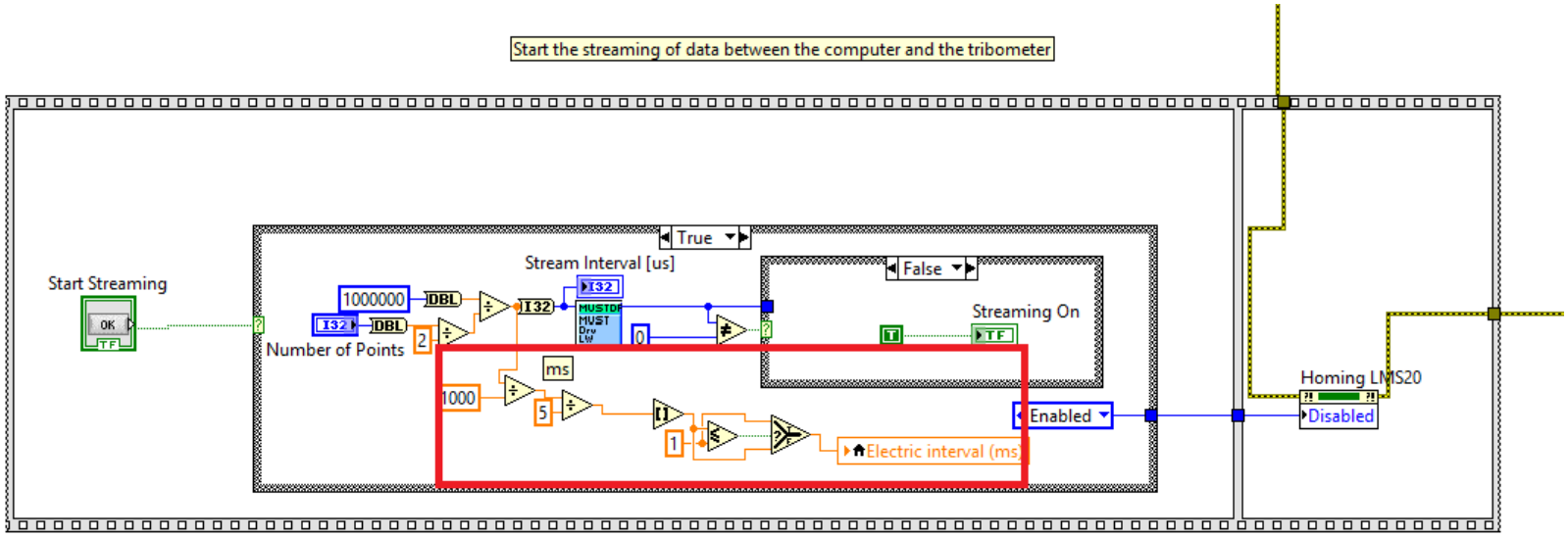

Figure 7.13: In the Start Streaming event of the tribologic program, the new program calculates the electrical interval (ms). This process is shown in the red square, the electrical interval is calculated and the value is limited by the minimum unit (1 ms) that the LabVIEW can used with the new programmed libraries.

2.3 Setting the power source

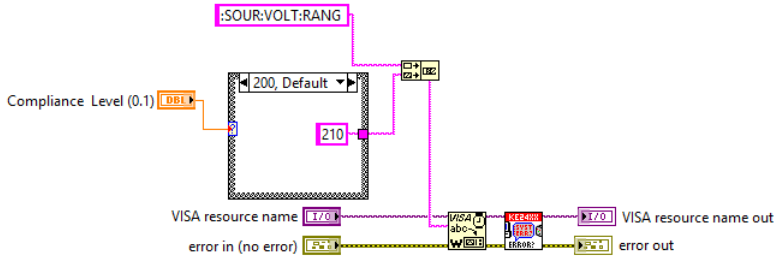

Figure 7.14: This Sub VI performs the configuration of the maximum compliance value required by the Keithley 2400 when this module is configured as a current source. The current value that is configured in the module is set by the user in each test..

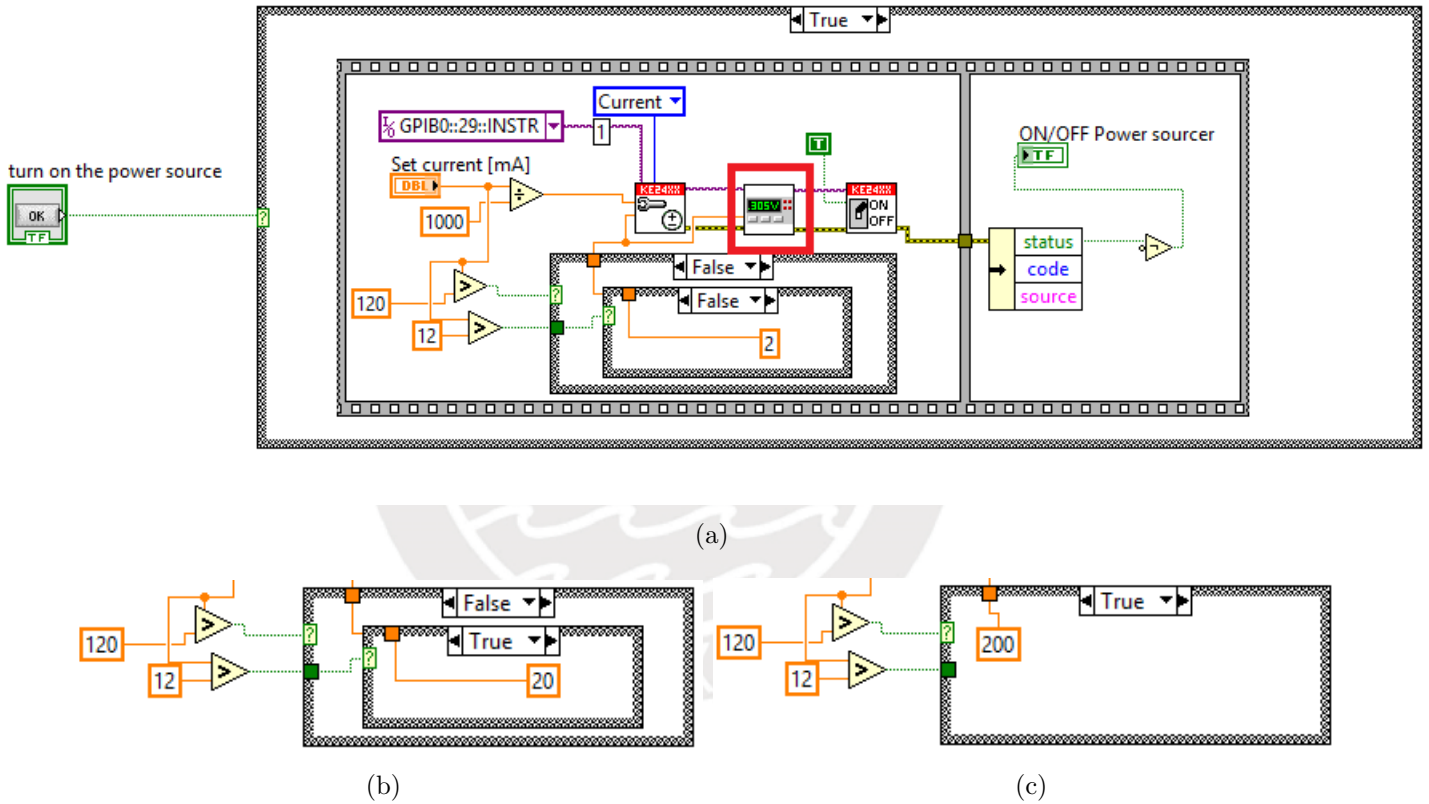

Figure 7.15: This event performs the configuration of the Keithley 2400 as a power supply. The red square shows the subVI mentioned in section 2.11, the current value supplied by the module is set by the user in each test..

2.4 Disconnection of the electrical modules during the test manually or by emergency.

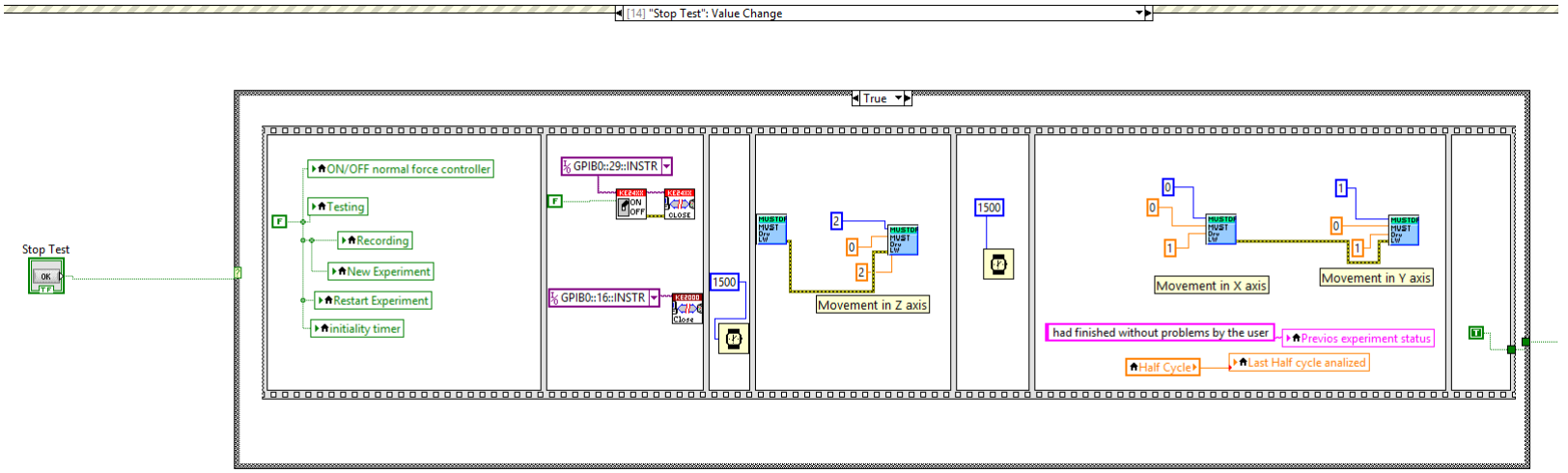

Figure 7.16: The experiment Stop Test has been updated to also disconnect the Keithley modules.

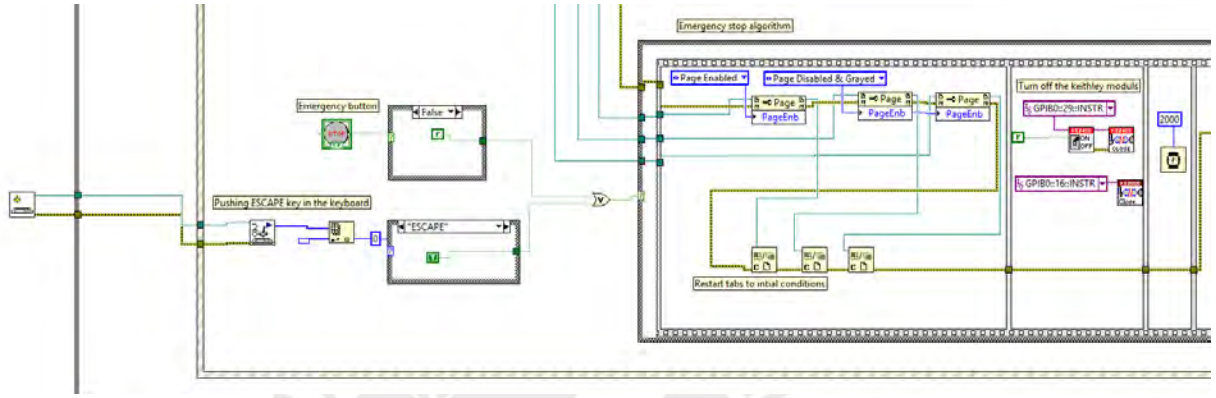

Figure 7.17: The emergency stop event algorithm has been updated to also disconnect the Keithley modules (a).

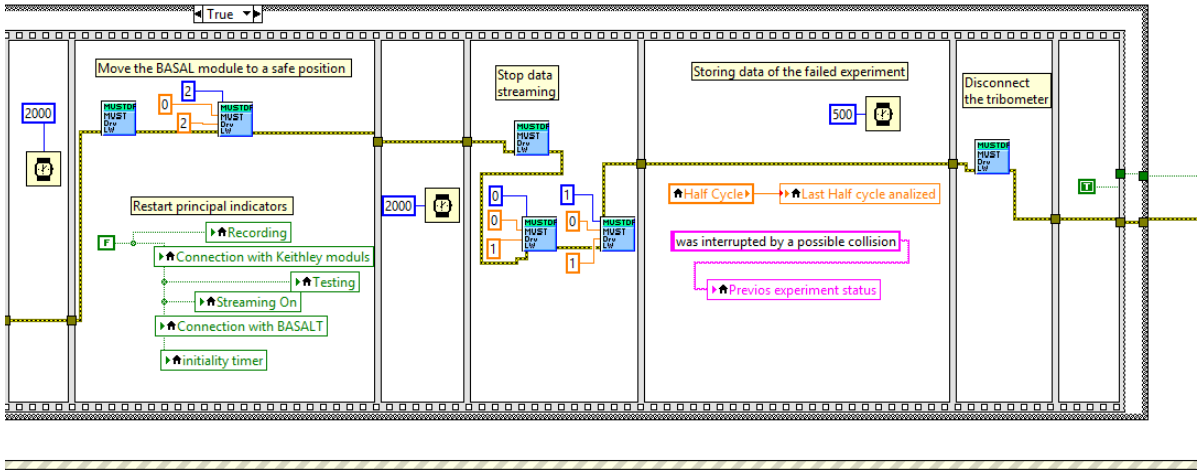

Figure 7.18: The emergency stop event algorithm has been updated to also disconnect the Keithley modules (b).

2.5 Simultaneous recording of electrical and tribological data

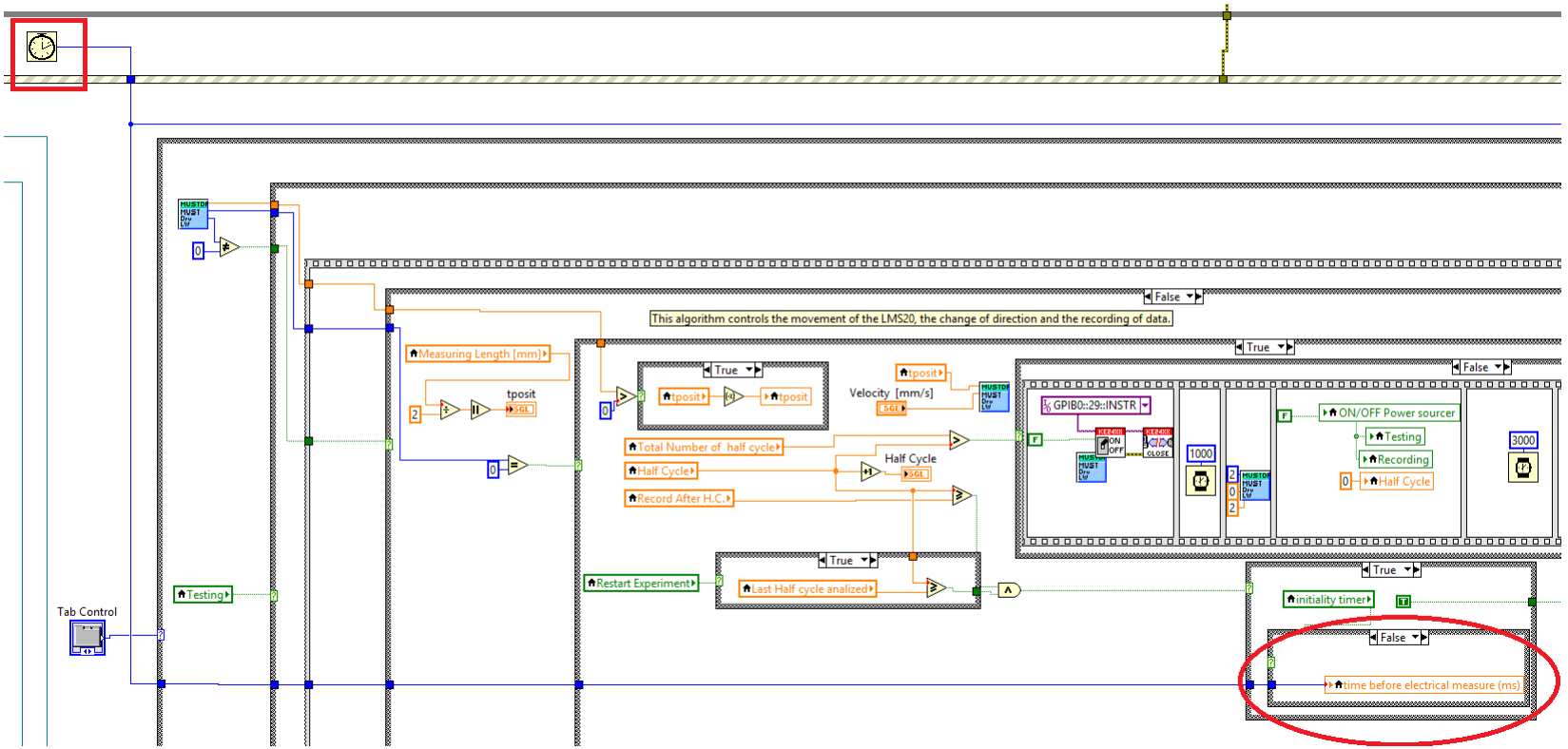

Figure 7.19: The new algorithm for recording electrical and tribological data simultaneously (a). The red square shows the timer used to define the moment when the electrical data are recorded. In addition, the red oval illustrates the algorithm for saving the timer value when the recording of the tribological data begins.

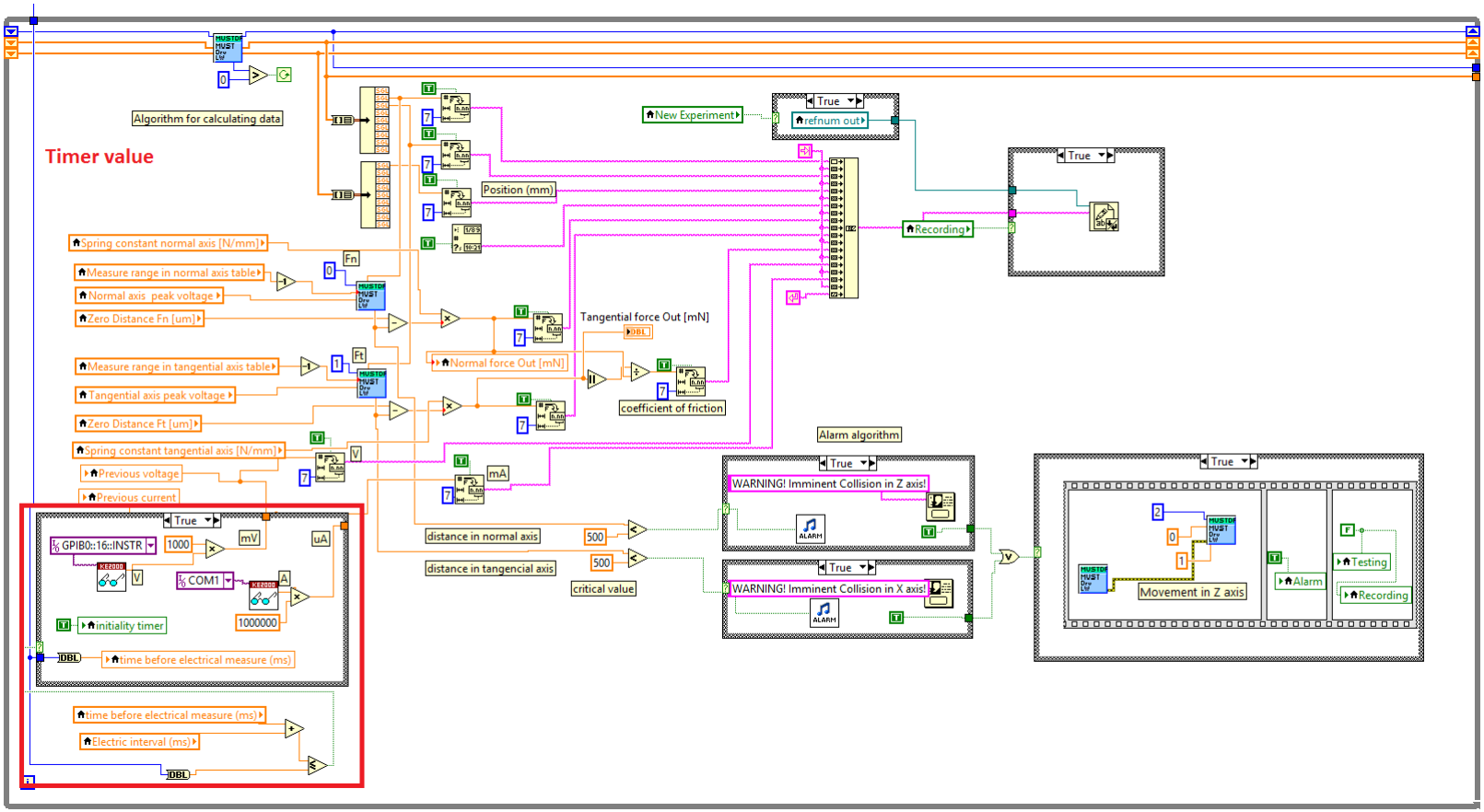

Figure 7.20: The new algorithm for recording electrical and tibological data simultaneously (b). The red square illustrates the logic of the last algorithm described in the section 2.4 for recording the values obtained from the tribometer and the Keithley devices (a).

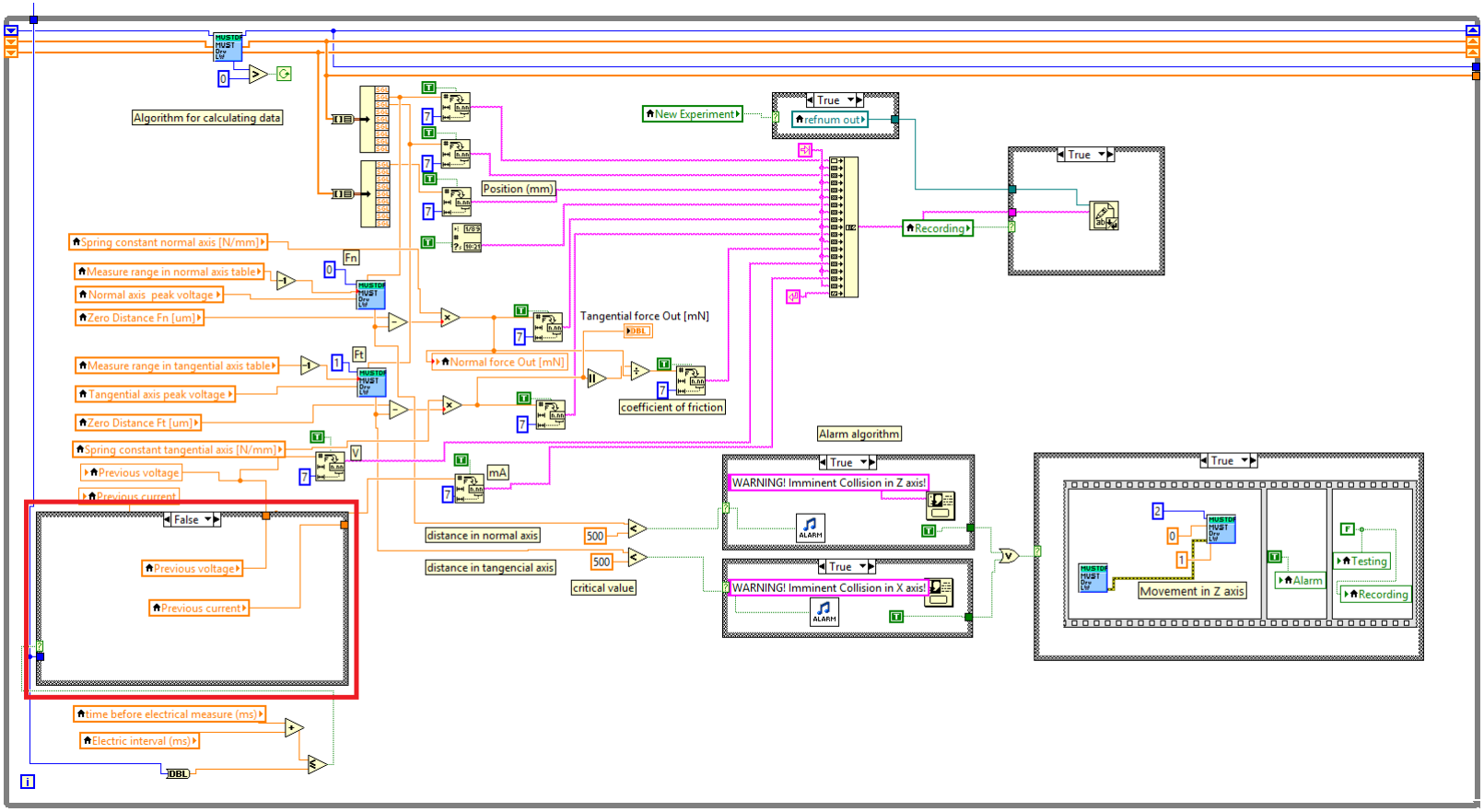

Figure 7.21: The new algorithm for recording electrical and tibological data simultaneously (c). The red square illustrates the logic of the last algorithm described in the section 2.4 for recording the values obtained from the tribometer and the Keithley devices(b).

3 Steps to perform the experiment using the GUI

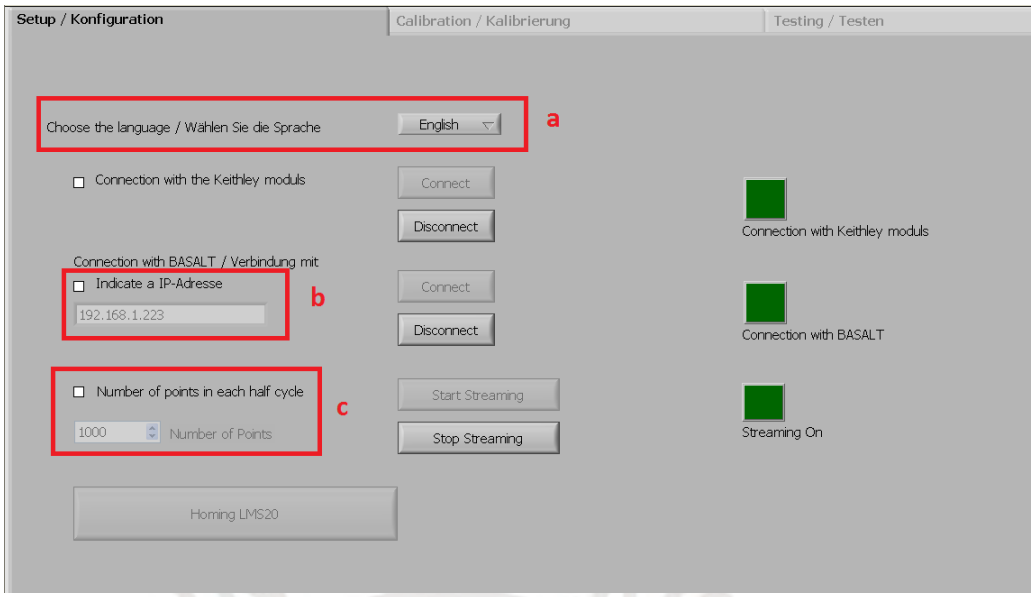

Figure 7.22: First part of the program (Setup). (a) The user has the option to change the language, (b) change the IP of the Basal module and (c) change the number of points in each half cycle

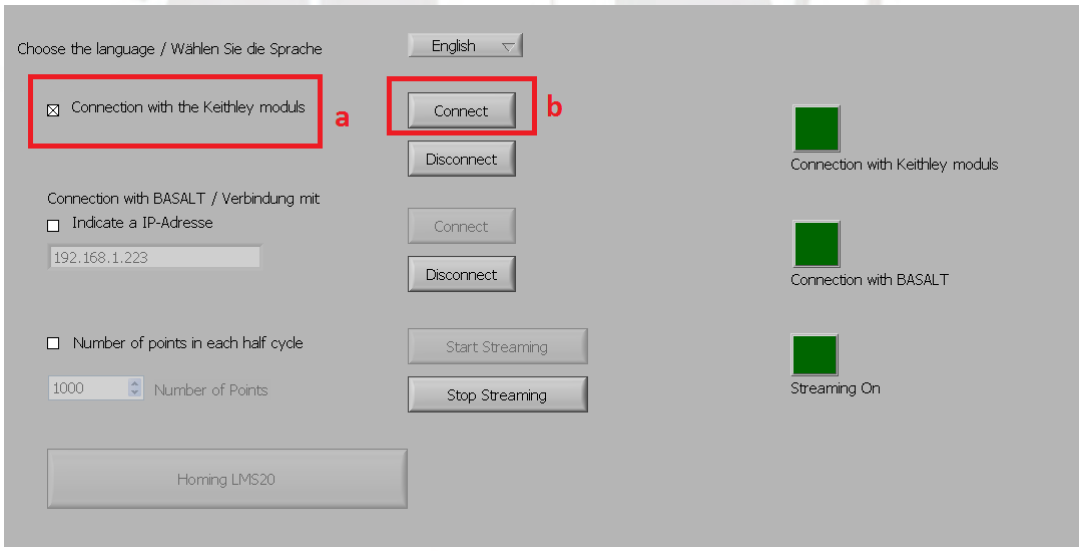

Figure 7.23: First part of the program (Setup). After choosing the language, the number of points in each half cycle and the IP, (a) the user must press the Connection with the Keithley moduls option. (b) Note that the button 'Connect' is enabled.

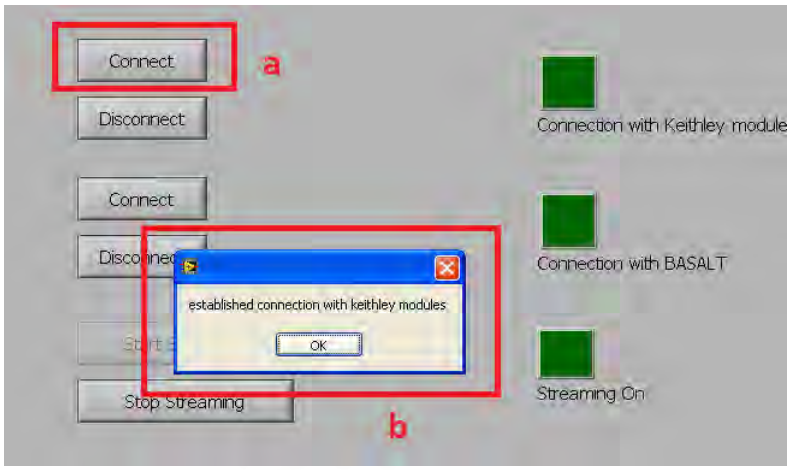

Figure 7.24: First part of the program (Setup). (a) Next, the user must click the 'Connect' button and the program will proceed to establish the connection. (b)Once the program establishes communication, a message with the status of the process is sent to the user.

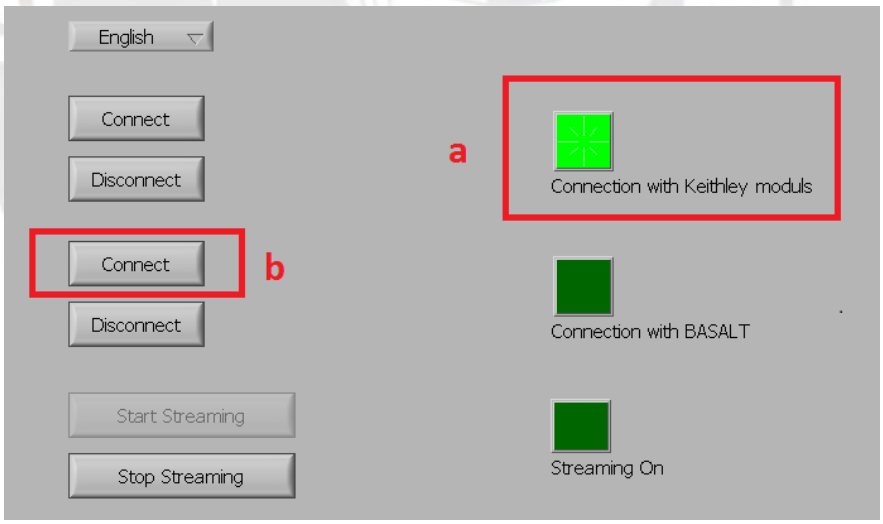

Figure 7.25: First part of the program (Setup). (a) Note that an LED indicator lights up to indicate that the connection with the Keithley modules has been established. (b) Then, the user must press the second 'Connect' button to establish communication with the tribometer.

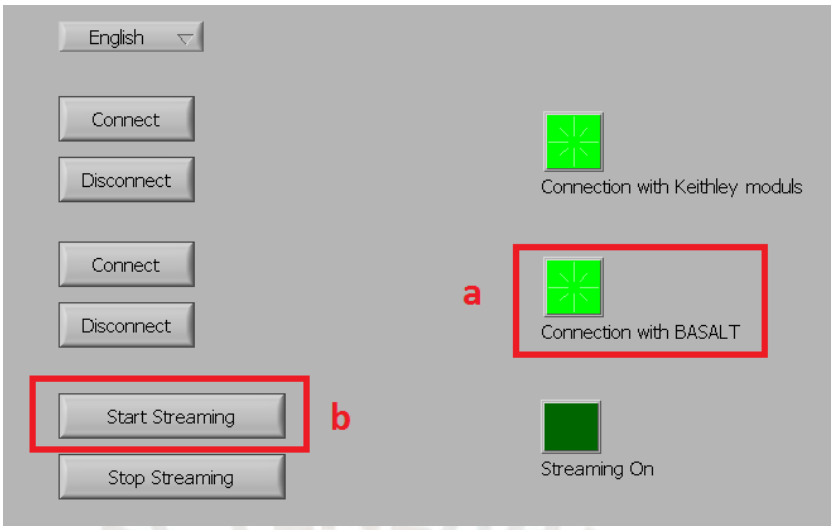

Figure 7.26: First part of the program (Setup). (a) Note that an LED indicator is turned on to indicate that the connection with BASALT has been established. (b) Once the connection is made, the 'Start Streaming' button is enabled.

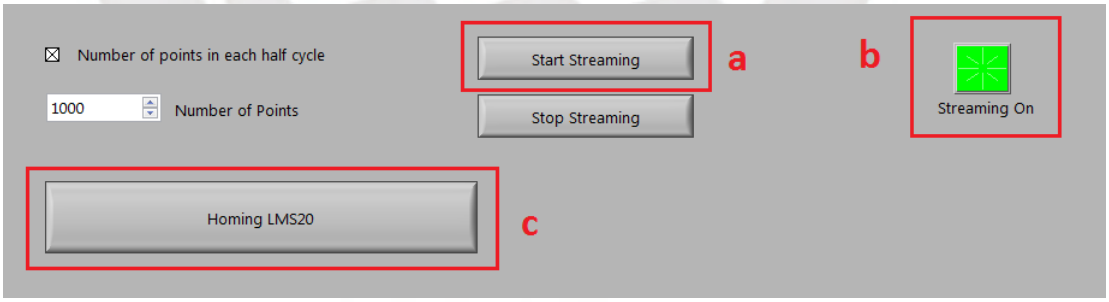

Figure 7.27: First part of the program (Setup). (a) Then the user must press the 'Start Streaming' button. (b) Note that a LED indicator lights up to indicate that the program is ready to start streaming and (c) the 'Homing LMS20' button is enabled.

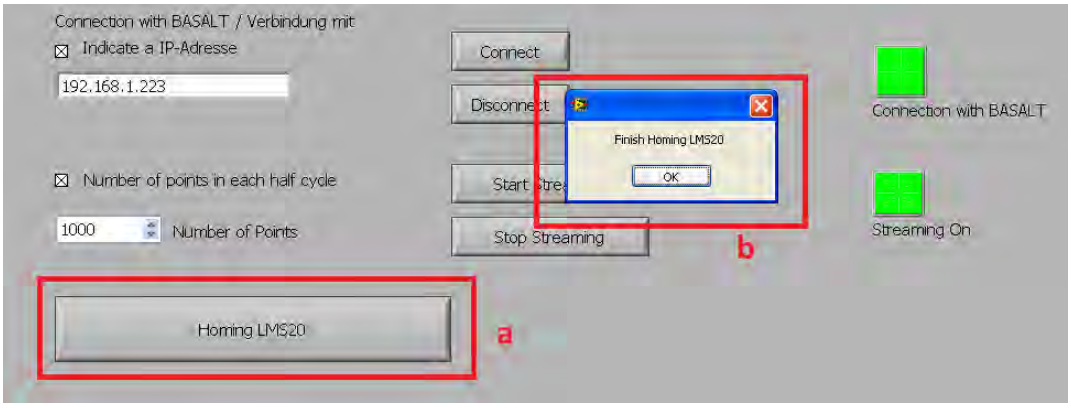

Figure 7.28: First part of the program (Setup). (a) After pressing the 'Homing LMS20' button, the user must wait until for the trbometer to complete its homing process before proceeding. (b) A pop-up appears when the homing is finished. Then the Calibration tab is enabled.

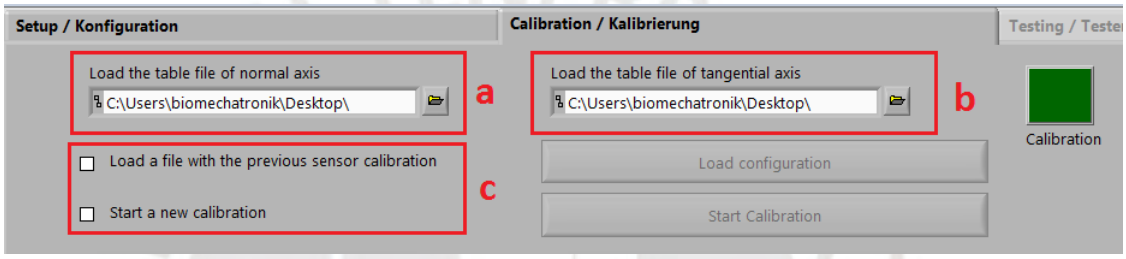

Figure 7.29: Second part of the program (Calibration). (a) The user must specify the location of the tables files for each sensor. These files contain information on the cantilevers available for the tribometer. One for the FOS sensor in the normal axis and (b) one for the FOS sensor in the tangential axis. (c) Note that calibration can be performed in two different ways: by loading a previous calibration file with the necessary data or by initiating a new calibration to find these values.

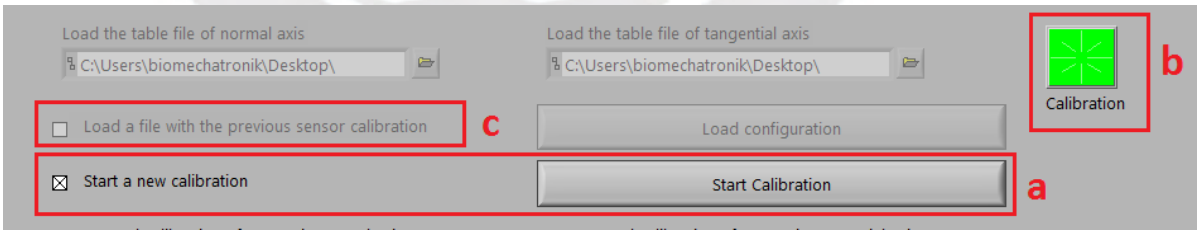

Figure 7.30: Second part of the program (Calibration). If the user decides to start a new calibration, (a) the 'Start Calibration' button is enabled. (b) Note that after pushing this button, a LED indicator is turned on and (c) the other option is disabled.

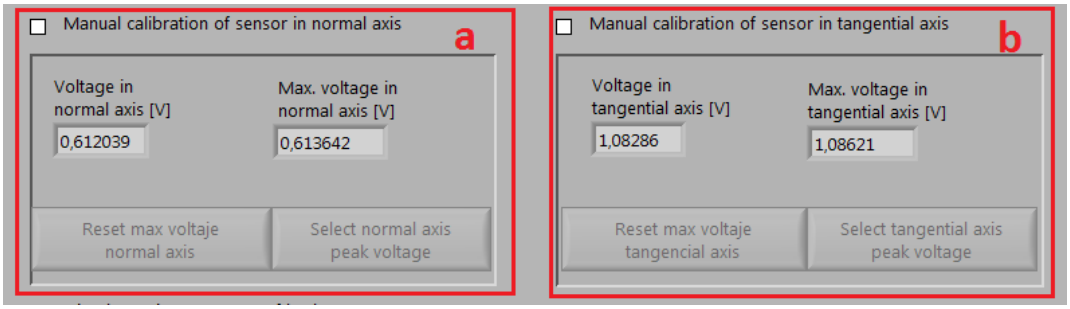

(a)

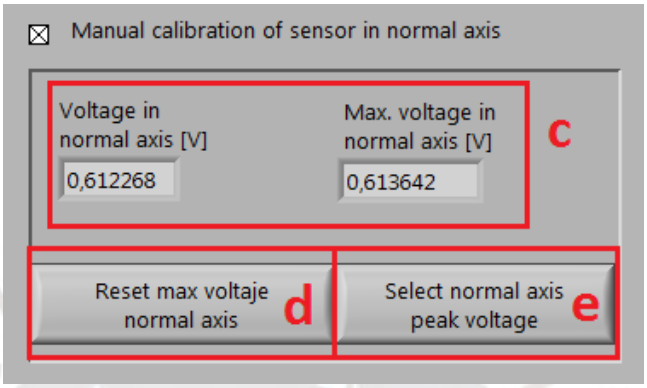

(b)

Figure 7.31: Second part of the program (Calibration). After pressing the 'Start Calibration' button, (a.a) manual calibration can be performed to find a peak voltage value for the normal axis and (a.b) for the tangential axis . The method is similar for both axes. (b.c) The user must manually bring the FOS sensor close to the mirror to find the maximum voltage value read by the sensor without hitting the mirror. (b.d) With the buttons, the user can reset the maximum voltage value and (b.e) after finding that value can store it in the program memory.

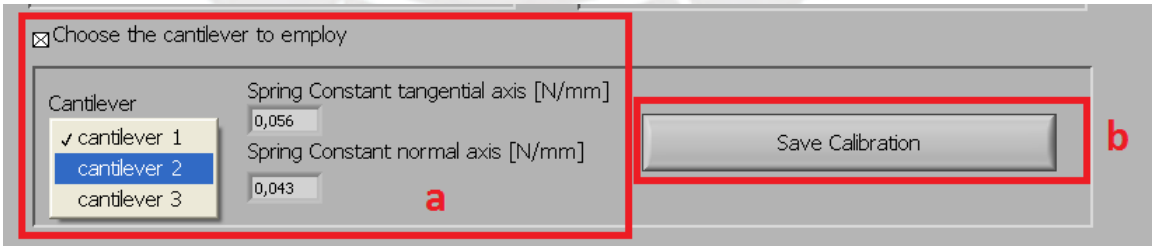

Figure 7.32: Second part of the program (Calibration). (a) After finding the maximum voltage values for both axis, the user must choose cantilever installed in the tribometer (the values of the spring constants and the accuracy of the normal force were set as default). (b) Then press the 'Save Calibration' button to create a file with the values of this calibration.

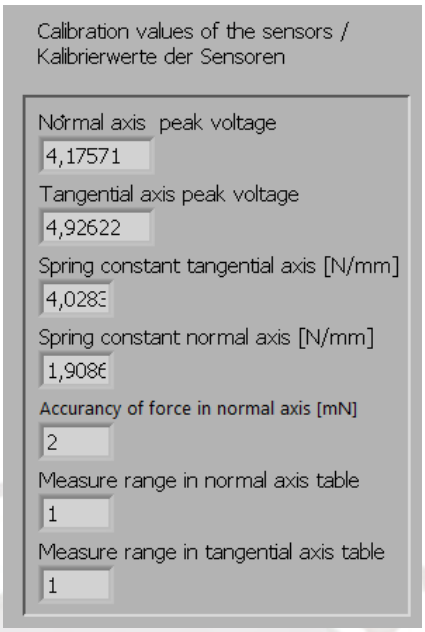

Figure 7.33: Second part of the program (Calibration). All calibration values are displayed at the top right corner of the interface (see Figure 2.14).

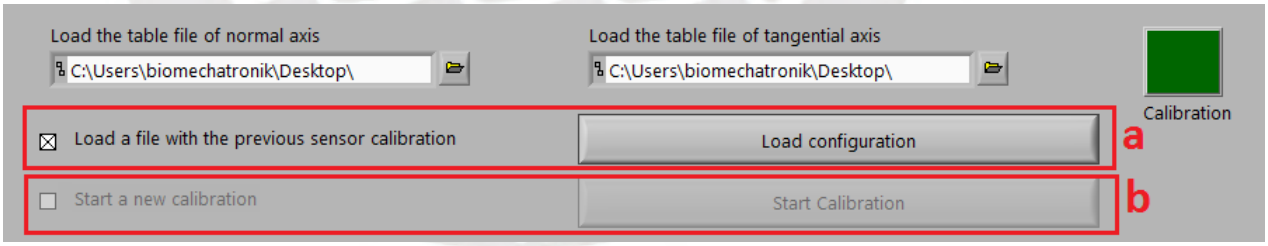

Figure 7.34: Second part of the program (Calibration). (a) If the user decides to load a previous calibration, the 'Load configuration' button is enabled. (b) Note that the other option is disabled. Additionally, after pressing this button and selecting the file with the previous configuration, the values from the previous calibration are displayed on the top right of the interface (Figure 7.33).

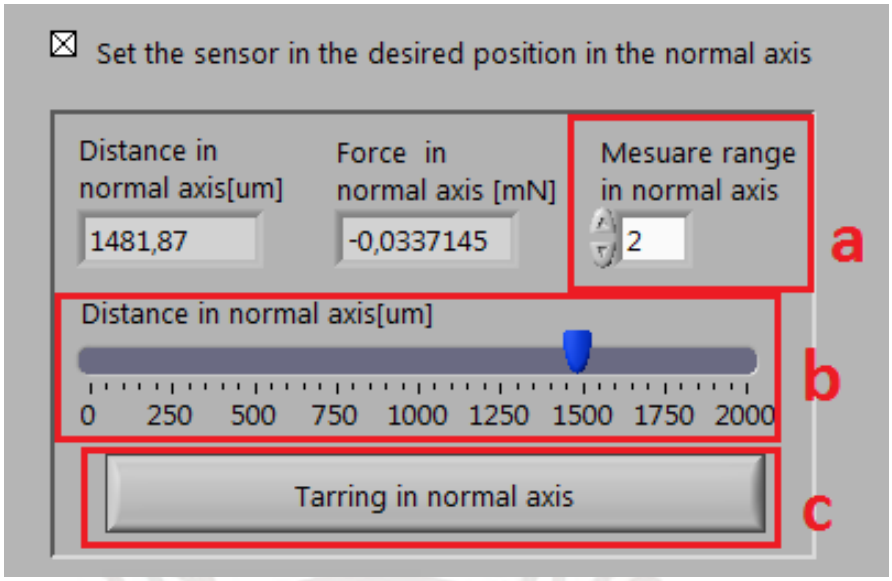

Figure 7.35: Second part of the program (Calibration). After storing the calibration values of the sensors in the program memory (Figure 7.33), it is necessary to store a new reference point for each sensor. (a) First, the measurement range must be changed to 2. (b) Next, the FOS sensor must be moved to a working position. Good positions include, for example, a distance of 1480 µm on the normal axis to use the maximum normal force value and a distance of 1000 µm on the tangential axis because the tangential force changes direction every half cycle. (c) Finally, the reference point is obtained after pressing the 'Tarring in normal axis' button.

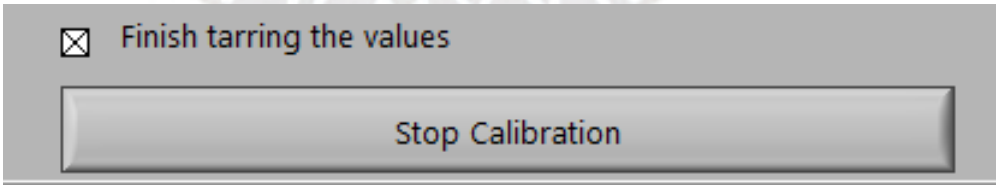

Figure 7.36: Second part of the program (Calibration). Finally, after tarring both sensors, the user must press the 'Stop calibration' button to complete the calibration process.

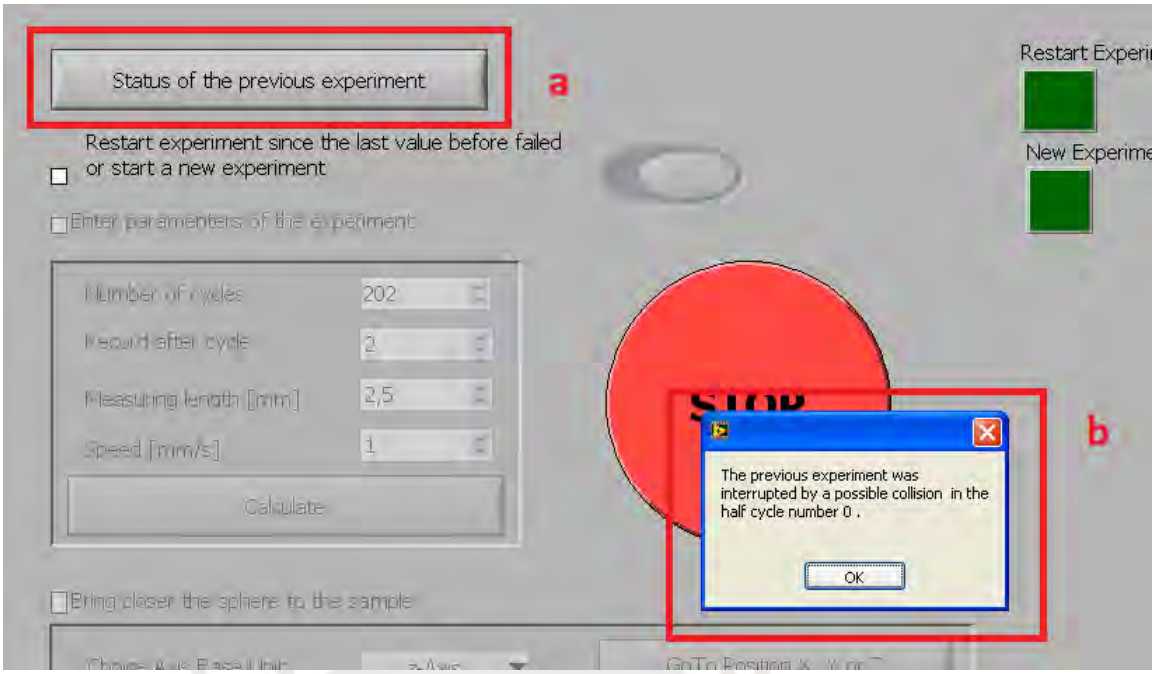

Figure 7.37: Third part of the program (Testing). (a) The user can request the status information of the previous experiment using the Status of the previous experiment button. (b) Immediately, a message describing such information is shown.

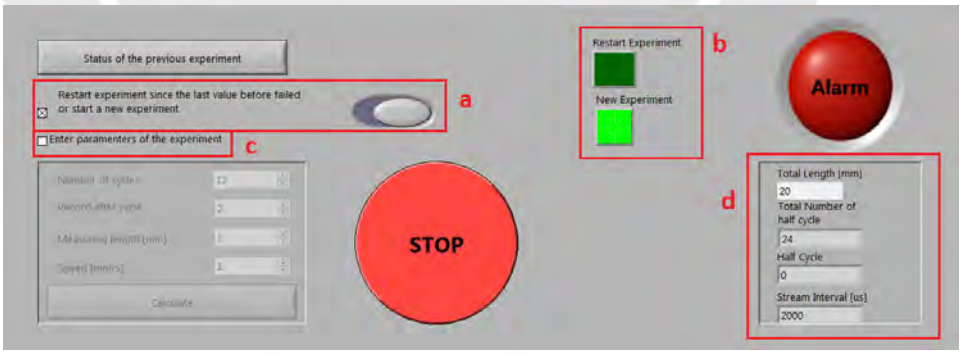

Figure 7.38: Third part of the program (Testing). (a) The user can choose between two options: restart the previous failed experiment or start a new experiment. The option chosen is displayed by two LEDs. (b) Depending on the user previous choice, the program requests the parameters for a new experiment or (c)it uses the values of the previous experiment shown in box d.

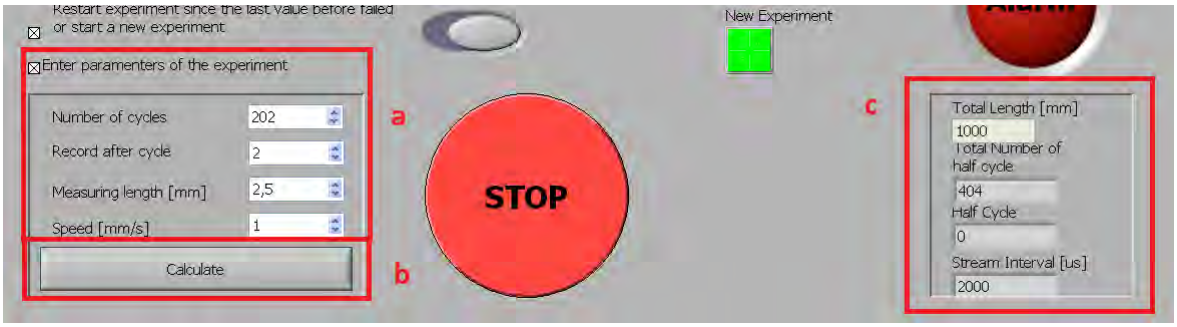

Figure 7.39: Third part of the program (Testing). (a) If the user chooses start a new experiment, the program prompts for its parameters. (b) After pressing the 'Calculate' button, the necessary values for conducting the experiment are calculated and displayed in box c.

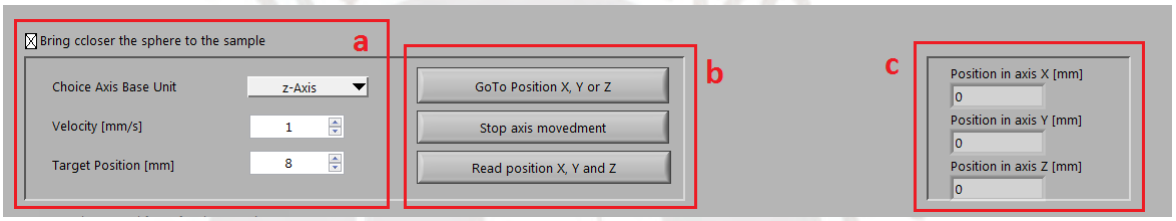

Figure 7.40: Third part of the program (Testing). After specifying the parameters of the experiment, the user must bring the sphere close to the sample. The options in box (a) allow the user to move the Basal module along the x, y, or z axes. The position and speed values are limited by the program according to the module specifications. Additionally, the buttons in box (b) are used to move the BASAL module. Finally, the absolute position of module can be verified in box (c) after pressing the button 'Read position X,Y and Z'.

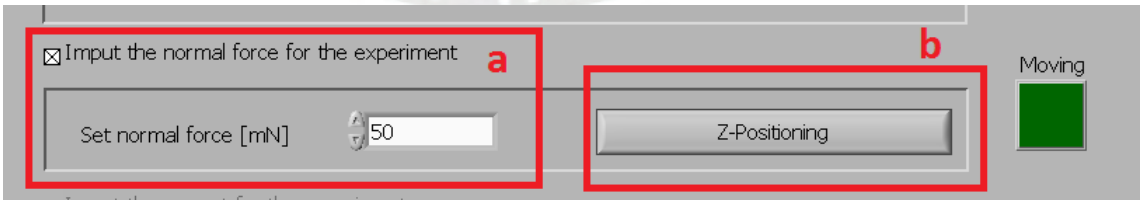

Figure 7.41: Third part of the program(Testing). (a) The next step is to enter the desired normal force for the experiment.(b) Next, the user presses the 'Z-Positioning' button to achieve the desired force.

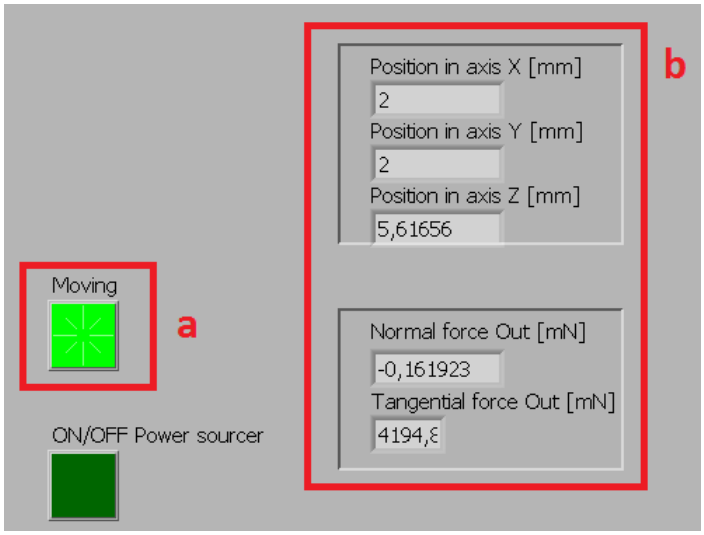

Figure 7.42: Third part of the program (Testing). (a) The interface indicates that the module is moving by a LED indicator. Also, the absolute position value of the BASAL module and the forces can be read in the indicators in box (b).

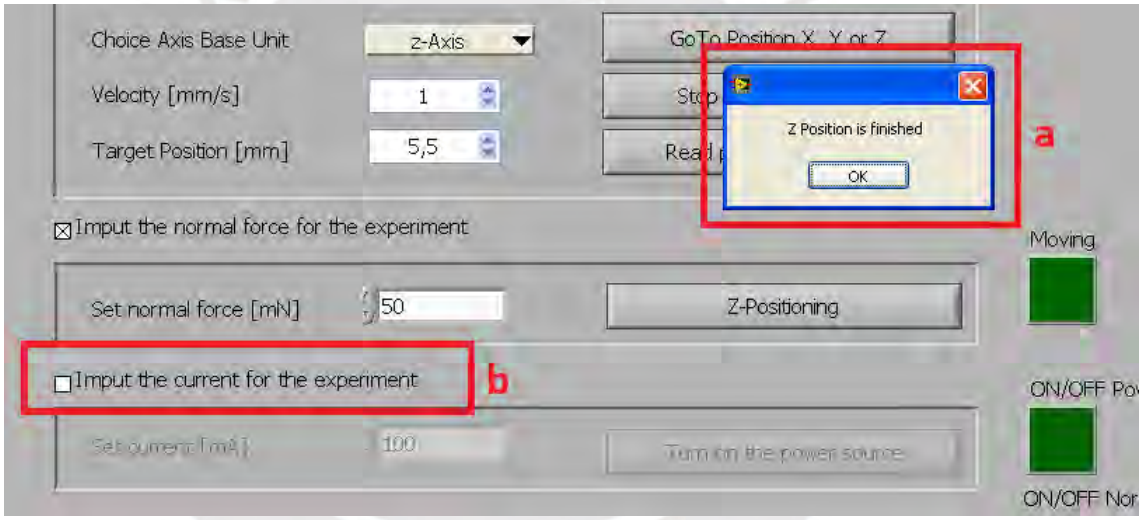

Figure 7.43: Third part of the program (Testing). (a) After obtaining the desired normal force, the program sends a message informing that the process has been completed. (b) Note that the 'Input the current for the experiment' option is enabled.

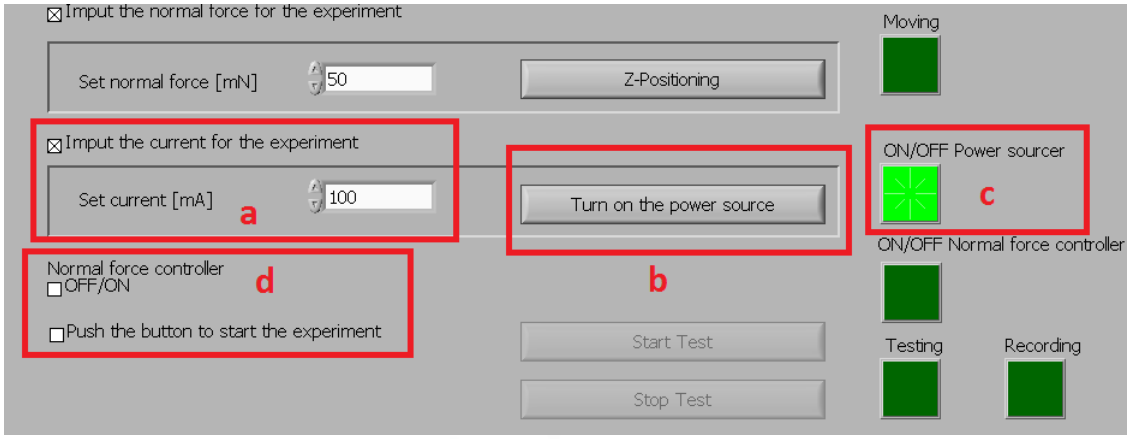

Figure 7.44: Third part of the program (Testing). (a) The next step is to enter the desired current source for the experiment. (b) Next, the user must press the 'Turn on the power source' button for the Keithley 2400 to supply the desired current. (c)The LED lights up when the Keithley 2400 is supplying current to the sample. (d) Note that the options to use the normal force controller algorithm during the experiment and the option to start the experiment were enabled.

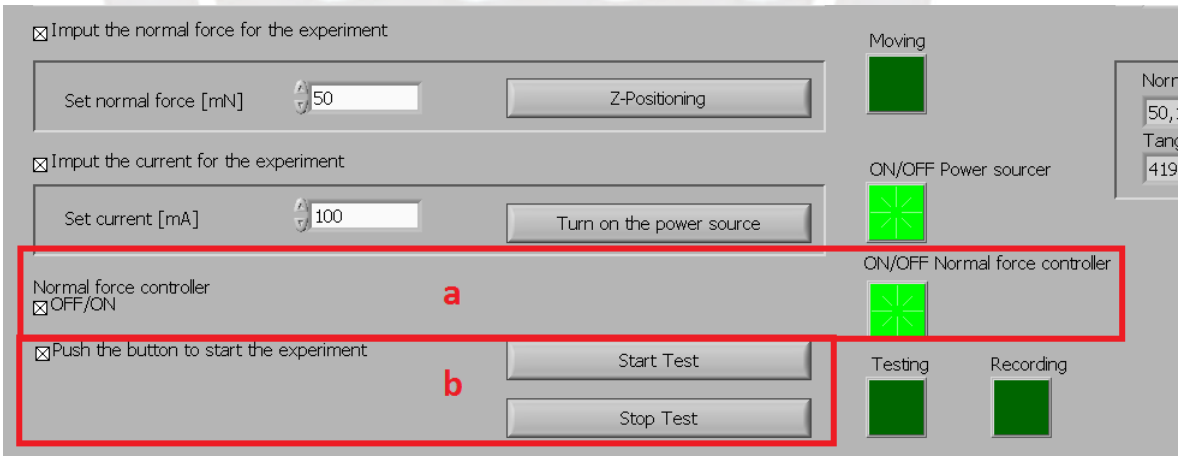

Figure 7.45: Third part of the program (Testing). (a) The user can choose whether to use the algorithm in box a (If selected, an LED lights up). (b) The experiment can be started after all the steps have been performed.

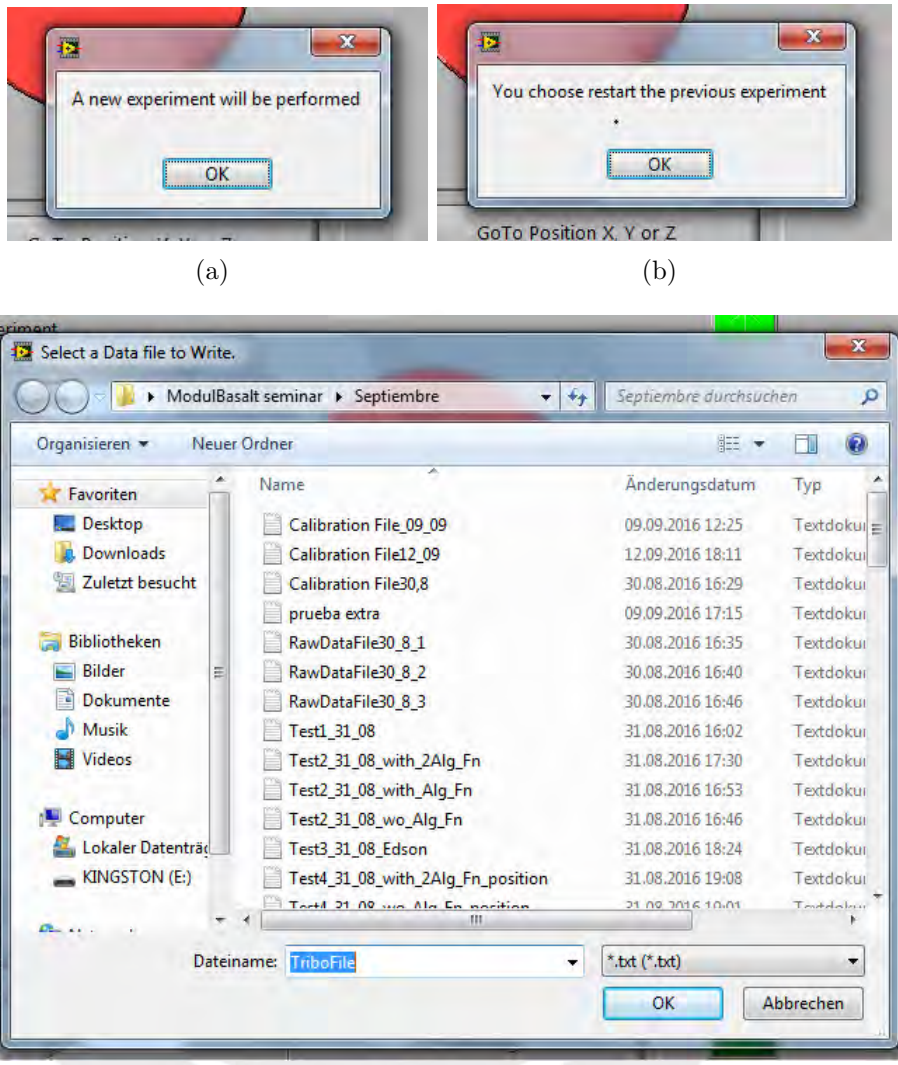

(a) (b)

(c)

Figure 7.46: Third part of the program (Testing). (a and b) The program sends a confirmation message based on the user's previous choice regarding the type of experiment after pressing the 'Start Test' button. (c) Next, the program prompts for the name of a file to store the data (Start New Experiment) or the location of the previous file where the experiment was stopped

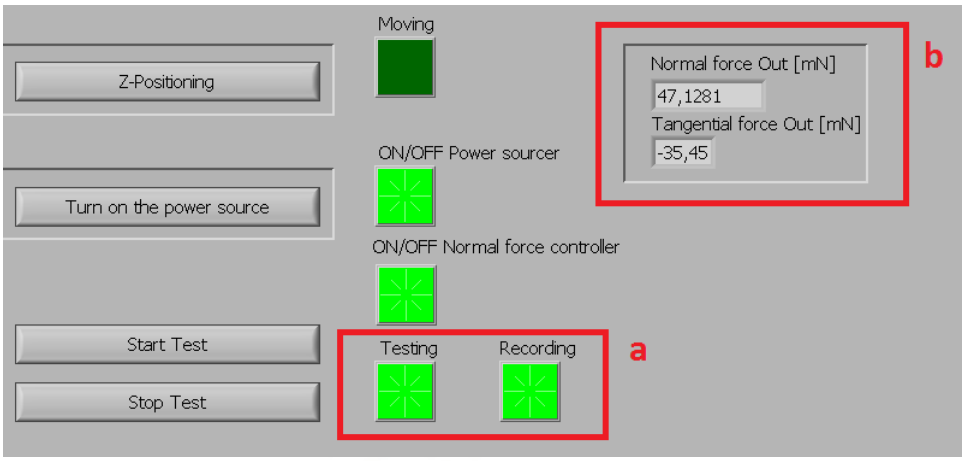

Figure 7.47: Third part of the program (Testing). (a) During the execution of the experiment, the program indicates its status using LED indicators. Additionally, the values of the forces read by the sensors are displayed in real-time in box (b).

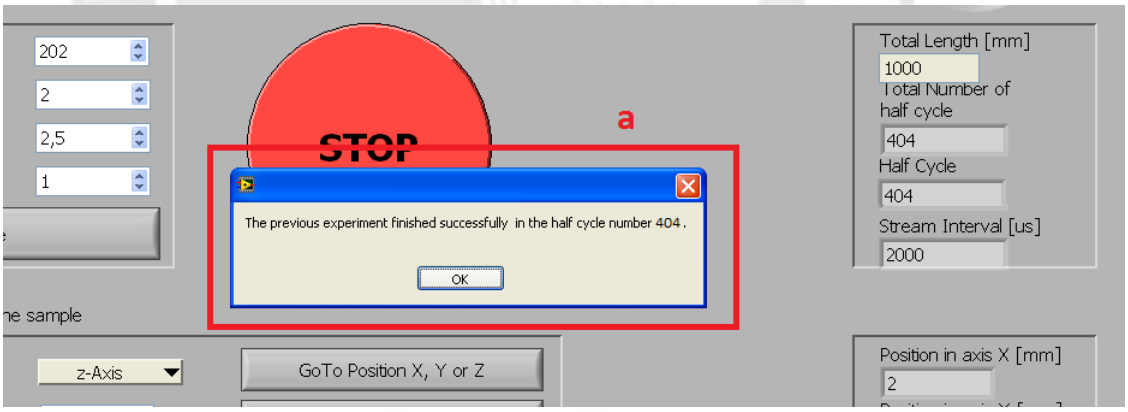

Figure 7.48: Third part of the program (Testing). (a) When the experiment is finished, the interface sends a message and initiates the shutdown sequence. First, the Keithley 2400 stops supplying current. Then, the tribometer head moves to the safety position, and the program continues running once the experiment is finished. The user can start a second experiment immediately after reviewing the status of the previous one.

Text file processing before using MATLAB

There are two main changes that the user must do before loading the text file obtained by the LabVIEW program into the post-processing program in MATLAB. However, is recommended to create a copy of the original file containing the test data and make the changes to the copy. Figure 8.1 shows an example of the copied text file obtained after conducting the experiment. The first change to be made to the copy for the proper execution of the MATLAB program is to delete all information about the experiment parameters. Figure 8.2 shows how the file must look at this point. Finally, the user must replace all commas with dots. This is very important because MATLAB commands cannot load text files with commas inside. To do this, select the Edit tab and choose the replace option. In the new window, enter the comma symbol (,) in the search field and the dot symbol (.) in the replacement field. After clicking on the replace all option, the text file should be similar to that shown in Figure 8.3.

```
[Input Current [mA]      100,0000000
Input Force [mN]         150,0000000
Number of Cycles         202,0000000
Record After Cycle       2,0000000
Total Length [mm]        1000,0000000
Measuring Length [mm]    2,5000000
Speed [mm/s]     1,0000000
Number of points         1000,0000000
Spring Constant Fn [N/mm]        1,9086000
Spring constant Ft [N/mm]        4,0283000

Fn (V)  Ft (V)  Position (mm)    Time    Normal force (mN)       Tangential force (mN)   Coefficient of friction Voltage (mV)    Current (uA)

0,7167925       1,4706645       -6,8400002      11:53:08        153,8813410     -38,9425281     0,2530686       6431,3982500    99969,4705000
0,7165636       1,4710460       -6,8400002      11:53:08        153,4507876     -38,2899946     0,2495262       6431,3982500    99969,4705000
0,7162585       1,4705882       -6,8400002      11:53:08        152,8767166     -39,0733298     0,2555872       6431,3982500    99969,4705000
0,7163348       1,4705882       -6,8400002      11:53:08        153,0202343     -39,0733298     0,2553475       6431,3982500    99969,4705000
0,7163348       1,4706645       -6,8400002      11:53:08        153,0202343     -38,9425281     0,2544927       6431,3982500    99969,4705000
0,7162585       1,4702067       -6,8400002      11:53:08        152,8767166     -39,7263550     0,2598588       6431,3982500    99969,4705000
0,7165636       1,4706645       -6,8400002      11:53:08        153,4507876     -38,9425281     0,2537786       6431,3982500    99969,4705000
0,7167162       1,4710460       -6,8400002      11:53:08        153,7378232     -38,2899946     0,2490603       6431,3982500    99969,4705000
0,7161822       1,4705119       -6,8400002      11:53:08        152,7331988     -39,2041316     0,2566838       6431,3982500    99969,4705000
0,7162585       1,4704356       -6,8400002      11:53:08        152,8767166     -39,3344416     0,2572952       6431,3982500    99969,4705000
0,7164111       1,4705119       -6,8400002      11:53:08        153,1637521     -39,2041316     0,2559622       6431,3982500    99969,4705000
0,7161059       1,4701304       -6,8400002      11:53:08        152,5896810     -39,8566650     0,2612016       6431,3982500    99969,4705000
0,7164111       1,4705882       -6,8400002      11:53:08        153,1637521     -39,0733298     0,2551082       6431,3982500    99969,4705000
0,7167162       1,4710460       -6,8400002      11:53:08        153,7378232     -38,2899946     0,2490603       6431,3982500    99969,4705000
0,7161822       1,4705882       -6,8400002      11:53:08        152,7331988     -39,0733298     0,2558274       6431,3982500    99969,4705000
0,7161059       1,4703593       -6,8400002      11:53:08        152,5896810     -39,4652433     0,2586364       6431,3982500    99969,4705000
0,7161822       1,4705882       -6,8400002      11:53:08        152,7331988     -39,0733298     0,2558274       6431,3982500    99969,4705000
0,7164111       1,4705882       -6,8400002      11:53:08        153,1637521     -39,0733298     0,2551082       6431,3982500    99969,4705000
0,7166399       1,4707408       -6,8400002      11:53:08        153,5943054     -38,8122181     0,2526931       6431,3982500    99969,4705000
0,7167162       1,4710460       -6,8400002      11:53:08        153,7378232     -38,2899946     0,2490603       6431,3982500    99969,4705000
```

Figure 8.1: The text file obtained after performing the test. This original text file contains all the parameters entered by the user before performing the experiment and all the data acquired during the experiment for further analysis.

Fn (V)	Ft (V)	Position (mm)	Time	Normal force (mN)	Tangential force (mN)	Coefficient of friction	Voltage (mV)	Current (uA)
0,7167925		1,4706645	-6,8400002	11:53:08	153,8813410	-38,9425281	0,2530686	6431,3982500	99969,4705000
0,7165636		1,4710460	-6,8400002	11:53:08	153,4507876	-38,2899946	0,2495262	6431,3982500	99969,4705000
0,7162585		1,4705882	-6,8400002	11:53:08	152,8767166	-39,0733298	0,2555872	6431,3982500	99969,4705000
0,7163348		1,4705882	-6,8400002	11:53:08	153,0202343	-39,0733298	0,2553475	6431,3982500	99969,4705000
0,7163348		1,4706645	-6,8400002	11:53:08	153,0202343	-38,9425281	0,2544927	6431,3982500	99969,4705000
0,7162585		1,4702067	-6,8400002	11:53:08	152,8767166	-39,7263550	0,2598588	6431,3982500	99969,4705000
0,7165636		1,4706645	-6,8400002	11:53:08	153,4507876	-38,9425281	0,2537786	6431,3982500	99969,4705000
0,7167162		1,4710460	-6,8400002	11:53:08	153,7378232	-38,2899946	0,2490603	6431,3982500	99969,4705000
0,7161822		1,4705119	-6,8400002	11:53:08	152,7331988	-39,2041316	0,2566838	6431,3982500	99969,4705000
0,7162585		1,4704356	-6,8400002	11:53:08	152,8767166	-39,3344416	0,2572952	6431,3982500	99969,4705000
0,7164111		1,4705119	-6,8400002	11:53:08	153,1637521	-39,2041316	0,2559622	6431,3982500	99969,4705000
0,7161059		1,4701304	-6,8400002	11:53:08	152,5896810	-39,8566650	0,2612016	6431,3982500	99969,4705000
0,7164111		1,4705882	-6,8400002	11:53:08	153,1637521	-39,0733298	0,2551082	6431,3982500	99969,4705000
0,7167162		1,4710460	-6,8400002	11:53:08	153,7378232	-38,2899946	0,2490603	6431,3982500	99969,4705000
0,7161822		1,4705882	-6,8400002	11:53:08	152,7331988	-39,0733298	0,2558274	6431,3982500	99969,4705000
0,7161059		1,4703593	-6,8400002	11:53:08	152,5896810	-39,4652433	0,2586364	6431,3982500	99969,4705000
0,7161822		1,4705882	-6,8400002	11:53:08	152,7331988	-39,0733298	0,2558274	6431,3982500	99969,4705000
0,7164111		1,4705882	-6,8400002	11:53:08	153,1637521	-39,0733298	0,2551082	6431,3982500	99969,4705000
0,7166399		1,4707408	-6,8400002	11:53:08	153,5943054	-38,8122181	0,2526931	6431,3982500	99969,4705000
0,7167162		1,4710460	-6,8400002	11:53:08	153,7378232	-38,2899946	0,2490603	6431,3982500	99969,4705000
0,7161822		1,4706645	-6,8400002	11:53:08	152,7331988	-38,9425281	0,2549709	6431,3982500	99969,4705000
0,7161822		1,4704356	-6,8400002	11:53:08	152,7331988	-39,3344416	0,2575369	6431,3982500	99969,4705000
0,7163348		1,4706645	-6,8400002	11:53:08	153,0202343	-38,9425281	0,2544927	6431,3982500	99969,4705000
0,7161059		1,4706645	-6,8400002	11:53:08	152,5896810	-38,9425281	0,2552108	6431,3982500	99969,4705000
0,7164111		1,4708934	-6,8400002	11:53:08	153,1637521	-38,5511064	0,2516986	6431,3982500	99969,4705000
0,7169452		1,4714274	-6,8400002	11:53:08	154,1683765	-37,6369694	0,2441290	6431,3982500	99969,4705000
0,7162585		1,4706645	-6,8400002	11:53:08	152,8767166	-38,9425281	0,2547316	6431,3982500	99969,4705000
0,7161059		1,4703593	-6,8400002	11:53:08	152,5896810	-39,4652433	0,2586364	6431,3982500	99969,4705000
0,7163348		1,4705882	-6,8400002	11:53:08	153,0202343	-39,0733298	0,2553475	6431,3982500	99969,4705000
0,7163348		1,4705882	-6,8400002	11:53:08	153,0202343	-39,0733298	0,2553475	6431,3982500	99969,4705000
0,7165636		1,4708934	-6,8400002	11:53:08	153,4507876	-38,5511064	0,2512278	6431,3982500	99969,4705000

Figure 8.2: The text file obtained after deleting the parameters entered by the user. All these changes must be made in one copy.

Fn (V)	Ft (V)	Position (mm)	Time	Normal force (mN)	Tangential force (mN)	Coefficient of friction	Voltage (mV)	Current (uA)
0.7167925		1.4706645	-6.8400002	11:53:08	153.8813410	-38.9425281	0.2530686	6431.3982500	99969.4705000
0.7165636		1.4710460	-6.8400002	11:53:08	153.4507876	-38.2899946	0.2495262	6431.3982500	99969.4705000
0.7162585		1.4705882	-6.8400002	11:53:08	152.8767166	-39.0733298	0.2555872	6431.3982500	99969.4705000
0.7163348		1.4705882	-6.8400002	11:53:08	153.0202343	-39.0733298	0.2553475	6431.3982500	99969.4705000
0.7163348		1.4706645	-6.8400002	11:53:08	153.0202343	-38.9425281	0.2544927	6431.3982500	99969.4705000
0.7162585		1.4702067	-6.8400002	11:53:08	152.8767166	-39.7263550	0.2598588	6431.3982500	99969.4705000
0.7165636		1.4706645	-6.8400002	11:53:08	153.4507876	-38.9425281	0.2537786	6431.3982500	99969.4705000
0.7167162		1.4710460	-6.8400002	11:53:08	153.7378232	-38.2899946	0.2490603	6431.3982500	99969.4705000
0.7161822		1.4705119	-6.8400002	11:53:08	152.7331988	-39.2041316	0.2566838	6431.3982500	99969.4705000
0.7162585		1.4704356	-6.8400002	11:53:08	152.8767166	-39.3344416	0.2572952	6431.3982500	99969.4705000
0.7164111		1.4705119	-6.8400002	11:53:08	153.1637521	-39.2041316	0.2559622	6431.3982500	99969.4705000
0.7161059		1.4701304	-6.8400002	11:53:08	152.5896810	-39.8566650	0.2612016	6431.3982500	99969.4705000
0.7164111		1.4705882	-6.8400002	11:53:08	153.1637521	-39.0733298	0.2551082	6431.3982500	99969.4705000
0.7167162		1.4710460	-6.8400002	11:53:08	153.7378232	-38.2899946	0.2490603	6431.3982500	99969.4705000
0.7161822		1.4705882	-6.8400002	11:53:08	152.7331988	-39.0733298	0.2558274	6431.3982500	99969.4705000
0.7161059		1.4703593	-6.8400002	11:53:08	152.5896810	-39.4652433	0.2586364	6431.3982500	99969.4705000
0.7161822		1.4705882	-6.8400002	11:53:08	152.7331988	-39.0733298	0.2558274	6431.3982500	99969.4705000
0.7164111		1.4705882	-6.8400002	11:53:08	153.1637521	-39.0733298	0.2551082	6431.3982500	99969.4705000
0.7166399		1.4707408	-6.8400002	11:53:08	153.5943054	-38.8122181	0.2526931	6431.3982500	99969.4705000
0.7167162		1.4710460	-6.8400002	11:53:08	153.7378232	-38.2899946	0.2490603	6431.3982500	99969.4705000
0.7161822		1.4706645	-6.8400002	11:53:08	152.7331988	-38.9425281	0.2549709	6431.3982500	99969.4705000
0.7161822		1.4704356	-6.8400002	11:53:08	152.7331988	-39.3344416	0.2575369	6431.3982500	99969.4705000
0.7163348		1.4706645	-6.8400002	11:53:08	153.0202343	-38.9425281	0.2544927	6431.3982500	99969.4705000
0.7161059		1.4706645	-6.8400002	11:53:08	152.5896810	-38.9425281	0.2552108	6431.3982500	99969.4705000
0.7164111		1.4708934	-6.8400002	11:53:08	153.1637521	-38.5511064	0.2516986	6431.3982500	99969.4705000
0.7169452		1.4714274	-6.8400002	11:53:08	154.1683765	-37.6369694	0.2441290	6431.3982500	99969.4705000
0.7162585		1.4706645	-6.8400002	11:53:08	152.8767166	-38.9425281	0.2547316	6431.3982500	99969.4705000
0.7161059		1.4703593	-6.8400002	11:53:08	152.5896810	-39.4652433	0.2586364		

Figure 8.3: The text file obtained after deleting the parameters entered by the user and replacing all commas with dots. Now the text file is ready to be loaded into the MATLAB program to process the data.

Upgrade of the MATLAB program

As explained earlier, there are two programs for performing the debugging process. The first is named *'Recording_data_of_the_triboelectrical_workstation.m'* and is to load the data from the text file into arrays that MATLAB can operate on. The second program is called *'Debuggin_data_of_the_triboelectrical_workstation.m'*. However, there are a few steps to follow before using these programs. The second program employs a special subroutine called *'regresion.m'*, so it is necessary to copy this MATLAB sub-program into the same directory as the two main programs. Next, the user must select the directory where the programs are located in the MATLAB interface. Figure 9.1 shows the MATLAB 2023 interface, displaying the current directory (a) and the button to change this directory (b). Click the button in the red box b and select the directory of the programs. Finally, open both programs and follow the instruction provided in the comments to execute the debugging process.The programs are shown in the following section.

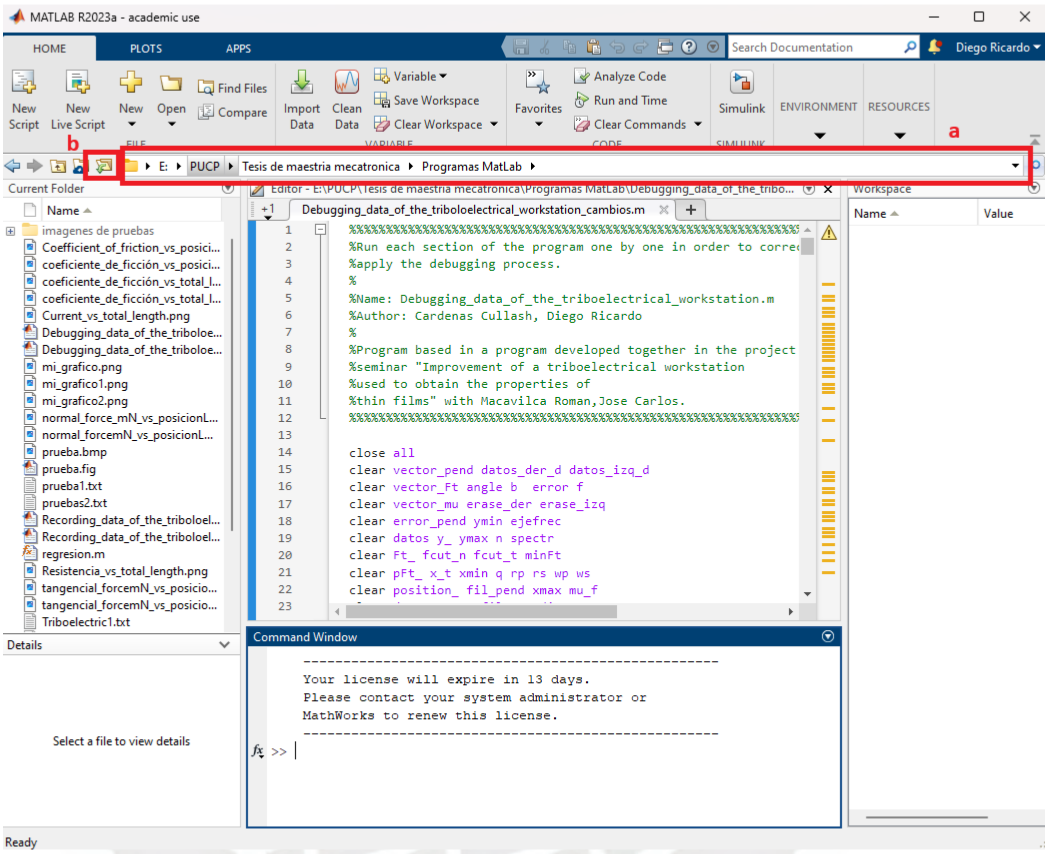

Figure 9.1: The text file obtained after deleting the parameters entered by the user and replacing all commas with dots. Now the text file is ready to be loaded into the MATLAB program to process the data.

```
function [a b]=regresion(x,y)
    n=length(x);
    a=zeros(2,1);
    b=zeros(2,1);

    % slope of regression line, a
    a(1)=(n*sum(x.*y)-sum(x)*sum(y))/(n*sum(x.^2)-sum(x)*sum(x));
    % intercepts in Y axis, b
    b(1)=(sum(y)-a(1)*sum(x))/n;

    % errorss of a and b
    sd2=sum((y-a(1)*x-b(1)).^2);
    a(2)=sqrt(sd2/(n-2))/sqrt(sum(x.^2)-sum(x)*sum(x)/n);
    b(2)=sqrt(sum(x.^2)/n)*a(2);
end
```

```
%Run each subsection of the program one by one in order to correctly
% apply the debugging process.
%(Right click and select 'Evaluated current section' to evaluate
% the program by parts)
%
%Name: Recording_data_of_the_triboelectrical_workstation.m
%Author: Cardenas Cullash, Diego Ricardo
%
%Program based in a program developed together in the project
%seminar "Improvement of a triboelectrical workstation
%used to obtain the properties of
%thin films" with Macavilca Roman,Jose Carlos.


% Program to collect data from the text file
close all
clear all
clc

%Introduce the name of the text file where the data will be obtained in
%the command importdata. Example:
%   filename: 'first_task.txt'
%
%NOTE: The name of the file must not have blank space in their name.
%   good name: 'First_task.txt', 'erste_1', 'task_01'
%   wrong name: 'first task.txt', 'erste 1', 'task 01'

filename = 'Triboelectric22.txt';

% Read file as table
opts = detectImportOptions(filename, ...
'Delimiter', '\t', 'VariableNamingRule', 'preserve');
dataTable = readtable(filename, opts);
dataTable.Properties.VariableNames = {'Fn', 'Ft', 'Position', 'Time', ...
'NormalForce', 'TangentialForce', 'CoefficientOfFriction', 'Voltage', ...
 'Current'};

% Create the first table with the mentioned values
tablaA1 = dataTable(:, {'NormalForce', 'TangentialForce', ...
'CoefficientOfFriction', 'Voltage', 'Current'});

% Create a second table with the remaining values
tablaA2 = dataTable(:, {'Fn', 'Ft', 'Position'});
% Create a table only with values of time
tablatime = dataTable(:, {'Time'});


[fil,~]=size(tablaA1); %Amount of data

% Convert to string if necessary
if iscell(dataTable.Time)
    dataTable.Time = string(dataTable.Time);
elseif ~ischar(dataTable.Time)
    dataTable.Time = string(dataTable.Time);
end

dataTable.Time = datetime(dataTable.Time, 'InputFormat', 'HH:mm:ss');
```

```
% Get first and last time value
primerTiempo = dataTable.Time(1);
ultimoTiempo = dataTable.Time(end);

% Calculate time in seconds since midnight
primerTiempoSegundos = seconds(primerTiempo - dateshift(primerTiempo,...
 'start', 'day'));
ultimoTiempoSegundos = seconds(ultimoTiempo - dateshift(ultimoTiempo,...
 'start', 'day'));
time_uno =primerTiempoSegundos ;
time_dos =ultimoTiempoSegundos ;

%Save the necessary data in different vectors
R=horzcat(tablaA2,tablaA1);
Fn_v=R(:,1);
Ft_v=R(:,2);
position=R(:,3);
Fn=R(:,4);
Ft=R(:,5);
mu=R(:,6);
Vol=R(:,7);
Curr=R(:,8);

%clean memory
clear A1 a j
clear A H MN S
clear A2
clear fil
clear i
```

```
%%%%%%%%%%%%%%%%%%%%%%%%%%%%%%%%%%%%%%%%%%%%%%%%%%%%%%%%%%%%%%%%%%%%%%%%%%%%5
%Run each subsection of the program one by one in order to correctly
% apply the debugging process.
%
%Name: Debugging_data_of_the_triboelectrical_workstation.m
%Author: Cardenas Cullash, Diego Ricardo
%
%Program based in a program developed together in the project
%seminar "Improvement of a triboelectrical workstation
%used to obtain the properties of
%thin films" with Macavilca Roman,Jose Carlos.
%%%%%%%%%%%%%%%%%%%%%%%%%%%%%%%%%%%%%%%%%%%%%%%%%%%%%%%%%%%%%%%%%%%%%%%%%%%%%

close all
clear vector_pend datos_der_d datos_izq_d
clear vector_Ft angle b  error f
clear vector_mu erase_der erase_izq
clear error_pend ymin ejefrec
clear datos y_ ymax n spectr
clear Ft_ fcut_n fcut_t minFt
clear pFt_ x_t xmin q rp rs wp ws
clear position_ fil_pend xmax mu_f
clear datos_p_neg fil_pos dim
clear datos_p_pos fil_pos_der Fn_prom_i
clear datos_p x_n mu row_vector
clear datos_izq Fn_prom  fny pas position_f
clear datos_der flag fm Fn Fn_f
clear fil_pFt_izq wn time_fil_pos
clear pFt_izq fil_pos_izq i2 vector_Ft_f
clear fil_pFt_der mu vector_Fn_f
clear pFt_der media_position_pend
clear position_izq vector_Fn
clear position_der p duration
clear Ft_izq max_mu pmedio_izq pos time_f
clear Ft_der pos_der var_Fn
clear datos_Ft_izq pmedio_der
clear datos_Ft_der pFt_der_d
clear mu_prom var_Fn_i vector_mu_f
clear mu_prom_i pos_izq S1d
clear mu_prom_f S1l
clear var_mu S2d time
clear var_mu_i S2l
clear var_mu_f j J k m
clear lentot ini_m resis_var
clear len i ini Vol_prom Vol_var
clear az a c d Curr_prom
clear bz col_pend h S MN
clear ad col_pos H resis_prom
clear bd cont Ft_f  Curr_var
clear vector_vol vector_curr vol_der vol_izq curr_der curr_izq
clear erase_pcurr_der erase_pcurr_izq erase_pvol_der erase_pvol_izq
clear pcurr_ pcurr_der pcurr_izq pvol_der pvol_izq
clear vector_resis resis_var_i resis_prom_i lentot_i Vol_var_i
clear Vol_prom_i Ft_v Fn_v Curr_var_i Curr_prom_i
clc
% Main information and their units
Fn=R{:,4};
```

```
Ft=R{:,5};
mu=R{:,6};
Vol=R{:,7}; %mV
Curr=R{:,8};%uA

%%
%Position values are incorrect, this error will appear after performing
%many experiments one after other.
[q,~]=size(R);
position = R{:, 3};
dataNumeric =position;
%The position will be escalated to fit the limits established in the
%experiment
semi_length = (max(dataNumeric) - min(dataNumeric)) / 2;
dataNumeric = dataNumeric - semi_length - min(dataNumeric);
position =dataNumeric;
%position values are correct now.

%%
%Position will be transformed in total length.
row_vector=length(position);
len_i=zeros(row_vector,1);
lentot_i=zeros(row_vector,1);
minFt=min(position);
for p=1:row_vector
   len_i(p,1)=position(p,1)-minFt;
end

for p=1:row_vector
   if p==1
       lentot_i(p,1)=len_i(p,1);
   end

   if p>1
       lentot_i(p,1)=lentot_i(p-1,1)+abs(len_i(p,1)-len_i(p-1,1));
   end
end



%Create new variables to work with this data
vector_Ft=[position,Ft];
vector_mu=[position,mu];
vector_Fn=[position,Fn];

%Calculate the average and variance of the initial tribological data
mu_prom_i=mean(mu);
var_mu_i=var(mu);
Fn_prom_i=mean(Fn);
var_Fn_i=var(Fn);

%Show the initial tribological data
%We must manually adjust the limit values of the graphs when
%analysing experiments with different forces to ensure all
%the data is displayed correctly
figure(1)
scatter(position, Fn, 1, 'k', 'filled')
```

```
ylabel('Normal Force (mN)')
xlabel('Position LMS20 (mm)')
xlim([-1.5 1.5]) % x-axis limits
%ylim([30 70])  % y-axis limits for a normal force of 50mN
ylim([130 170])  % y-axis limits for a normal force of 150mN
%title('Normal Force vs Position')
saveas(gcf, 'normal_forcemN_vs_posicionLMS20.png')
% Save the figure as PNG file

figure(2)
scatter(vector_Ft(:,1),vector_Ft(:,2), 1, 'k', 'filled')
xlim([-1.5 1.5]) % x-axis limits
%ylim([-70 50])  % y-axis limits for a normal force of 50mN
ylim([-140 120])  % y-axis limits for a normal force of 150mN
%title('Tangential force vs Position')
xlabel('Position LMS20 (mm)')
ylabel('Tangential Force (mN)')
saveas(gcf, 'tangencial_forcemN_vs_posicionLMS20.png')
% Save the figure as PNG file


figure(3)
scatter(vector_mu(:,1),vector_mu(:,2), 1, 'k', 'filled')
xlim([-1.5 1.5]) % x-axis limits
ylim([0 1])  % y-axis limits
%title('Coefficient of friction vs Position')
xlabel('Position LMS20 (mm)')
ylabel('Coefficient of friction')
saveas(gcf, 'Coefficient_of_friction_vs_posicionLMS20.png')
% Save the figure as PNG file

clear semi_length  row_vector minFt p
clear flag len_i minFt
%%
%Electric analysis

resis=Vol./Curr;%Ohm
resis= resis*1000;
Curr_prom_i=mean(Curr);%mV
Vol_prom_i=mean(Vol);%uA
resis_prom_i=mean(resis);%Ohm (49-54)

%Calculate the average and variance of the initial tribological data
Curr_var_i= var(Curr);
Vol_var_i=var(Vol);
resis_var_i=var(resis);

%Create new variables to work with this data
vector_curr=[position,Curr];
vector_vol=[position,Vol];
vector_resis=[position,resis];

%Show the initial electrical data
figure(4)
plot(lentot_i,Vol)
title('voltage')
```

```
figure(5)
plot(lentot_i,Curr)
title('corriente')

figure(6)
plot(lentot_i,resis)
title('resistencia')

%%
%From this point forward, filters will be performed
duration =time_dos-time_uno;%in seconds

fm=q/duration;%Sampling frequency=#sample/time(s
pas=1/fm; %Period in seconds
fny=fm/2;

%A new vector with the time data is created
time(q,1)=0;
for i=1:q
    if i==1
       time(i,1)=0;
    end
    if i>1
        time(i,1)=time(i-1,1)+duration/q;
    end
end

%Show the aplication of the filter
figure(7)
subplot(4,1,1)
plot(time(:,1),vector_Ft(:,2))
title('Tangential Force vs Time')
xlabel('Time (s)')
ylabel('Tangential Force (mN)')

subplot(4,1,2)
dim=q*pas;
ejefrec=[0:1/dim:(q-1)/dim];
spectr=abs(fft(Ft));
spectr=spectr/max(spectr);
plot(ejefrec,spectr,'linewidth',2);
xlabel('Frequency (Hz)')
title('Spectrum of the signal amplitude')
axis([0 max(ejefrec) 0 max(spectr)])

%Filter values defined to the filter for the tangential axis
wp=[0.001 0.990];
ws=[0.45 0.55];
rp=15;
rs=35;

%Creation and application of the butterworth filter
[n,wn]=buttord(wp,ws,rp,rs);
[b,a]=butter(n,wn,'stop');
fcut_t=wn*fny % cutoff frequency
[h,f]=freqz(b,a,[],fm);
```

```
subplot(4,1,3)
plot(f,abs(h));
axis([0 max(f) 0 max(abs(h))])
xlabel('Frequency (Hz)')
ylabel('H |j\omega|')
title('Response of the Butterworth Filter')

x_t=filter(b,a,vector_Ft(:,2)); %
subplot(4,1,4)
plot(time,x_t,'linewidth',2)
xlabel('Time (s)')
title('Filtered Signal by the Butterworth filter')
ylabel('F_t (mN)')

clear n wn a b h f
clear  i
clear  n mn b a wp ws rp rs h f
clear ejefrec
clear spectr
%%
%Filter for the normal force
%%%%
%Show the aplication of the passband filter
%%%%
figure(8)
subplot(4,1,1)
plot(time(:,1),vector_Fn(:,2))
title('Normal Force vs Time')
xlabel('Time (s)')
ylabel('Normal Force (mN)')
axis([0 max(time) 135 165])

subplot(4,1,2)
dim=q*pas;
ejefrec=[0:1/dim:(q-1)/dim];
spectr=abs(fft(Fn));
plot(ejefrec,spectr,'linewidth',2);
xlabel('Frequency (Hz)')
title('Spectrum of the signal amplitude')
axis([0 max(ejefrec) 0 max(spectr)])

Filter values defined to the filter for the normal axis
wp=0.005;
ws=0.15;
rp=15;
rs=50;

%Creation and application of the bandpass filter
[n,wn]=buttord(wp,ws,rp,rs);
[b,a]=butter(n,wn,'low');
fcut_n=wn*fny; %cutoff frequency
[h,f]=freqz(b,a,[],fm);

subplot(4,1,3)
plot(f,abs(h));
axis([0 max(f) 0 max(abs(h))])
xlabel('Frequency (Hz)')
```

```
ylabel('H |j\omega|')
title('Response of the Butterworth Filter')

x_n=filter(b,a,vector_Fn(:,2));
subplot(4,1,4)
plot(time,x_n)
xlabel('Time (s)')
title('Filtered Signal by the Butterworth filter')
ylabel('F_t (mN)')
 %axis([0 max(time) 135 165])
 %axis([260 300 135 165])

%Create new variables
time_fil_pos=find(time>0.5);
time_f=time(time_fil_pos);
Ft_f=x_t(time_fil_pos);
Fn_f=x_n(time_fil_pos);

figure(9)
subplot(2,1,1)
plot(time,vector_Fn(:,2))
title('Normal Force vs Time')
xlabel('Time (s)')
ylabel('Normal Force (mN)')
subplot(2,1,2)
plot(time_f,Fn_f)
xlabel('Time (s)')
title('Filtered Signal by the Butterworth filter')
ylabel('F_t (mN)')

clear  n mn b a wp ws rp rs h f
clear dim pas fny  fm wn
clear ejefrec spectr time_fil_pos
%%
%The recognition of constant slope zones algorithm begins
%
Ft_=vector_Ft(:,2);
h=50;
error=0.005;
max_mu=max(vector_mu(:,2));
position_=vector_Ft(:,1);
flag = 0;
for i2=1:8000
    vector_pend(h,1)=0;
    matriz_positionFt(h,1)=0;

    for k=1:h
        %Calculation of the slope
        slope=(Ft_(i2+k,1)-Ft_(i2+(1-1),1))/(position_(i2+k,1)- ...
        position_(i2+(1-1),1));
        angle=atan(slope)*180/pi;
        vector_pend(k,1)=angle;
        matriz_positionFt(k,1)=position_(i2+k,1);
        %the position value is stored in first column
        matriz_positionFt(k,2)=Ft_(i2+k,1);
        %the Ft value is stored in second column
    end
```

```
    [fil_pend,col_pend]=size(vector_pend);
    error_pend(fil_pend-1,1)=0;
    for m=2:fil_pend
        %Calculation of the error of the slope
        error_pend(m-1,1)=abs((abs(vector_pend(m,1)) ...
        -abs(vector_pend(2-1,1)))/abs(vector_pend(2-1,1)));
    end
    %It finds wich error values are in the range of the desired error and
    %gives the row number.
    pos=find(abs(error_pend(:,1))<error);
    [fil_pos,col_pos]=size(pos);
    if fil_pos==fil_pend-1

        if flag==0
           datos= matriz_positionFt;
        end
        if flag>0
           datos=[datos; matriz_positionFt];
        end
        flag=flag+1;
    end
end
figure(10)
plot(datos(:,1),datos(:,2),'o','markersize',2)
title('Sample_1')
xlabel('Position (mm)')
ylabel('F_t (mN)')

clear vector_pend matriz_positionFt slope col_pend
clear angle   fil_pend k  m
clear error_pend flag i2 fil_pos col_pos
%%
%Analysing the point when the tangential force were highest and lowest of
%all the data and applied the previous algorithm in the nearby of these
%points.
[a b]= size(Ft_);
 c=max(Ft_);
 d= min(Ft_);
for i=1: a
if Ft_(i)==c
    cont1=i;
end
if Ft_(i)==d
    cont2=i;
end
end

%Samples 8000, nearby to cont1 (maximum value)
if cont1>(a-4000)
    cont1 = a-4001-h;
end
if cont1<8000;
   cont1=4001;
end
m=8000;
ini=round(cont1-m/2);
```

```
ini_m= ini+m;
flag=1;
for i2=ini:ini_m
    vector_pend(h,1)=0;
    matriz_positionFt(h,1)=0;

    for k=1:h
        %Slope calculation
        slope=(Ft_(i2+k,1)-Ft_(i2+(1-1),1))/ ...
        (position_(i2+k,1)-position_(i2+(1-1),1));
        angle=atan(slope)*180/pi;
        vector_pend(k,1)=angle;
        matriz_positionFt(k,1)=position_(i2+k,1);
        %the position value is stored in first column
        matriz_positionFt(k,2)=Ft_(i2+k,1);
        %the Ft value is stored in second column
    end

    [fil_pend,col_pend]=size(vector_pend);
    error_pend(fil_pend-1,1)=0;
    for m=2:fil_pend
        %Calculation of slope error
        error_pend(m-1,1)=abs((abs(vector_pend(m,1)) ...
        -abs(vector_pend(2-1,1)))/abs(vector_pend(2-1,1)));
    end
    %Find the error values that are in the desired error range and
    %give the row number.
    pos=find(abs(error_pend(:,1))<error);
    [fil_pos,col_pos]=size(pos);
    if fil_pos==fil_pend-1
        if flag>0
            datos=[datos; matriz_positionFt];
        end
        flag=flag+1;
    end
end

%Samples 8000, nearby to cont2 (minimum value)
m=8000;
if cont2<8000;
   cont2=4001;
end
if cont2>(a-4000)
    cont2 = a-4001-h;
end

ini=cont2-m/2;
ini_m= ini+m;
flag=1;
for i2=ini:ini_m
    vector_pend(h,1)=0;
    matriz_positionFt(h,1)=0;

    for k=1:h
        %Slope calculation
        slope=(Ft_(i2+k,1)-Ft_(i2+(1-1),1))/ ...
        (position_(i2+k,1)-position_(i2+(1-1),1));
```

```
        angle=atan(slope)*180/pi;
        vector_pend(k,1)=angle;
        matriz_positionFt(k,1)=position_(i2+k,1);
        %the position value is stored in first column
        matriz_positionFt(k,2)=Ft_(i2+k,1);
        %the Ft value is stored in second column
    end

    [fil_pend,col_pend]=size(vector_pend);
    error_pend(fil_pend-1,1)=0;
    for m=2:fil_pend
        %Calculation of slope error
        error_pend(m-1,1)=abs((abs(vector_pend(m,1))...
        -abs(vector_pend(2-1,1)))/abs(vector_pend(2-1,1)));
    end
    %It finds wich error values are in the range of the desired error and
    %gives the row number.
    pos=find(abs(error_pend(:,1))<error);
    [fil_pos,col_pos]=size(pos);
    if fil_pos==fil_pend-1
        if flag>0
           datos=[datos; matriz_positionFt];
        end
        flag=flag+1;
    end
end

figure(10)
plot(datos(:,1),datos(:,2),'o','markersize',2)
title('Sample')
xlabel('Position (mm)')
ylabel('F_t (mN)')
%
clear flag a b c d i cont1 cont2  vector_pend
clear matriz_positionFt fil_pend col_pend
clear error_pend m pos fil_pos col_pos
clear ini ini_m k error i2
clear slope angle
%%
clc
close all
%Repeated values stored in the matrix "datos" are erased.
[UniXY,Index]=unique(datos,'rows');
DupIndex=setdiff(1:size(datos,1),Index);
datos(DupIndex,:)=[];

%Matrix "datos" is separated in left and right side.
%Left Side
clear vector_pend
clear error_pend
clear matriz_positionFt
clear slope

media_position_pend=mean(datos(:,1));
pos_izq=find(datos(:,1)<media_position_pend);
[fil_pos_izq,~]=size(pos_izq);
datos_izq(fil_pos_izq,2)=0;
```

```
for j=1:fil_pos_izq
    datos_izq(j,2)=datos(pos_izq(j,1),2);
    datos_izq(j,1)=datos(pos_izq(j,1),1);
end
figure(11)
plot(datos_izq(:,1),datos_izq(:,2),'o','markersize',2)
title('Left line')
xlabel('Position (mm)')
ylabel('F_t (mN)')
%
clear Index pos_izq fil_pos_izq j
clear UniXY DupIndex
%%
%Identify the desired area to erase
[d f]= size(datos_izq);

for i=1:d
     k =datos_izq(i,1);
    if k<-1.18
        temp_izq(i)= datos_izq(i,2);
    end
end
a=max(temp_izq);
for i=1:d
    if datos_izq(i,2)==a
        b= datos_izq(i,1);
    end
end

p=0;
for i=1:d
    if datos_izq(i,1)<=b
        if p==0
        datos_izq_d=[datos_izq(i,1) datos_izq(i,2)];
        end
        if p>0
         datos_izq_d=[datos_izq_d;[datos_izq(i,1) datos_izq(i,2)]];
        end
        p=p+1;
    end
end
figure(11)
plot(datos_izq_d(:,1),datos_izq_d(:,2),'o','markersize',2)
title('Left line')
xlabel('Position (mm)')
ylabel('F_t (mN)')

%Variables with the required information
datos_izq = datos_izq_d;
S1l=min(datos_izq(:,1));
S1d=max(datos_izq(:,1));

clear temp_izq
clear a d f i p
clear b k datos_izq_d
clc
%%
```

```
%Right Side
pos_der=find(datos(:,1)>media_position_pend);
[fil_pos_der,~]=size(pos_der);
datos_der(fil_pos_der,2)=0;
for j=1:fil_pos_der
    datos_der(j,2)=datos(pos_der(j,1),2);
    datos_der(j,1)=datos(pos_der(j,1),1);
end
figure(12)
plot(datos_der(:,1),datos_der(:,2),'o','markersize',2)
title('Right line')
xlabel('Position (mm)')
ylabel('F_t (mN)')

clear fil_pos_der j
%%
%Identify the desired area to erase
clear temp_der a b d f datos_der_d p

[d f]= size(datos_der);
for i=1:d
    if datos_der(i,1)> 1.18
        temp_der(i)= datos_der(i,2);
    end
end
a=min(temp_der);
for i=1:d
    if datos_der(i,1)> 1.18
    if datos_der(i,2)==a
       b= datos_der(i,1);
    end
    end
end

p=0;
for i=1:d
    if datos_der(i,1)>=b
        if p==0
        datos_der_d=[datos_der(i,1) datos_der(i,2)];
        end
        if p>0
         datos_der_d=[datos_der_d;[datos_der(i,1) datos_der(i,2)]];
        end
        p=p+1;
    end
end

figure(12)
plot(datos_der_d(:,1),datos_der_d(:,2),'o','markersize',2)
title('Right line')
xlabel('Position (mm)')
ylabel('F_t (mN)')

datos_der = datos_der_d;
S2l=min(datos_der(:,1));
S2d=max(datos_der(:,1));
```

```
clear temp_der
clear a d f i p
clear b k datos_der_d

%The data located between the abscissas corresponding to "S1d"
%and "S2l" is separated.

pFt_izq=find(position_(:,1)<S1d);
%Data whose position is less than limit "S1d"
pFt_der=find(position_(:,1)>S2l);
%Data whose position is more than limit "S2l"

[fil_pFt_izq,~]=size(pFt_izq);
Ft_izq(fil_pFt_izq,1)=0;
position_izq(fil_pFt_izq,1)=0;

[fil_pFt_der,~]=size(pFt_der);
Ft_der(fil_pFt_der,1)=0;
position_der(fil_pFt_der,1)=0;

for f=1:fil_pFt_izq
    Ft_izq(f,1)=Ft_(pFt_izq(f,1),1);
    position_izq(f,1)=position_(pFt_izq(f,1),1);
end

for f=1:fil_pFt_der
    a=pFt_der(f,1);
    Ft_der(f,1)=Ft_(a);
    position_der(f,1)=position_(a);
end

pFt_=[position_izq,Ft_izq;position_der,Ft_der];
figure(13)
plot(pFt_(:,1),pFt_(:,2),'o','markersize',2)
title('Data to identify')
xlabel('Position (mm)')
ylabel('F_t (mN)')

clear pFt_izq pFt_der
clear f a
%%
%It is proceeded to identify the linear regression
%The function "regresion" is used.

[az ,bz]=regresion(position_izq,Ft_izq);

figure(14)
plot(position_izq,Ft_izq,'ro','markersize',2,'MarkerEdgeColor', ...
'r','markerfacecolor','b')

%Extreme values are calculated,it is needed to plot the line
xmin=min(position_izq);
ymin=az(1)*xmin+bz(1);
xmax=max(position_izq);
ymax=az(1)*xmax+bz(1);
line([xmin xmax],[ymin ymax]);
xlabel('Position (mm)')
```

```
ylabel('F_t (mN)')
title('Data to identify and linear regression - Left side')

clear  S1d S1l S2d S2l
clear  xmin ymin xmax ymax
%%
%%%%%%%%%%%%%%%%%%%%%%%%%%%%%%%%%%%%%%%%%%%%%%%%%%%%%%%%%%%%%%%%%%%%55
%%%%%%%%%%%%%%%%%%%%%%%%%%%%%%%%%%%%%%%%%%%%%%%%%%%%%%%%%%%%%%%%%%%%55
flag=0;
for i=1:fil_pFt_izq
    y_=az(1)*position_izq(i,1)+bz(1);
    pFt_izq=[position_izq(i,1),Ft_izq(i,1)];
    %Data whose tangential force is higher than the
    %correspondent "y" value of the line, for the
    %same position, is stored in matrix "erase_izq".
    if Ft_izq(i,1)>=y_
        if flag==0
            erase_izq=pFt_izq;
        end
        if flag>0
            erase_izq=[erase_izq;pFt_izq];
        end
        flag=flag+1;
    end
end

clear az bz i flag pFt_izq  y_
%%
[ad ,bd]=regresion(position_der,Ft_der);

figure(15)
plot(position_der,Ft_der,'ro','markersize',2,'MarkerEdgeColor',...
'r','markerfacecolor','b')

%Extreme values are calculated,it is needed to plot the line
xmin=min(position_der);
ymin=ad(1)*xmin+bd(1);
xmax=max(position_der);
ymax=ad(1)*xmax+bd(1);
line([xmin xmax],[ymin ymax]);
xlabel('Position (mm)')
ylabel('F_t (mN)')
title('Data to identify and linear regression - Right side')

%%
flag=0;
for i=1:fil_pFt_der
    y_=ad(1)*position_der(i,1)+bd(1);
    pFt_der=[position_der(i,1),Ft_der(i,1)];
    %Data whose tangential force is lower than the
    %correspondent "y" value of the line, for the
    %same position, is stored in matrix "erase_der".
    if Ft_der(i,1)<y_
        if flag==0
            erase_der=pFt_der;
        end
        if flag>0
```

```
            erase_der=[erase_der;pFt_der];
        end
        flag=flag+1;
    end
end

clear fil_pFt_izq ad bd
clear  xmin ymin xmax ymax
clear flag i  y_ pFt_der
%%
%Data stored in matrixes "erase_der" and "erase_izq" are eliminated from
%original matrixes "vector_mu" and "vector_Ft".

%Result after applied the first part of the program
vector_mu(ismember(vector_Ft,erase_izq,'rows'),:)=[];
vector_Fn(ismember(vector_Ft,erase_izq,'rows'),:)=[];
vector_curr(ismember(vector_Ft,erase_izq,'rows'),:)=[];
vector_vol(ismember(vector_Ft,erase_izq,'rows'),:)=[];
vector_Ft(ismember(vector_Ft,erase_izq,'rows'),:)=[];


vector_mu(ismember(vector_Ft,erase_der,'rows'),:)=[];
vector_Fn(ismember(vector_Ft,erase_der,'rows'),:)=[];
vector_curr(ismember(vector_Ft,erase_der,'rows'),:)=[];
vector_vol(ismember(vector_Ft,erase_der,'rows'),:)=[];
vector_Ft(ismember(vector_Ft,erase_der,'rows'),:)=[];

%calculated the new average and variance
mu_prom=mean(vector_mu(:,2));
var_mu=var(vector_mu(:,2));
Fn_prom=mean(vector_Fn(:,2));
var_Fn=var(vector_Fn(:,2));

vector_resis=[vector_vol(:,1) ,vector_vol(:,2)./vector_curr(:,2)*1000];
%Ohm
Curr_prom=mean(vector_curr(:,2));%mV
Vol_prom=mean(vector_vol(:,2));%uA
resis_prom=mean(vector_resis(:,2));

Curr_var= var(vector_curr(:,2));
Vol_var=var(vector_vol(:,2));
resis_var=var(vector_resis(:,2));

%%
%Show previous results
figure(16)
scatter(vector_Ft(:,1),vector_Ft(:,2),1.5)
title('Tangential force without transition zones')
xlabel('Position (mm)')
ylabel('F_t (mN)')

figure(17)
scatter(vector_mu(:,1),vector_mu(:,2),1.5)
ylim([0 (max_mu+0.02)])
title('Coefficient of friction without valleys')
xlabel('Position (mm)')
ylabel('\mu')
```

```
figure(18)
scatter(vector_Fn(:,1),vector_Fn(:,2),1.5)
title('Normal Force without transition zones')
xlabel('Position (mm)')
ylabel('F_n')

clear fil_pFt_der

%%
%Position will be transformed in total length.
%%%
[row_vector,~]=size(vector_Ft);
len(row_vector,1)=0;close all

lentot(row_vector,1)=0;
minFt=min(vector_Ft(:,1));

for p=1:row_vector
   len(p,1)=vector_Ft(p,1)-minFt;
end

for p=1:row_vector
   if p==1
       lentot(p,1)=len(p,1);
   end

   if p>1
       lentot(p,1)=lentot(p-1,1)+abs(len(p,1)-len(p-1,1));
   end
end

%%
%Calculate the absolute value of tangential force in order to
% show the reults against the total length
[l,me]=size(vector_Ft);
val_abs_ft(l,1)=0;
for ia=1:l
    if vector_Ft(ia,2)<=0
        val_abs_ft(ia,1) =vector_Ft(ia,2)*(-1);
    else
        val_abs_ft(ia,1) =vector_Ft(ia,2);
    end
end
Ft_prom=mean(val_abs_ft(:,1));
var_Ft=var(val_abs_ft(:,1));

%%
%Show the result of this first part of the program
figure(19)
scatter(lentot(:,1),val_abs_ft(:,1),1.5)
title('Tangential force without transition zones')
xlabel('Total length (mm)')
ylabel('F_t (mN)')

figure(20)
scatter(lentot(:,1),vector_Fn(:,2),1.5)
```

```
title('Normal force without transition zone')
xlabel('Total length (mm)')
ylabel('F_n')

figure(21)
scatter(lentot(:,1),vector_mu(:,2),1.5)
title('Coefficient of friction without valleys')
xlabel('Total length (mm)')
ylabel('\mu')

figure(22)
scatter(lentot(:,1),vector_vol(:,2),1.5)
title('Voltage without transition zone')
xlabel('Total length (mm)')
ylabel('Voltage')

figure(23)
scatter(lentot(:,1),vector_curr(:,2),1.5)
title('Current without valleys')
xlabel('Total length (mm)')
ylabel('Current')

figure(24)
scatter(lentot(:,1),vector_resis(:,2),1.5)
title('Electrical resistence without valleys')
xlabel('Total length (mm)')
ylabel('Electrical resistence')


%%
%The process will be repeated to the filtered tangential data
%%%%
%%%%
% Ft_fil=x_t; %Replace the value of the filtered tangential force
% Fn_fil=x_n; %Replace the value of the filtered normal force

%From here the values of the
%Identify the values of time higher than 0.5 seconds
clear time_fil_pos
clear time_f
clear Ft_f
clear Fn_f
close all

time_fil_pos=find(time>0.5);
time_f=time(time_fil_pos);
position_f=position_(time_fil_pos);
%%
%Position will be transformed in total length.
%%%
row_vector=length(position_f);
len_f=zeros(row_vector,1);
lentot_f=zeros(row_vector,1);
minFt=min(position_f);
clear p
for p=1:row_vector
   len_f(p,1)=position_f(p,1)-minFt;
```

```
end

for p=1:row_vector
   if p==1
       lentot_f(p,1)=len_f(p,1);
   end

   if p>1
       lentot_f(p,1)=lentot_f(p-1,1)+abs(len_f(p,1)-len_f(p-1,1));
   end
end

%%
Ft_f=x_t(time_fil_pos);
Fn_f=x_n(time_fil_pos);
vector_Ft_f=[position_f,Ft_f];
vector_Fn_f=[position_f,Fn_f];
mu_f=zeros(length(time_f),1);

%The coefficient of friction will be calculated with the filterend normal
%and tangential forces
for j=1:length(time_f)
    mu_f(j,1)=abs(Ft_f(j,1))/Fn_f(j,1);
end
vector_mu_f=[position_f,mu_f];
figure(33)
plot(position_f,Fn_f)
figure(34)
plot(position_f,Ft_f)
figure(35)
plot(position_f,mu_f)
figure(36)
plot(lentot_f,mu_f)
clear vector_pend
clear matriz_positionFt
clear error_pend
clear flag
clear slope x_t

%%
flag=0;
h=50;
error=0.05;
for i2=1:8000
    vector_pend=zeros(h,1);
    for k=1:h
        %Slope calculation
        slope=(Ft_f(i2+k,1)-Ft_f(i2+k-1,1))/...
        (position_f(i2+k,1)-position_f(i2+k-1,1));
        angle=atan(slope)*180/pi;
        vector_pend(k,1)=angle;
        matriz_positionFt(k,1)=position_f(i2+k,1);
        %the position value is stored in first column
        matriz_positionFt(k,2)=Ft_f(i2+k,1);
        %the Ft value is stored in second column
    end
```

```
    [fil_pend,~]=size(vector_pend);
    error_pend(fil_pend-1,1)=0;
    for m=2:fil_pend
        %Slope calculation error
        error_pend(m-1,1)=abs((abs(vector_pend(m,1))- ...
        abs(vector_pend(2-1,1)))/abs(vector_pend(2-1,1)));
    end
    %It finds which error values are in the range of the desired error and
    %gives the row number.
    pos=find(abs(error_pend(:,1))<error);
    [fil_pos,~]=size(pos);
    if fil_pos==fil_pend-1

        if flag==0
           datos_f= matriz_positionFt;
        end
        if flag>0
           datos_f=[datos_f; matriz_positionFt];
        end
        flag=flag+1;
    else

    end
end

%%
%Analysing the point when the tangential force were highest and lowest of
%all the data and applied the previous algorithm in the nearby os these
%points in the filter data.
[a b]= size(Ft_f);
 c=max(Ft_f);
 d= min(Ft_f);
for i=1: a
if Ft_f(i)==c
    cont1=i;
end
if Ft_f(i)==d
    cont2=i;
end
end

%Samples 8000, nearby to cont1 (maximum value)
if cont1>(a-4000)
    cont1 = a-4001-h;
end
if cont1<8000;
   cont1=4001;
end
m=8000;
ini=round(cont1-m/2);
ini_m= ini+m;
flag=1;

for i2=ini:ini_m
    vector_pend=zeros(h,1);
    matriz_positionFt(h,1)=0;
    for k=1:h
```

```
        %Slope calculation
        slope=(Ft_f(i2+k,1)-Ft_f(i2+k-1,1))/(position_f(i2+k,1)- ...
        position_f(i2+k-1,1));
        angle=atan(slope)*180/pi;
        vector_pend(k,1)=angle;
        matriz_positionFt(k,1)=position_f(i2+k,1);
        %the position value is stored in first column
        matriz_positionFt(k,2)=Ft_f(i2+k,1);
        %the Ft value is stored in second column
    end

    [fil_pend,~]=size(vector_pend);
    error_pend(fil_pend-1,1)=0;
    for m=2:fil_pend
        %Slope calculation error
        error_pend(m-1,1)=abs((abs(vector_pend(m,1))- ...
        abs(vector_pend(2-1,1)))/abs(vector_pend(2-1,1)));
    end
    %It finds wich error values are in the range of the desired error and
    %gives the row number.
    pos=find(abs(error_pend(:,1))<error);
    [fil_pos,~]=size(pos);
    if fil_pos==fil_pend-1
        if flag>0
           datos_f=[datos_f; matriz_positionFt];
        end
        flag=flag+1;
    else
    end
end

%Samples 8000, nearby to cont1 (minimum value)
m=8000;
if cont2>(a-4000)
    cont2 = a-4001-h;
end
if cont2<8000;
   cont2=4001;
end
ini=cont2-m/2;
ini_m= ini+m;
flag=1;

for i2=ini:ini_m
    vector_pend=zeros(h,1);
    matriz_positionFt(h,1)=0;
    for k=1:h
        %Slope calculation
        slope=(Ft_f(i2+k,1)-Ft_f(i2+k-1,1))/(position_f(i2+k,1)- ...
        position_f(i2+k-1,1));
        angle=atan(slope)*180/pi;
        vector_pend(k,1)=angle;
        matriz_positionFt(k,1)=position_f(i2+k,1);
        %the position value is stored in first column
        matriz_positionFt(k,2)=Ft_f(i2+k,1);
        %the Ft value is stored in second column
    end
```

```
    [fil_pend,~]=size(vector_pend);
    error_pend(fil_pend-1,1)=0;
    for m=2:fil_pend
        %Slope calculation error
        error_pend(m-1,1)=abs((abs(vector_pend(m,1))- ...
        abs(vector_pend(2-1,1)))/abs(vector_pend(2-1,1)));
    end
    %It finds wich error values are in the range of the desired error and
    %gives the row number.
    pos=find(abs(error_pend(:,1))<error);
    [fil_pos,~]=size(pos);
    if fil_pos==fil_pend-1
        if flag>0
           datos_f=[datos_f; matriz_positionFt];
        end
        flag=flag+1;
    else
    end
end
%%
%Repeated values stored in the matrix "datos_f" are erased.
[UniXY,Index]=unique(datos_f,'rows');
DupIndex=setdiff(1:size(datos_f,1),Index);
datos_f(DupIndex,:)=[];

%Matrix "datos_f" is separated in left and right side.
%Left Side
clear vector_pend
clear matriz_positionFt
clear slope
clear i2
clear flag
clear DupIndex
clear UniXY
clear Index
clear poz_izq
clear poz_der
clear Ft_izq
clear Ft_der
clear pFt_izq
clear pFt_der
clear pFt_
clear position_fizq
clear Ft_izq
clear position_fder
clear Ft_der
clear datos_f_izq pos_izq media_position_pend

media_position_pend=mean(datos_f(:,1));
pos_izq=find(datos_f(:,1)<media_position_pend);
[fil_pos_izq,~]=size(pos_izq);
datos_f_izq(fil_pos_izq,2)=0;
for j=1:fil_pos_izq
    datos_f_izq(j,2)=datos_f(pos_izq(j,1),2);
    datos_f_izq(j,1)=datos_f(pos_izq(j,1),1);
end
```

```
figure(37)
plot(datos_f_izq(:,1),datos_f_izq(:,2),'o','markersize',2)
title('Left line')
xlabel('Position (mm)')
ylabel('F_t (mN)')

%%
% Same as before, identifying the desired area to erase in the filter
% data
close all
clear d f temp_izq a b datos_f_izq_d
[d f]= size(datos_f_izq);

for i=1:d
    if datos_f_izq(i,1)<-1.1
        temp_izq(i)= datos_f_izq(i,2);
    end
end
a=max(temp_izq);
for i=1:d

    if datos_f_izq(i,2)==a
        b= datos_f_izq(i,1);
    end

end

p=0;
for i=1:d
    if datos_f_izq(i,1)<= b
        if p==0
        datos_f_izq_d=[datos_f_izq(i,1) datos_f_izq(i,2)];
        end
        if p>0
         datos_f_izq_d=[datos_f_izq_d;...
         [datos_f_izq(i,1) datos_f_izq(i,2)]];
        end
        p=p+1;
    end
end
figure(37)
plot(datos_f_izq_d(:,1),datos_f_izq_d(:,2),'o','markersize',2)
title('Left line')
xlabel('Position (mm)')
ylabel('F_t (mN)')
clear datos_f_izq
datos_f_izq = datos_f_izq_d;

%%
S1l=min(datos_f_izq(:,1));
S1d=max(datos_f_izq(:,1));
clear datos_f_der pos_der fil_pos_der
%Right Side
pos_der=find(datos_f(:,1)>media_position_pend);
[fil_pos_der,~]=size(pos_der);
datos_f_der(fil_pos_der,2)=0;
for j=1:fil_pos_der
```

```
    datos_f_der(j,2)=datos_f(pos_der(j,1),2);
    datos_f_der(j,1)=datos_f(pos_der(j,1),1);
end
figure(38)
plot(datos_f_der(:,1),datos_f_der(:,2),'o','markersize',2)
title('Right line')
xlabel('Position (mm)')
ylabel('F_t (mN)')

%%
% Same as before, identifying the desired area to erase in the filter
% data
clear datos_f_der_d temp_izq a b d f p
[d f]= size(datos_f_der);

for i=1:d
    if datos_f_der(i,1)>1.1
        temp_der(i)= datos_f_der(i,2);
    end
end
a=min(temp_der);
for i=1:d
     if datos_f_der(i,1)>1.1
    if datos_f_der(i,2)==a
        b= datos_f_der(i,1);
    end
     end
end


p=0;
for i=1:d

    if datos_f_der(i,1)>=b
        if p==0
        datos_f_der_d=[datos_f_der(i,1) datos_f_der(i,2)];
        end
        if p>0
         datos_f_der_d=[datos_f_der_d;...
         [datos_f_der(i,1) datos_f_der(i,2)]];
        end
        p=p+1;
    end
end

figure(38)
plot(datos_f_der_d(:,1),datos_f_der_d(:,2),'o','markersize',2)
title('Right line')
xlabel('Position (mm)')
ylabel('F_t (mN)')
clear datos_der
datos_f_der = datos_f_der_d;
%%

S2l=min(datos_f_der(:,1));
S2d=max(datos_f_der(:,1));
pmedio_izq=0.5*(S1l+S1d);
```

```
pmedio_der=0.5*(S2l+S2d);

%The data located between the abscissas corresponding
%to "S1d" and "S2l" is separated.

pFt_izq=find(position_f(:,1)<S1d);
%Data whose position is less than limit "S1d"
pFt_der=find(position_f(:,1)>S2l);
%Data whose position is more than limit "S2l"
[fil_pFt_izq,~]=size(pFt_izq);
[fil_pFt_der,~]=size(pFt_der);
Ft_izq(fil_pFt_izq,1)=0;
position_fizq(fil_pFt_izq,1)=0;
Ft_der(fil_pFt_der,1)=0;
position_fder(fil_pFt_der,1)=0;

for f=1:fil_pFt_izq
    Ft_izq(f,1)=Ft_f(pFt_izq(f,1),1);
    position_fizq(f,1)=position_f(pFt_izq(f,1),1);
end

for f=1:fil_pFt_der
    Ft_der(f,1)=Ft_f(pFt_der(f,1),1);
    position_fder(f,1)=position_f(pFt_der(f,1),1);
end

pFt_=[position_fizq,Ft_izq;position_fder,Ft_der];
figure(39)
plot(pFt_(:,1),pFt_(:,2),'o','markersize',2)
title('Data to identify')
xlabel('Position (mm)')
ylabel('F_t (mN)')
%%

%It is proceeded to identify the linear regression
%The function "regresion" is used.

[az bz]=regresion(position_fizq,Ft_izq);
figure(40)
plot(position_fizq,Ft_izq,'ro','markersize',2,...
'MarkerEdgeColor','r','markerfacecolor','b')

%Extreme values are calculated, it is needed to plot the line
xmin=min(position_fizq);
ymin=az(1)*xmin+bz(1);
xmax=max(position_fizq);
ymax=az(1)*xmax+bz(1);
line([xmin xmax],[ymin ymax]);
xlabel('Position (mm)')
ylabel('F_t (mN)')
title('Data to identify and linear regression - Left side')
flag=0;
for i=1:fil_pFt_izq
    y_=az(1)*position_fizq(i,1)+bz(1);
    pFt_izq=[position_fizq(i,1),Ft_izq(i,1)];
    %Data whose tangential force is higher than the correspondent "y"
    % value of the line, for the same position,
```

```
    % is stored in matrix "erase_izq".
    if Ft_izq(i,1)>y_
        if flag==0
            erase_izq=pFt_izq;
        end
        if flag>0
            erase_izq=[erase_izq;pFt_izq];
        end
        flag=flag+1;
    end
end
%%
[ad bd]=regresion(position_fder,Ft_der);

figure(41)
plot(position_fder,Ft_der,'ro','markersize',2,'MarkerEdgeColor', ...
'r','markerfacecolor','b')

%Extreme values are calculated, it is needed to plot the line
xmin=min(position_fder);
ymin=ad(1)*xmin+bd(1);
xmax=max(position_fder);
ymax=ad(1)*xmax+bd(1);
line([xmin xmax],[ymin ymax]); %recta
xlabel('Position (mm)')
ylabel('F_t (mN)')
title('Data to identify and linear regression - Right side')
flag=0;
for i=1:fil_pFt_der
    y_=ad(1)*position_fder(i,1)+bd(1);
    pFt_der=[position_fder(i,1),Ft_der(i,1)];
    %Data whose tangential force is lower than the correspondent "y" value
    %of the line, for the same position, is stored in matrix "erase_der".
    if Ft_der(i,1)<y_
        if flag==0
            erase_der=pFt_der;
        end
        if flag>0
            erase_der=[erase_der;pFt_der];
        end
        flag=flag+1;
    end
end

%Data stored in matrices "erase_der" and "erase_izq" are eliminated from
%original matrices "vector_mu" and "vector_Ft".

%%
%Calculate the final result after appliying the two part of the program
vol_f=Vol(time_fil_pos);
curr_f=Curr(time_fil_pos);

vector_vol_f=[position_f,vol_f];
vector_curr_f=[position_f,curr_f];

vector_curr_f(ismember(vector_Ft_f,erase_izq,'rows'),:)=[];
vector_vol_f(ismember(vector_Ft_f,erase_izq,'rows'),:)=[];
```

```
vector_mu_f(ismember(vector_Ft_f,erase_izq,'rows'),:)=[];
vector_Fn_f(ismember(vector_Ft_f,erase_izq,'rows'),:)=[];
vector_Ft_f(ismember(vector_Ft_f,erase_izq,'rows'),:)=[];

vector_curr_f(ismember(vector_Ft_f,erase_der,'rows'),:)=[];
vector_vol_f(ismember(vector_Ft_f,erase_der,'rows'),:)=[];
vector_mu_f(ismember(vector_Ft_f,erase_der,'rows'),:)=[];
vector_Fn_f(ismember(vector_Ft_f,erase_der,'rows'),:)=[];
vector_Ft_f(ismember(vector_Ft_f,erase_der,'rows'),:)=[];

%Calculate the final average and variance of the text file
mu_prom_f=mean(vector_mu_f(:,2));
var_mu_f=var(vector_mu_f(:,2));
Fn_prom_f=mean(vector_Fn_f(:,2));
var_Fn_f=var(vector_Fn_f(:,2));

vector_resis_f=[vector_vol_f(:,1) ,vector_vol_f(:,2)./ ...
vector_curr_f(:,2)*1000];%mOhm
Curr_prom_f=mean(vector_curr_f(:,2));%mV
Vol_prom_f=mean(vector_vol_f(:,2));%uA
resis_prom_f=mean(vector_resis_f(:,2));

Curr_var_f= var(vector_curr_f(:,2));
Vol_var_f=var(vector_vol_f(:,2));
resis_var_f=var(vector_resis_f(:,2));

%%
%Calculate the tangential force for this second part
clear erase_der
clear erase_izq
clear position_fder
clear position_fizq
clear position_fpend
clear pFt
clear row_vector
clear position_fder
clear val_f_abs_ft
clear val_f_abs_mu

[l,me]=size(vector_Ft_f);
val_f_abs_ft(l,1)=0;
for ia=1:l
    if vector_Ft_f(ia,2)<=0
        val_f_abs_ft(ia,1) =vector_Ft_f(ia,2)*(-1);
    else
        val_f_abs_ft(ia,1) =vector_Ft_f(ia,2);
    end
end
Ft_prom_f=mean(val_f_abs_ft(:,1));
var_Ft_f=var(val_f_abs_ft(:,1));

%%
%Calculate the total length for this second part
clear row_vector
clear len_f
clear lentot_f
[row_vector,~]=size(vector_Ft_f);
```

```
len_f(row_vector,1)=0;
lentot_f(row_vector,1)=0;
minFt=min(vector_Ft_f(:,1));

for p=1:row_vector
   len_f(p,1)=vector_Ft_f(p,1)-minFt;
end
for p=1:row_vector
   if p==1
       lentot_f(p,1)=len_f(p,1);
   end
   if p>1
       lentot_f(p,1)=lentot_f(p-1,1)+abs(len_f(p,1)-len_f(p-1,1));
   end
end
clear j
clear i
clear len_f


%%
%Show final results
%We must manually adjust the limit values of the graphs when
%analysing experiments with different forces to ensure all
figure(42)
scatter(vector_Ft_f(:,1),vector_Ft_f(:,2),1, 'k', 'filled')
xlim([-1.5 1.5]) % x-axis limits
%ylim([-70 50])  % y-axis limits for a normal force of 50mN
ylim([-140 120])  % y-axis limits for a normal force of 150mN
title('Tangential force without transition zones')
xlabel('Position LMS20 (mm)')
ylabel('Tangential Force (mN)')

figure(43)
scatter(vector_mu_f(:,1),vector_mu_f(:,2),1,'k', 'filled')
ylim([0 1])
xlim([-1.5 1.5]) % x-axis limits
title('Coefficient of friction without transition zones')
xlabel('Position LMS20 (mm)')
ylabel('Coefficient of friction')

figure(44)
scatter(vector_Fn_f(:,1),vector_Fn_f(:,2),1,'k', 'filled')
title('Normal Force without transition zones')
xlim([-1.5 1.5]) % x-axis limits
%ylim([30 70])  % y-axis limits for a normal force of 50mN
ylim([130 170])  % y-axis limits for a normal force of 150mN
xlabel('Position (mm)')
ylabel('Normal Force (mN)')

figure(45)
scatter(lentot_f(:,1),vector_mu_f(:,2),1,'k', 'filled')
title('Coeficient of friction without transition zones ...
%and with filter process')
xlabel('Total length (mm)')
ylabel('Coefficient of friction')
ylim([0 1])
```

```
xlim([0 1000])

figure(50)
scatter(lentot_i,mu,1, 'k', 'filled')
title('Coeficient of friction')
xlabel('Total length (mm)')
ylabel('Coefficient of friction')
ylim([0 1])
xlim([0 1000])

figure(46)
scatter(lentot_f(:,1),val_f_abs_ft,1.5)
title('Tangential force without transition zones and with filter process')
xlabel('Total length (mm)')
ylabel('F_t (mN)')

figure(47)
scatter(lentot_f(:,1),vector_vol_f(:,2),2,'k', 'filled')
title('Voltage without transition zone and with filter process')
xlabel('Total length (mm)')
ylabel('Voltage (mV)')
ylim([0 12000])
xlim([0 1000])

figure(48)
scatter(lentot_f(:,1),vector_curr_f(:,2),2,'k', 'filled')
title('Current without valleys and with filter process')
xlabel('Total length (mm)')
ylabel('Current (\mu A)')
ylim([99900 100000])
xlim([0 1000])

figure(49)
scatter(lentot_f(:,1),vector_resis_f(:,2),2,'k', 'filled')
title('Electrical resistence without valleys and with filter process')
xlabel('Total length (mm)')
ylabel('Electrical resistence (Ohm)')
ylim([0 120])
xlim([0 1000])

%%
%Final cleaning variable before export the data in the variables
clear me ymin temp q   pmedio_izq p
clear ia y_ xmin row_vector pos pFt_der
clear l ymax xmax temp_izq  pmedio_der pFt_izq
clear minFt media_position_pend max_mu m k
clear ini_m ini h flag fil_pos_izq fil_pos_der
clear fil_pos fil_pend fil_pFt_izq fil_pFt_der
clear fcut_t fcut_n f  error_pend error d cont1 cont2
clear d c bz bd b az ad a S2l S2d S1l S1d
clear vol_f curr_f x_n pFt_ len angle Ft_der Ft_izq Ft_f Ft_
clear Fn_f temp_der
close all
```

,